WOOD AND FIBER SCIENCE

The Sustainable Natural Materials Journal

Volume 57, Number 3, 2025 (ISSN 0735-6161)

Open Access

JOURNAL OF THE

SWST – International Society of Wood Science and Technology

EDITORIAL AND PUBLICATION POLICY

Wood and Fiber Science as the official publication of the Society of Wood Science and Technology publishes open access papers with both professional and technical content. Original papers of professional concern, or based on research of international interest dealing with the science, processing, and manufacture of wood and composite products of wood or wood fiber origin will be considered.

All manuscripts are to be written in US English, the text should be proofread by a native speaker of English prior to submission. Any manuscript submitted must be unpublished work not being offered for publication elsewhere.

Papers will be reviewed by referees selected by the editor and will be published in approximately the order in which the final version is received. Research papers will be judged on the basis of their contribution of original data, rigor of analysis, and interpretations of results; in the case of reviews, on their relevancy and completeness.

Color photos/graphics will be offered at no additional cost to authors. The Open Access fee will be $1800/article for SWST members and $2000/article for nonmembers. Reduced rates are available for authors based in developing countries.

Technical Notes

Authors are invited to submit Technical Notes to the Journal. A Technical Note is a concise description of a new research finding, development, procedure, or device. The length should be **no more than two printed pages in WFS**, which would be five pages or less of double-spaced text (TNR12) with normal margins on 8.5 x 11 paper, including space for figures and tables. In order to meet the limitation on space, figures and tables should be minimized, as should be the introduction, literature review and references. The Journal will attempt to expedite the review and publication process. As with research papers, Technical Notes must be original and go through a similar double-blind, peer review process.

On-line Access to *Wood and Fiber Science* Back Issues

SWST is providing readers with a means of searching all articles in *Wood and Fiber Science* from 1968 to present.

Visit the SWST website at https://www.swst.org and go to Wood & Fiber Science Online. Click on either SWST Member Publication access (SWST members) or Subscriber Publication access (Institution Access). All must login with their email and password on the https://www.swst.org site or use their ip authentication if they have a site license.

As an added benefit to our current subscribers, you can now access the electronic version of every printed article along with exciting enhancements that include:

- IP authentication for institutions (only with site license)
- Enhanced search capabilities
- Email alerting of new issues
- Custom links to your favorite titles

(ISSN 0735-6161)

WOOD AND FIBER SCIENCE

JOURNAL OF THE SOCIETY OF WOOD SCIENCE AND TECHNOLOGY

VOLUME 57 JULY 2025 NUMBER 3

CONTENTS

Articles

MUDJI SUSANTO, MASUMI HASEGAWA, GANIS LUKMANDARU, SETIYO BUDI, MASHUDI, LILIANA BASKOROWATI, IDA LUH GEDE NURTJAHJANINGSIH, RINA LAKSMI HENDRATI, SUGENG PUDJIONO, DEDI SETIADI, SUMARDI, RATIH DAMAYANTI, BUDIMAN ACHMAD, ANDY BHERMANA, YUSUF SIGIT AHMAD FAUZAN, AND FANNY HIDAYATI
Genetic variations in wood properties of third generation *Acacia mangium* Willd. progeny tests from Sumatra, Indonesia 111

CHENG-JUNG LIN, BING-SYUN PENG, PO-HENG LIN, AND CHIEH-YU CHANG
Spatiotemporal dynamics of termite infestation in urban *Araucaria cunninghamii*: A case study in Taipei 122

DEVON PESSLER, EVA HAVIAROVA, AND MARK FRENCH
A survey of woods for acoustic guitar soundboards 136

EMMANUEL A. BOAKYE, JENNIFER KLUTSCH, CYRIAC S. MVOLO, AND ANDRE G. DUARTE
Near-infrared spectral signatures differentiate blue stain and brown rot fungi in conifer and broadleaf trees.... 147

Genetic variations in wood properties of third generation *Acacia mangium* Willd. progeny tests from Sumatra, Indonesia

*Mudji Susanto**
Research Center for Applied Botany, National Research and Innovation Agency, Indonesia, Email: mudj003@brin.go.id

Masumi Hasegawa
Department of Agro-environmental Sciences, Faculty of Agriculture, Kyushu University, Japan, Email: kmgtmsm@agr.kyushu-u.ac.jp

Ganis Lukmandaru
Faculty of Forestry, Universitas Gadjah Mada, Indonesia, Email: glukmandaru@ugm.ac.id

Setiyo Budi
Forest Tree Seed Center, Ministry of Forestry, Indonesia, Email: budi101279@gmail.com

Mashudi
Research Center for Applied Botany, National Research and Innovation Agency, Indonesia, Email: mash006@brin.go.id

Liliana Baskorowati
Research Center for Applied Botany, National Research and Innovation Agency, Indonesia, Email: lili020@brin.go.id

Ida Luh Gede Nurtjahjaningsih
Research Center for Applied Botany, National Research and Innovation Agency, Indonesia, Email: ilgn001@brin.go.id

Rina Laksmi Hendrati
Research Center for Applied Botany, National Research and Innovation Agency, Indonesia, Email: rina032@brin.go.id

Sugeng Pudjiono
Research Center for Applied Botany, National Research and Innovation Agency, Indonesia, Email: suge017@brin.go.id

Dedi Setiadi
Research Center for Applied Botany, National Research and Innovation Agency, Indonesia, Email: dedi024@brin.go.id

Sumardi
Research Center for Applied Botany, National Research and Innovation Agency, Indonesia, Email: suma027@brin.go.id

Ratih Damayanti
Directorate of Environment, Maritime, Natural Resources, and Nuclear Policy National Research and Innovation Agency, Indonesia, Email: ratih.damayanti@brin.go.id

Budiman Achmad
Research Centre for Macro Economics and Finance, National Research and Innovation Agency, Indonesia, Email: budi071@brin.go.id

Andy Bhermana
Research Centre for Research Center for Food Crops, National Research and Innovation Agency, Indonesia, Email: andy008@brin.go.id

Yusuf Sigit Ahmad Fauzan
Research Center for Applied Botany, National Research and Innovation Agency, Indonesia, Email: yusu009@brin.go.id

Fanny Hidayati
Faculty of Forestry, Universitas Gadjah Mada, Indonesia, Email: fanny_hidayati@ugm.ac.id

(Received 19 March 2025)

Abstract. *Acacia mangium* Willd. is a fast-growing tree commonly used in pulp and paper production. Despite extensive planting, there is a need for genetic improvement to enhance wood properties for better pulp output. This study assessed genetic variations in moisture content, pilodyn penetration, specific gravity, fiber length, cell wall thickness, lumen diameter, and cellulose content in a third-generation progeny test of *A. mangium* in South Sumatra, involving 52 families. Averages for 3-year-old *A. mangium* were as follows: pilodyn penetration at 11.22 mm, moisture content at 117.18%, specific gravity at 0.44, fiber length at 1.01 mm, and alpha cellulose at 68.03%. Phenotypic variation of wood properties ranged from 3.53% to 19.62%, while genotypic variation was between 1.83% and 9.91%. There was a strong genetic correlation between pilodyn penetration and wood properties (specific gravity, holocellulose, and alpha cellulose) with individual heritability of wood properties estimates (h^2_i) from 0.09 to 0.37. Significant family differences were found in pilodyn penetration, specific gravity, fiber length, holocellulose, and alpha cellulose, with genetic gains of wood properties between 1.78% and 9.72%.

Keywords: *Acacia mangium*; Genetic improvement; Wood properties; Pulp production; Heritability estimates

* Corresponding author

Introduction

Acacia mangium Willd. is a key species in the pulp and paper industry, particularly in tropical regions of Southeast Asia, where it has become a favored plantation species due to its rapid growth, adaptability to varied climates, and valuable wood properties (Hegde et al. 2013). Since the 1990s, Indonesia has widely cultivated *A. mangium* on marginal lands across the country, promoting it as a sustainable resource to meet the rising demand in the pulp and paper sector (Sutedjo and Warsudi 2017; Goreti et al. 2021). This species is distributed in several regions, such as Riau, South Sumatra, West Java, South Kalimantan, East Kalimantan, West Papua, and Maluku province (Figure 1). However, initial plantations were established using unimproved seeds, which limited wood productivity and quality (Suyanto and Soedjoko 2007; Krisnawati et al. 2011; Goreti et al. 2021).

To address these limitations, the Indonesian Ministry of Environment and Forestry (MoEF), in collaboration with the Japan International Cooperation Agency (JICA) and Musi Hutan Persada Company, initiated a breeding program in 1993. This program began with a first-generation progeny test and was later extended to second- and third-generation trials focused on growth enhancement. However, these trials initially did not assess wood property traits critical for pulp production, such as specific gravity, fiber length, lignin, and cellulose content, which directly affect pulp yield and quality (Nisatmanto and Kurinobu 2002; Susanto et al. 2013; Nirsatmanto 2016; Sunarti et al. 2022). Given the industry's need for both high growth rates and quality wood, improving the genetic traits of *A. mangium* relevant to pulp properties has become essential.

The pulp and paper industry requires raw materials characterized by substantial wood increments and superior quality. The quality of wood is indicated by pulp output; thus, investigations into pulp-related wood qualities are essential for tree selection in third-generation progeny tests. Qualities such as specific gravity and fiber length are critical determinants of tree species' utility for pulp manufacturing. The primary chemical constituents of wood that constitute cell walls (cellulose and lignin) and extractive substances, together with their distribution inside the cell walls, influence the characteristics of pulp and paper (Pereira et al. 2003). Fengel and Wegener (1995) indicated that several wood properties affecting pulp production for paper comprise specific gravity, moisture content, fiber dimensions, wood extractives, lignin, and cellulose. The potential for genetic improvement in morphological traits and wood properties has been validated (Harwood et al. 2015).

This study therefore aimed to identify genetic variations in wood properties related to pulp production in third-generation *A. mangium* progeny trials. Key wood characteristics evaluated were pilodyn penetration, moisture content, specific gravity, fiber length, and chemical contents (lignin, holocellulose, alpha cellulose) to determine their impact on pulp output. Estimated genetic parameters, including heritability and genetic gain, were used to assess the potential for genetic improvement of these traits. Genetic correlations between pilodyn penetration and wood properties were used to develop efficient selection criteria for high-quality trees in breeding programs without

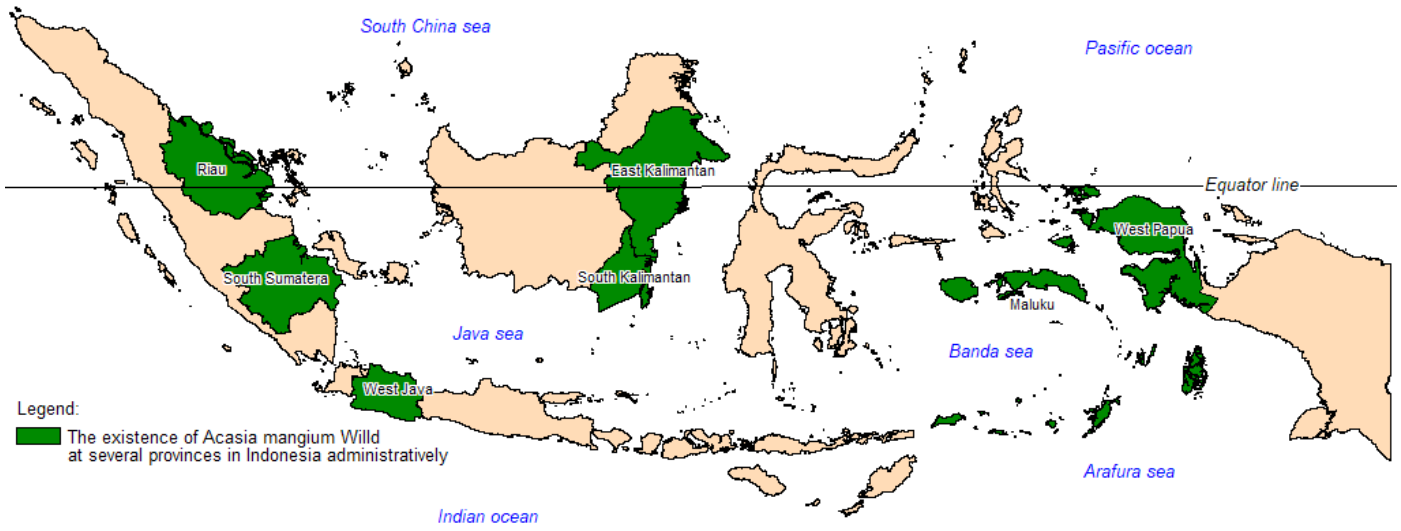

Figure 1. Spatial distribution of *Acacia mangium* Willd. in Indonesia.

causing damage to standing trees. Ultimately, the study aims to provide insights for optimizing *A. mangium* breeding programs focused on enhancing wood properties crucial for the pulp and paper industry in Indonesia.

Materials and Methods

Trial site, genetic material and experimental design

The third-generation progeny test of *A. mangium* was conducted in the Subanjeriji Trial, located at latitude 3.4°S and longitude 103.7°E. The trial was established at an elevation of 110 m above sea level in South Sumatra on podzolic soil. The average minimum temperature of the coldest month was 23°C, while the average maximum temperature of the hottest month was 33°C. Annual precipitation was 2,082 mm, with peak rainfall occurring from December to March and minimal rainfall in June. Humidity levels varied from 29% to 73%.

The progeny test comprised 52 open-pollinated families from the second-generation progeny test of *A. mangium* (Oriomo-Papua New Guinea provenance) during the Subanjeriji Trial. The experimental arrangement comprised 30 replications (blocks) utilizing a row-column pattern (incomplete block design) at group B-3 in Figure 2. Each plot consisted of a single row of four trees, with a spacing of 4 m between rows and 3 m between trees within each row. Only 10 blocks were used for measuring the wood properties (Figure 2).

Wood sample collection and wood properties measurement

A total of 326 trees (52 families with different replications of each family with a range of 3 to 11 trees) of 3-year-old third-generation *A. mangium* progeny were measured. Pilodyn penetration was measured on standing trees using a Pilodyn tester (6 J Forest, Proceq, Switzerland) with three positions were obtained for each tree at 50 cm above the ground after removing the bark (Ishiguri et al. 2008; Hidayati et al. 2013a; Hidayati et al. 2013b). The mean values of pilodyn penetration were calculated for each tree.

The average diameter of the sample trees was 20.85 cm (±3.49 cm). The sample trees were cut and wood discs samples were taken 50 cm above the ground. Wood samples were obtained from 52 families (the same number of the trees as for pilodyn testing) The discs were used to measure green specific gravity, green moisture content, fiber length, cell wall thickness, lumen diameter, lignin content, extractive content, alpha-cellulose content, and holocellulose content. Radial strips (2 cm in width, 2 cm in thickness, and length dependent on tree diameter) were prepared from each disk for measuring moisture content and specific gravity. Green specific gravity was determined from pith to bark. Blocks were obtained from one side with respect to the pith of the disk. Green specific gravity was calculated as the ratio of oven-dry mass to green volume, as determined by the water displacement method.

Measurements of fiber dimensions (fiber length, lumen diameter, and cell wall thickness) were conducted using a micrometer. Small strip specimens were macerated with Franklin's solution (100% glacial acetic acid [CH_3COOH] and 50% hydrogen peroxide [$H_2O_{2]}$ at a 1:10 ratio) for measuring fiber dimensions. The macerated fibers were stained with 1% safranin, cleared with alcohol, then mounted with Canada balsam. Images were captured using a digital camera attached to a microscope. A total of 50 wood fibers were measured for fiber length. Lumen diameter and cell wall thickness were also measured, using the macerated sample. Three positions of each fiber were measured for lumen diameter and cell wall thickness, then averaged. Ten fibers were measured for every sample, then averaged for each sample.

Wood samples were extracted for the analysis of wood chemistry, according to Technical Association of the Pulp and Paper Industry (TAPPI) standard T 204 cm-97 (1997). Lignin and alpha-cellulose contents were quantified utilizing TAPPI T 222 om-2 (2006) and TAPPI T 203 cm 99 (1999). Holocellulose content in wood samples was analyzed utilizing the acid chlorite method (Browning 1967).

Data Analysis

Common general linear models described by Hocking et al. (1978), Setiadi et al. (2021), Baskorowati et al. (2022), Purwanto et al. (2022), and Susanto et al. (2024) were utilized in this research. An analysis of variance (ANOVA) was carried out in order to investigate differences among families on the basis of the linear model presented below:

$$Y_{ijkl} = \mu + R_i + F_j + e_{ijk} \quad (1)$$

where, Y_{ijkl} = plot mean at j^{th} family and i^{th} replicate; μ = overall mean; R_i = effect of the i^{th} replicate; F_j = effect of the j^{th} family; and E_{ijk} = residual error with a mean of zero.

Individual tree heritabilities (h^2_i) was calculated based on Williams et al. (2002):

$$h^2_i = 1/r * \sigma^2_f/\sigma^2_p \quad (2)$$

where, r = coefficient of relationship; σ^2_f = variance between families; σ^2_p = phenotypic variance = ($\sigma^2_f + \sigma^2_m$); and σ^2_m = variance between plot.

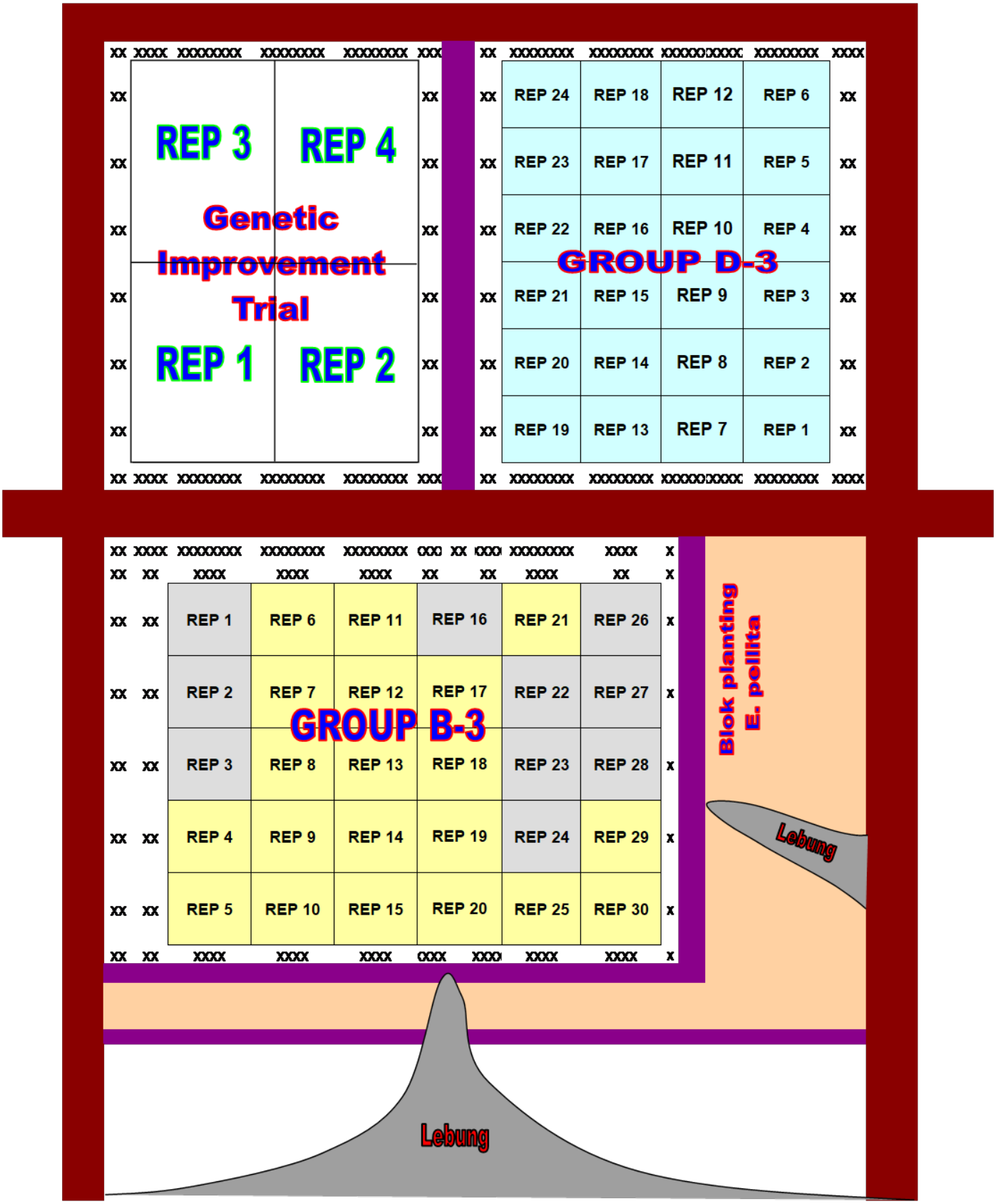

Figure 2. Layout of research plot at the Subanjeriji Trial.

Phenotypic coefficient of variation (PCV) (%) and genotypic coefficient of variation (GCV) were estimated according to Burton and DeVane (1953).

$$PCV = \frac{\sqrt{\sigma^2 p}}{\bar{x}} \times 100 \quad (3)$$

$$GCV = \frac{\sqrt{\sigma^2 g}}{\bar{x}} \times 100 \quad (4)$$

where, $\sigma^2 g$ = variance component of genotypic = $\sigma^2 A$; $\sigma^2 A$ = variance component of additive = $1/r * \sigma^2_f$; $\sigma^2 p$ = variance component of phenotypic; and $\bar{x}$ = mean of value of wood properties.

Genetic correlations (denoted r_g) were calculated according methodologies described by Williams et al. (2002):

$$r_g = \frac{Cov_f(X,Y)}{[\sigma^2_f(x) \cdot \sigma^2_f(y)]^{1/2}} \quad (5)$$

where, $Cov_f(X,Y)$ = covariance of the two traits at family level; $\sigma^2_f(x)$ = family-level variance components of trait (x); and $\sigma^2_f(y)$ = family-level variance components of trait (y).

Expected genetic gain (denoted ΔG) in the trial was estimated based on Shelbourne (1992):

$$\Delta G = i \cdot \sigma^2_p \cdot h^2_i \quad (6)$$

where, I = selection intensity; σ^2_p = phenotypic variance; and h^2_i = individual heritability for the trait of interest.

Results

Measurements and analyses of wood properties in 3-year-old *A. mangium* progeny trials at Subanjeriji in South Sumatra are shown in Tables 1–4. The mean and range of wood qualities evaluated, together with the genetic and phenotypic variety are presented in Table 1.

The range of phenotypic coefficients of variation of wood properties in the progeny trials ranged from 3.53% to 19.62% (Table 1), indicating that the phenotypic variance of wood properties was relatively small. The genotypic coefficient of variance in the progeny test was from 1.83% to 9.91%. This indicated that the genetic variation was also low. Individual heritability estimates for wood properties in the study ranged from low to high (h^2_i = 0.09 to 0.37), indicating that not all wood properties were strongly controlled by genetics.

Pilodyn penetration, moisture content, specific gravity, fiber length, holocellulose content, and alpha cellulose content all differed significantly amongst families (Table 2). Cell wall thickness, lumen diameter, extractive content, and lignin content did not differ significantly between families.

The genetic and phenotypic correlations between wood properties in the third-generation *A. mangium* progeny test at Subanjeriji are displayed in Table 3. Several wood properties exhibited significant genetic and phenotypic relationships among themselves (Table 3). Strong negative and positive genetic correlations are essential in tree selection activities based on wood characteristics.

The evaluation of genetic gain for wood properties of 3-year-old *A. mangium* in the third-generation progeny test in the Subanjeriji Trial is shown in Table 4. Estimated genetic gains for wood qualities from 3-year-old *A. mangium* in the third-generation progeny test in the Subanjeriji Trial are presented in Table 4. Genetic gain ranged from 1.78% to 9.72%, contingent upon a selection intensity of 10% for identifying the superior trees within the progeny test population.

Table 1. Mean, phenotypic coefficient of variation (PCV), genotypic coefficient of variation (GCV) and individual heritability (h^2_i) of *Acacia mangium* wood properties.

Wood property	Variation ranges	$\bar{x}$±SD	PCV (%)	GCV (%)	h^2_i
Pilodyn penetration	7.50–15.75 (mm)	11.22 (±1.42) mm	11.69	6.36	0.30
Moisture content	51.50–330.18 (%)	117.18 (±32.90) %	10.15	5.77	0.15
Specific gravity	0.22–0.72	0.44 (±0.07)	16.70	9.91	0.37
Fiber length	0.76–1.20 (mm)	1.01 (±0.06) mm	5.77	3.13	0.35
Cell wall thickness	2.41–5.00 (µm)	3.05 (±0.41) µm	13.56	4.27	0.09
Lumen diameter	7.59–19.44 (µm)	12.32 (±2.13) µm	17.33	6.34	0.13
Extractive content	1.60–7.14 (%)	3.64 (±1.15) %	19.62	9.11	0.24
Lignin content	19.35–39.45 (%)	24.10 (±5.57) %	11.85	5.46	0.21
Holocellulose content	63.63–83.95 (%)	74.83 (±3.93) %	3.53	1.83	0.27
Alpha cellulose content	53.08–68.82 (%)	68.03 (±3.86) %	9.99	6.09	0.37

Notes: $\bar{x}$±SD = Mean and standard deviation.

Table 2. Analysis of variance (ANOVA) of *Acacia mangium* wood properties.

Wood properties / Variance Sources	Df	MS	Pr>F
Pilodyn penetration			
Replications	9	7.633	<0.0001**
Families	51	3.683	<0.0001**
Error	740	1.236	
Moisture content			
Replications	9	0.004	<0.2171**
Families	51	0.004	<0.0491*
Error	740	0.002	
Specific gravity			
Replications	9	0.061	<0.0001**
Families	51	0.007	<0.0001**
Error	262	0.003	
Fiber length			
Replications	9	0.006	0.0525
Families	51	0.005	0.0038**
Error	267	0.002	
Cell wall thickness			
Replications	9	0.358	0.0200*
Families	51	0.137	0.7390
Error	267	0.160	
Lumen diameter			
Replications	9	2.455	0.8410
Families	51	5.272	0.2152
Error	267	4.505	
Extractive content			
Replications	9	0.923	0.0428
Families	51	0.650	0.0529
Error	264	0.468	
Lignin content			
Replications	9	12.702	0.0948
Family	51	10.122	0.0768
Error	264	7.579	
Holocellulose content			
Replications	9	15.976	0.0074**
Family	51	9.271	0.0235*
Error	264	6.202	
Alpha cellulose content			
Replication	9	470.365	< 0.0001**
Family	51	61.353	< 0.0001**
Error	269	26.973	

Notes: ns = not significant; * = significant at level of 0.05; ** = significant at level of 0.01.

Discussion

Significant differences among families were observed for pilodyn penetration, specific gravity, fiber length, holocellulose content, and alpha cellulose content. The findings indicated that pilodyn penetration, moisture content, specific gravity, fiber length, holocellulose content, and alpha cellulose content were influenced by family variation, suggesting genetic control. These wood properties must be considered in forestry breeding programs to meet the seedling needs for wood quality suitable for pulp production. Specific gravity, fiber length, holocellulose content, and alpha cellulose concentration are essential for pulp production (Arisman 1996; Lestari 2012).

Wood properties revealed that the third-generation *A. mangium* progeny test showed significant variances among individual trees (Table 1). This signifies that wood properties must be acknowledged as genetic variables in the breeding of *A. mangium* and establishes a basis for choosing the most suitable trees with superior wood quality. The selection of trees for wood qualities is based on individual heredity. Fiber length, specific gravity, extractives content, lignin content, alpha cellulose content, and holocellulose content demonstrate significant heritability; hence, these wood qualities need meticulous attention in tree selection to obtain superior wood quality.

Alpha-cellulose is essential for assessing cellulose purity. The presence of lignin and extractives adversely affects pulp quality. Nonetheless, there was no substantial difference between families in the progeny test regarding lignin and extractive content; so, these two factors may be excluded from consideration in tree selection, since they do not influence the quality of the resultant pulp. This study revealed significant variability in wood properties among 3-year-old third-generation *A. mangium* (Table 1). Thus, wood characteristics must be considered within the genetic criteria for the breeding of *A. mangium.*

Average specific gravity of the third generation of *A. mangium* at the age of 3 years was 0.44, with a variation range that extended from 0.22 to 0.72. This indicates that the trees possess qualities that are suitable for pulp production. Other research indicates that the ideal specific gravity range of *A. mangium* for pulp production is 0.37 to 0.46 (Arisman 1996). Susanto et al. (2013) examined the specific gravity of 17 provenances in the first generation of 5-year-old *A. mangium* progeny tests in Wonogiri, Central Java, and found that variances in specific gravity between provenances ranged from 0.40 to 0.47. Specific gravity of the trees from both the first and third generations provided promising potential for pulp manufacturing.

Table 3. Genetic (above the cross) and phenotypic correlation (under the cross) between wood properties of *Acacia mangium.*

	PP	SG	Ext	HC	Lig	AC	FL	LD	CW	MC
PP		-0.67	-0.98	-0.22	0.58	-0.96	0.00	-0.48	0.55	0.46
SG	-0.68		0.16	0.03	-0.24	0.53	-0.32	0.00	0.00	0.61
Ext	0.01	0.06		0.34	0.60	-0.57	-0.43	0.00	0.00	0.00
HC	0.16	0.25	0.08		-0.92	-0.08	-0.43	0.72	-0.54	0.00
Lig	-0.13	0.17	0.23	-0.90		-0.11	0.45	-0.65	0.37	0.00
AC	-0.12	0.25	-0.04	0.06	0.01		-0.01	0.00	0.44	0.00
FL	0.32	0.12	-0.02	0.10	-0.10	-0.03		0.00	0.00	-0.50
LD	0.13	0.08	0.06	-0.04	-0.06	0.04	0.00		-0.82	0.00
CW	0.11	0.06	-0.02	-0.05	0.04	-0.13	0.14	-0.03		0.00
MC	0.35	-0.49	0.00	0.00	0.00	0.00	0.19	0.00	0.00	

Notes: PP = Pilodyn penetration; SG = Specific gravity; Ext = Extractive content;
HC = Holocellulose content; Lig = Lignin content; AC = Alpha cellulose;
FL = Fiber length; LD = Lumen diameter; CW= Cell wall thickness; MC = moisture content

This study revealed that the average cell wall thickness was 3.05 µm, with a range from 2.41 to 5.00 µm. Average lumen diameter was 12.27 µm, with a range from 7.59 to 19.44 µm. Average fiber length was 1.01 mm, with a range from 0.76 to 1.2 mm. Variability in cell wall thickness, lumen diameter, and fiber length in progeny tests are of fundamental importance in breeding trials. Although the average fiber length in the third-generation progeny test was greater than that for the first generation of *A. mangium* in Pelaihari, South Kalimantan, at 22 months of age, at 0.89 mm (Susanto et al. 2012), it was shorter than the fiber length of the first generation at the Wonogiri Trial at the age of 5 years, which was 1.04 mm (Susanto et al. 2013). The generational differences, geographic variations, and age when fiber length was measured are factors that contribute to the variations in fiber length in *A. mangium*. Variations in fiber length of *A. mangium* trees have also been studied in Central Java (Hasegawa et al. 2009).

Average extractive content of 3-year-old third-generation *A. mangium* was 3.64%, lignin content was 24.10%, holocellulose content was 74.83%, and alpha cellulose content was 68.03%. The lower alpha cellulose content demonstrated that it is appropriate for use as a raw material in the paper industry (Lestari 2012). In contrast to the findings of other investigations on *Eucalyptus pellita*, the results of this specific inquiry are presented in Table 5.

Extractive content of *A. mangium* was lower than that of *E. globulus*, which was reported at 6% in West Ridgley, Tasmania (Poke et al. 2005), and lower than the extractive content of *Acacia melanoxylon* in Portugal (Lourenço et al. 2008). Lignin level was lower than that of *E. globulus*, which was 28.48%. Holocellulose and alpha cellulose content were superior to those of other species: *E. globulus* has a holocellulose content of 42.40% (Poke et al. 2005); *Antocephalus* spp. a holocellulose content of 39.20%; and *Falcataria moluccana* exhibited holocellulose and alpha cellulose contents of 63.39% and 40.43%, respectively (Indrawan et al. 2015). The reduced extractives

Table 4. Genetic gain estimation of *Acacia mangium* wood properties.

Traits	$\sigma^2 p$	i	h^2_i	ΔG %
Pilodyn penetration (mm)	1.32	1.75	0.30	6.16
Moisture content (%)	5.74	1.75	0.15	1.51
Specific gravity	0.07	1.75	0.37	9.72
Fiber length (mm)	0.06	1.75	0.35	3.57
Cell wall thickness (µ)	0.41	1.75	0.09	1.78
Lumen diameter (µ)	2.13	1.75	0.13	4.01
Extractive content (%)	0.71	1.75	0.24	6.95
Lignin content (%)	2.85	1.75	0.21	4.22
Holocellulose content (%)	2.64	1.75	0.27	1.77
Alpha cellulose content (%)	6.80	1.75	0.37	6.53

Notes: $\sigma^2 p$ = variance component of phenotypic; i = selection intensity; h^2_i = individual heritability; ΔG % = % genetic gain of population mean in progeny test.
Selection proportion was 10%.

Table 5. Alpha cellulose, lignin, and extractive contents of *Eucalyptus pellita* in three locations.

Alpha cellulose (%)	Lignin (%)	Extractive (%)	Location
49.02	29.49	—	South Kalimantan (Lukmandaru et al. 2016)
48.45	29.82	5.87	Central Java (Fatimah et al. 2015)
—	29.90	10.11	East Kalimantan (Taufiqhaqiqi et al. 2022)

and lignin contents, along with elevated holocellulose and alpha cellulose levels in the *A. mangium* progeny test at Subanjeriji, are crucial for breeding initiatives aimed at enhancing seed quality for the pulp and paper sector.

The third-generation *A. mangium* progeny test revealed medium to high individual heritability for pilodyn penetration, holocellulose content, lignin content, extractive content, specific gravity, fiber length, and alpha-cellulose content (Table 2). Moderate to high individual heritability was seen in first-generation *A. magium* progeny tests in Peleihari, South Kalimantan, and Wonogiri, Central Java, as well as in *E. urophylla* progeny tests in Vietnam and *E. niten*s progeny tests in East Victoria, Australia. The individual heritability values for pilodyn penetration were 0.62 in *A. mangium* in Peleihari and 0.30 in Wonogiri, 0.42 in *E. urophylla,* and 0.60 in *E. nitens*. The individual heritabilities for specific gravity were 0.35 in *A. mangium* in Pelaihari and 0.57 in Wonogiri, 0.60 in *E. urophylla*, and 0.73 in *E. nitens* (Greaves et al. 1996; Kien et al. 2008; Susanto et al. 2012; Susanto et al. 2013).

Despite exhibiting moderate to high heritability, these wood properties do not inherently possess a large genetic coefficient of variation (GCV) (Table 2). The genetic variation of wood properties is low, as evidenced by their GCV and PCV being less than 20%. However, values with GCV or PCV over 5% included pilodyn penetration, moisture content, specific gravity, lumen diameter, extractives, lignin, and alpha cellulose. These wood properties exhibited more additive genetic variance; hence, these should be factored into tree selection. Research on genetic coefficient of variation and heritability concerning tree selection based on wood density and growth in forest trees has been conducted by Cornelius (1994).

The wood properties studied showed low genetic variation (Table 2). Low genetic variation in wood properties means that the tree selection will yield genetic gains in accordance with genetic diversity (Table 4). Decreased additive variance of wood properties resulted from the *A. mangium* tree population being a third-generation progeny test, which had undergone a selection process for genetic value, hence reducing genetic diversity. Investigations on the reduction of additive variance across succeeding generations indicated that additive variance diminished during several selection cycles, leading to decreased genetic variation relative to the initial generation (van der Werf and de Boer 1990).

The substantial negative genetic correlation between pilodyn penetration and specific gravity, extractive content, and alpha cellulose indicated that pilodyn penetration may be effective in tree selection (Table 3). Minimal damage to the tree makes it much simpler to choose trees based on the characteristics of the wood in the standing tree. An increase in holocellulose content will result in a reduction in lignin and extractive content, while an increase in wood density may also reduce lignin content. This negative correlation between these wood properties is highly advantageous for pulp and paper production. The strong correlation between pilodyn penetration and other wood properties is advantageous for the selection of trees in *A. mangium* progeny assays to optimize pulp and paper production. Rapid tree selection has the potential to enhance alpha cellulose, while simultaneously reducing the amounts of lignin and extractive content. Cown and Hutchison (1983) found a strong correlation between pilodyn penetration and basic density in *Pinus radiata* in New Zealand and suggested that this device could have an application for rapid non-destructive measurement of wood properties. The pilodyn has a long history of use as a non-destructive method for evaluating density in tree breeding programs (Sprague et al. 1983; Woods et al. 1995; Hansen 2000). Wood density and pilodyn pin penetration were significantly negatively correlated (Wei and Borralho 1997; Wu et al. 2010, 2011; Hidayati et al. 2019). Research on the pilodyn for assessing genetic improvements of wood density and selecting *Cryptomeria japonica* trees has been conducted in Japan (Fukatsu et al. 2011).

Genetic or phenotypic correlations between moisture content and other wood properties, such as extractives, holocellulose, lignin, alpha cellulose, lumen diameter, and cell wall thickness were weak. Moisture content was poorly correlated with pilodyn penetration, specific gravity, and fiber length, suggesting that moisture content does not impact other wood qualities relevant to the selection process. A significant negative genetic correlation was found between pilodyn penetration and specific gravity in the first-generation *A. mangium* progeny test in Pelaihari, South Kalimantan, with r_g = -0.83, and in Wonogiri, Central Java, with r_g = -0.91 (Susanto et al. 2012, 2013). Strong negative correlations between pilodyn pin penetration and basic density were also found in *P. radiata* with r = -0.80 (Cown and Hutchison 1983). Other progeny tests have revealed strong negative phenotypic and genetic correlations between pilodyn pin penetration and specific gravity in various species, including *E. urophyla* in Guangxi Zhuang Autonomous Region, with r_g = -1.00 and r_p = -0.80 (Wei and Borralho 1997); *C. japonica* in Japan, with r_p = -0.92 (Yamashita et al. 2007); and *E. urophyla* in Vietnam, with r_g = -0.86 (Kien et al. 2008), as well as *E. nitens* in eastern Victoria, Australia, with r_g = -0.92 and r_p = -0.59 (Greaves et al. 1996).

Our research suggests that the negative genetic and phenotypic correlations between fiber length and other wood properties were weak. As a result, it is useful to select trees with high alpha cellulose or holocellulose contents without diminishing fiber length. A study on *E. globulus* in Northwestern Tasmania revealed a weak genetic correlation (r_g = 0.21) between the fiber length and specific gravity (Apiolaza et al. 2005). A weak genetic correlation was observed in the *A. mangium* progeny test between specific gravity and fiber length, extractive content and holocellulose content, lignin content and specific gravity, and lignin content and cell thickness. A weak or moderate correlation between these wood properties implied that they were insufficient for estimating wood properties.

Specific gravity, fiber length, holocellulose content, and alpha cellulose were anticipated to improve by 9.72%, 3.57%, 1.77%, and 6.53%, respectively, following selection at 3 years of age (Table 4). The projections in wood properties may be considered cautious, due to the exclusion of some factors from these computations. Concurrently, extractive content and lignin content may decrease by 6.95% and 4.22%, respectively (Table 4). However, it is important to note that for the families in Subanjeriji, this degree of improvement is necessary to align the selected population's wood properties with those of the *A. mangium* plantation in Indonesia. This study's results demonstrate significant improvements in the commercial wood quality of *A. mangium* by selection and breeding. A program is now in progress in South Sumatra involving the progeny test of *A. mangium* at the Subanjeriji trial, aimed at converting it into a seedling seed orchard. The anticipated result of utilizing improved *A. mangium* seeds is a more efficient pulp and paper industry in Indonesia, yielding higher profits for companies and thus providing a stronger incentive to replace declining plantations with superior germplasm. An anticipated substantial advantage from a more efficient *A. mangium* is expected for several pulp and paper facilities in Indonesia.

Conclusions

Analysis of wood properties and genetic parameters in the third-generation offspring test of *A. mangium* indicated that genetic variations in wood properties were relatively low; however, there were moderate to high heritability values for attributes such as pilodyn penetration, holocellulose content, lignin content, extractive content, specific gravity, fiber length, and alpha-cellulose content. Consequently, these wood properties can serve as a basis for tree selection to enhance wood quality. Pilodyn penetration, which was strongly genetically correlated with wood properties, can be employed for tree selection to improve wood quality without causing damage to the tree stem. Concurrently, specific gravity, fiber length, holocellulose content, and alpha cellulose can be enhanced, while diminishing extractive content and lignin, thus improving the quality of the resultant wood for pulp production.

Acknowledgments:

Authors thank Mohammad Naiem, Eko Bhakti Hardiyanto, T.A. Prayitno, Junji Matsumura, Koki Fujita for their help in the research; PT. Musi Hutan Persada (MHP) for *Acacia mangium* progeny test at Subanjeriji, South Sumatra; Ministry of Forestry, Indonesia; Gadjah Mada University and Kyushu University for their supporting in the research; Staffs of PT. MHP for their help in the wood sample collection and field measurement.

Authors' contributions

Mudji Susanto: Conceptualization, methodology, investigation, wood chemical analysis, parameter genetic analysis, writing original draft, and editing. Masumi Hasegawa: Review on article and supervision on lab. for wood analysis. Ganis Lukmandaru: Review on chemical analysis. Setiyo Budi: Fiber dimension analysis. Mashudi: Wood sample preparation. Liliana Baskorowati: Review on article and editing. ILG Nurtjahjaningsih: Review on genetic. Rina Laksmi H: Review on method. Sugeng Pudjiono: Data curation. Dedi Setiadi: Checking data for analysis. Sumardi: Data preparation of wood chemical properties. Ratih Damayanti: Review on wood properties. Budiman Achmad: Data analysis. Andy Bhermana: Writing for spatial distribution of *Acacia mangium* and visualization; Yusuf Sigit Ahmad Fauzan: Data preparation of wood physical properties. Fanny Hidayati: Review on wood physical properties analysis and editing.

References

Apiolaza, LA, Raymond CA, Yeo BJ (2005) Genetic variation of physical and chemical wood properties of *Eucalyptus globulus*. Silvae Genet 54(1–6):160–166. https://doi.org/10.1515/sg-2005-0024

Arisman H (1996) A tree improvement program for a pulpwood plantation project in Sumatra, Indonesia. In A Widyatmoko AYPBC Suhaendi H Furukoshi T, eds. Tropical Plantation Establishment Improving Productivity Through Genetic Practices, Proceedings International Seminar 19–21 December 1996, Yogyakarta Indonesia. Yogyakarta: Forest Tree Improvement Research and Development Institute Part IV 20-26.

Baskorowati L, Purwanto, Hendrati RL, Setiahadi R, Susanto M, Nurtjahyaningsih I, Mashudi, Kurniawan A, Pudjiono S, Setiadi D, Sumardi (2022) The approach in selecting the best genetic resistance against invasive aphid for indigenous tropical *Pinus merkusii* Jungh. et de Vriese in Indonesia. Forests 13(3):451. https://doi.org/https://doi.org/10.3390/f13030451

Browning BL (1967) Methods of wood chemistry. Interscience Publishers. A Division of John Wiley and Sons.

Burton GW, DeVane EH (1953) Estimating heritability in tall fescue (*Festuca arundinacea*) from replicated clonal material. Agron J 45(10):478–481. https://doi.org/https://doi.org/10.2134/agronj1953.00021962004500100005x

Cornelius J (1994) Heritabilities and additive genetic coefficients of variation in forest trees. Can J For Res 24(2):372–379. https://doi.org/10.1139/x94-050

Cown DJ, Hutchison JD (1983) Wood density as an indicator of the bending properties of pinus radiata poles. N Z J For Sci 13(1):87–99. https://www.scionresearch.com/__data/assets/pdf_file/0009/36477/NZJFS-1311983COWN87_99.pdf

Fatimah S, Susanto M, Lukmandaru G (2015) Study of chemical components of *Eucalyptus pellita* F. Muell from trees plus second generation offspring test results in Wonogiri, Central Java. Jurnal Ilmu Kehutanan 7(1):57. https://doi.org/10.22146/jik.6138

Fengel D, Wegener G (1995) Wood: chemical, ultrastructure, reactions. Gadjah Mada University Press.

Fukatsu E, Tamura A, Takahashi M, Fukuda Y, Nakada R, Kubota M, Kurinobu S (2011) Efficiency of the indirect selection and the evaluation of the genotype by environment interaction using pilodyn for the genetic improvement of wood density in *Cryptomeria japonica*. J For Res 16:128–135. https://doi.org/doi.org/10.1007/s10310-010-0217-6

Goreti T, Muin A, Burhanuddin B (2021) Diversity of undergrowth of *Acacia mangium* plants on Mandor Green Hill, Landak Regency. Jurnal Hutan Lestari, 9(1):14. https://doi.org/10.26418/jhl.v9i1.45320

Greaves BL, Borralho NMG, Raymond CA, Farrington A (1996) Use of a pilodyn for the indirect selection of basic density in *Eucalyptus nitens*. Can J For Res 26(9):1643–1650. https://doi.org/10.1139/x26-185

Hansen CP (2000) Application of the pilodyn in forest tree improvement. Danida Forest Seed Centre, Denmark, pp. 1–11.

Harwood CE, Hardiyanto EB, Yong WC (2015) Genetic improvement of tropical acacias: achievements and challenges. South For 77(1):11–18. https://doi.org/10.2989/20702620.2014.999302

Hasegawa M, Wakimoto R, Yoshida E, Shimizu K, Kondo R, Widyatmoko A, Nirsatmanto A, Shiraishi S (2009) Provenance variation in growth and wood properties of *A. mangium* and *A. auriculiformis* in Central Java, Indonesia: selecting potential hybrid parents for good provenance. Bulletin of Kyushu University Forestry 90(25–37).

Hegde M, Palanisamy K, Yi JS (2013). *Acacia mangium* Willd. - A fast growing tree for tropical plantation. J For Environ Sci 29(1):1–14. https://doi.org/10.7747/JFS.2013.29.1.1

Hidayati F, Lukmandaru G, Indrioko K, Sunarti S, Nirsatmanto A (2019) Variation in tree growth characteristics, pilodyn penetration, and stress-wave velocity in 65 families of *Acacia mangium* trees planted in Indonesia. J Korean Wood Sci Tech 47(5):633–643. https://doi.org/10.5658/WOOD.2019.47.5.633

Hidayati F, Ishiguri F, Iizuka K, Makino K, Takashima Y, Danarto S, Winarni WW, Irawati D, Na'iem M, Yokota S (2013a) Variation in tree growth characteristics, stress-wave velocity, and pilodyn penetration of 24-year-old teak (*Tectona grandis*) trees originating in 21 seed provenances planted in Indonesia. J Wood Sci 59(6):512–516. https://doi.org/10.1007/s10086-013-1368-9

Hidayati F, Ishiguri F, Iizuka K, Makino K, Tanabe J, Marsoem SN, Na'iem M, Yokota S, Yoshizawa N (2013b) Growth characteristics, stress-wave velocity, and pilodyn penetration of 15 clones of 12-year-old *Tectona grandis* trees planted at two different sites in Indonesia. J Wood Sci 59(3):249–254. https://doi.org/10.1007/s10086-012-1320-4

Hocking RR, Hackney OP, Speed FM (1978) The Analysis of Linear Models with Unbalanced Data. In Contributions to Survey Sampling and Applied Statistics (pp. 133–151) Elsevier. https://doi.org/10.1016/B978-0-12-204750-3.50016-2

Indrawan DA, Efiyanti L, Tampubolon RM, Roliadi H (2015) The manufacture of pulp for wrapping paper from alternative fiber stuffs. Jurnal Penelitian Hasil Hutan 33(4):283–302.

Ishiguri F, Matsui R, Iizuka K, Yokota S, Yoshizawa N (2008) Prediction of the mechanical properties of lumber by stress-wave velocity and Pilodyn penetration of 36-year-old Japanese larch trees. Holz Als Roh- Und Werkstoff 66(4):275–280. https://doi.org/10.1007/s00107-008-0251-7

Kien ND, Jansson G, Harwood C, Almqvis C, Thin HH (2008) Genetic variation in wood basic density and pilodyn penetration and their relationships with growth, stem straightness, and branch size for *Eucalyptus urophylla* in Northern Vietnam. N Z J For Sci 38(1):160–175.

Krisnawati H, Kallio M, Kanninen M (2011) *Acacia mangium* Willd.: Ecology, silviculture and productivity. CIFOR. https://www.cifor-icraf.org/publications/pdf_files/Books/BKrisnawati1101.pdf

Lestari SDW (2012) Holoselulosa. Saridewei Site. https://sardewforester.blogspot.com/2012/01/ holoselulosa.html

Lourenço A, Baptista I, Gominho J, Pereira H (2008) The influence of heartwood on the pulping properties of *Acacia melanoxylon* wood. J Wood Sci 54(6):464–469. https://doi.org/10.1007/s10086-008-0972-6

Lukmandaru G, Zumaini, UF, Soeprijadi D, Nugroho WD, Susanto M (2016) Chemical properties and fiber dimension of *Eucalyptus pellita* from the 2nd generation of progeny tests in Pelaihari, South Borneo, Indonesia. J Korean Wood Sci Tech 44(4):571–588. https://doi.org/10.5658/WOOD.2016.44.4.571

Nirsatmanto A, Kurinobu S (2002) Trend of within-plot selection practiced in two seedling seed orchards of *Acacia mangium* in Indonesia. J For Res 7: 49−52. https://doi.org/10.1007/BF02762598

Nirsatmanto A (2016) Recycled genetic resource as an optional srategy in advanced generation breeding for tropical species: a case study in optimizing genetic resource for *Acacia mangium* breeding program. Pp 762−772 in Siregar PDCA et al. (eds) Proceedings of International Conference of Indonesia Forestry Researchers. III. Forestry Research to Support Sustainable Timber Production and Selfsufficiency in Food, Energy, and Water. 21−22 October 2016, Bogor.

Pereira H, Graca J, Rodrigues JC (2003) Wood chemistry in relation to quality. In Wood Quality and its Biological Basic (pp. 53–67).

Poke FS, Wright JK, Raymond CA (2005) Predicting extractives and lignin contents in *Eucalyptus globulus* using near infrared reflectance analysis. JWCT 24(1), 55–67. https://doi.org/10.1081/WCT-120035944

Purwanto, Baskorowati L, Sumarton P, Hendrati RL, Susanto M, Mashudi, Setiadi D, Nurtjahyaningsih I, Pudjiono S, Kurniawan A, Putra PYAW, Sumardi (2022) Evaluation of aphid resistance and oleoresin production in indigenous tropical pine (*Pinus merkusii* Jungh. & de Vriese). Forests 13: 977. https://doi.org/10.3390/f13070977

Setiadi D, Susanto M, Baskorowati L, Mashudi, Pudjiono S (2021) Genetic variation of *Gmelina arborea* Roxb in Trenggalek, East Java. IOP Conference Series: Earth and Environmental Science. https://doi.org/10.1088/1755-1315/914/1/012014

Shelbourne CJA (1992) Genetic gains from different kinds of breeding population and seed or plant production population. South Afr For J 160(1):49–65. https://doi.org/10.1080/00382167.1992.9630411

Sprague JR, Talbert JT, Jett JB, Bryant RL (1983) Utility of the pilodyn in selection for mature wood specific gravity in loblolly pine. For Sci 29(4):696–701. https://doi.org/10.1093/forestscience/29.4.696

Sunarti S, Nirsatmanto A, Brawner J, Setyaji T, Kartikaningtyas D, Handayani BR, Surip, Hidayati F (2022) Effect of genetic gain in diameter and wood density on advanced generation breeding strategy of *Acacia mangium* in Indonesia. J Trop For Sci 34(1): 92–102. https://doi.org/10.26525/jtfs2022.34.1.92

Susanto M, Baskorowati L, Hendrati RL, Nurtjahjaningsih ILG, Mashudi, Pudjiono S, Setiadi D, Sumardi, Santoso Sulistiadi HB, Fauzan YSA, Achmad B, Hadiyan Y, Haryjanto L (2024) Growth of indigenous mountainous Indonesian *Hibiscus macrophyllus* in agroforestry system from various age, seed sources and slopes. For Sci Technol 20(3):300–308. https://doi.org/10.1080/21580103.2024.2385181

Susanto M, Naiem M, Hardiyanto EB, PrayitnoTA (2012) Genetic parameter analysis of wood properties in combination of provenance and progeny

trial of *Acacia mangium* in South Kalimantan. Jurnal Pemuliaan Tanaman Hutan 6(3):131–142.

Susanto M, Naiem M, Hardiyanto EB, Prayitno TA (2013) Genetic variation of wood properties in progeny trial of *Acacia mangium* on 5 years old in Wonogiri, Central Java. Jurnal Manusia Dan Lingkungan 20(3):312–323. https://doi.org/https://doi.org/10.22146/jml.18499

Sutedjo, Warsudi (2017) Measuring the invasive properties of *Acacia mangium* Willd. in the Bukit Soeharto Research and Education Forest. Jurnal Hutan Tropis 1(1):82–89. https://doi.org/10.32522/u-jht.v1i1.795

Suyanto, Soedjoko MA (2007) Invasion of *Acacia mangium* into Galam Forest Wildlife Reserve, Pelaihari Tanah Laut. Warta Konservasi Lahan Basah, 15(18–19).

TAPPI (1997) T 204 cm-97, Solvent extractives of wood and pulp. Technical Association of the Pulp & Paper Industry Publications.

TAPPI (1999) T 203 cm-99, Alpha-, beta- and gamma-cellulose in pulp. Technical Association of the Pulp & Paper Industry Publications. https://webstore.ansi.org/standards/tappi/203cm99

TAPPI (2006) TAPPI T 222 om-02, Acid-insoluble lignin in wood and pulp Technical Association of the Pulp & Paper Industry Publications.

Taufiqhaqiqi M, Hudaya D, Septiana HA, Ramadhan R, Yuliansyah Y, Suwinarti W, Amirta R (2022) Analysis of theultimate wood composition of a forest plantation species, *Eucalyptus pellita*, to estimate its bioelectricity potency. Biodiversitas 23(5):2389–2394. https://doi.org/10.13057/biodiv/d230516

van der Werf JH, de Boer IJ (1990) Estimation of additive genetic variance when base populations are selected. JAS 68(10):3124. https://doi.org/10.2527/1990.68103124x

Wei X, Borralho NMG (1997) Genetic control of wood basic density and bark thickness and their relationships with growth traits of *Eucalyptus urophylla* in South East China. Silvae Genet 46(4):245–250.

Williams ER, Matheson AC, Harwood CE (2002) Experimental Design and Analysis for Tree Improvement. CSIRO Publishing.

Woods JH, Kolotelo D, Yanchuk AD (1995) Early selection of coastal Douglas-fir in a farm-field test environment. Silvae Genet 44:178–186

Wu S-J, Xu J-M., Li G-Y, Risto V, Lu Z-H, Li B-Q, Wang W (2010) Use of the pilodyn for assessing wood properties in standing trees of Eucalyptus clones. J For Res 21: 68–72. https://doi.org/10.1007/s11676-010-0011-5

Wu S-J, Xu J-M, Li G-Y, Risto V, Lu Z-H, Li B-Q, Wang W (2011) Estimation on basic density and modulus of elasticity of eucalypt clones in Southern China using non-destructive methods. JTFS 23:51–56. https://www.jstor.org/stable/23616879

Yamashita K, Okada N, Fujiwara T (2007) Use of the pilodyn for estimating basic density and its applicability to density-based classifying of *Cryptomera japonica* green logs. Mokuzai Gakkaishi 53(2):72–81.

Spatiotemporal dynamics of termite infestation in urban *Araucaria cunninghamii*: A case study in Taipei

*Cheng-Jung Lin**
Senior Researcher
Forest Products Utilization Division, Taiwan Forestry Research Institute
53 Nanhai Rd., Taipei 10066, Taiwan
zzlin@tfri.gov.tw

Bing-Syun Peng
Associate Researcher
Chiayi Research Center, Taiwan Forestry Research Institute
53 Nanhai Rd., Taipei 10066, Taiwan
bspeng@tfri.gov.tw

*Po-Heng Lin**
Assistant Researcher
Forest Products Utilization Division, Taiwan Forestry Research Institute
53 Nanhai Rd., Taipei 10066, Taiwan
afarmer@tfri.gov.tw

Chieh-Yu Chang
Assistant
Forest Products Utilization Division, Taiwan Forestry Research Institute
53 Nanhai Rd., Taipei 10066, Taiwan
cychang@tfri.gov.tw

(Received 19 March 2025)

Abstract. Termite feeding on the trunk cross-sections of *Araucaria cunninghamii* in Taipei, Taiwan, was examined using 2D stress wave imaging (FAKOPP system). Six inspections were conducted at 2-month intervals to monitor six trees. 2D cross-sectional stress wave velocity images were created at different heights (30–180 cm) to assess termite feeding damage. Termite damage, quantified as damage ratio (DR, %), ranged from 0% to 55% across different trees and heights, with maximum increases of up to 21% in DR observed over a 2-month period. In the investigated cases, termites primarily fed on the interior of tree trunks. The feeding pattern typically extended longitudinally, then proceeded in a tangential (circular) direction, and finally moved radially. This study identified *Coptotermes formosanus* as a key termite species involved. Typically, termites prioritized feeding on the earlywood over the latewood. The periods with the highest damage to trunk cross-sections due to termite feeding occurred during seasons with higher temperatures and relative humidity. Damage initially appeared near the heartwood or the boundary between the heartwood and sapwood, gradually expanding into the heartwood. Of the six trees monitored for the full study duration (after one tree was felled for validation), subterranean termite tunneling was observed as the primary pattern in three trees, while aerial swarm invasion patterns were inferred for two trees based on initial damage locations.

Keywords: Termite; Feeding behavior;Visual tree assessment; Nondestructive technique; *Coptotermes formosanus; Araucaria cunninghamii*

Introduction

Termites are integral to ecosystems, contributing to processes like nutrient cycling and decomposition (Myer and Forschler 2018), but certain species, particularly wood-feeders, simultaneously present potential threats to forest ecology and trees. Certain termite species, such as those belonging to the genus *Coptotermes*, are notorious for their wood-feeding habits, with a particular inclination for devouring the interiors of living trees, posing significant risks to their structural integrity. This propensity poses a substantial risk to both the structural stability and overall health of trees. Therefore, a comprehensive exploration of termite behavior and their potential tree-related damage is important for assessing risk.

In Taiwan, hoop pine (*Araucaria cunninghamii* Aiton ex D. Don.) is commonly planted as an ornamental tree in parks,

* Corresponding author

roadsides, and campuses throughout Taipei due to its aesthetic appeal and adaptability to urban environments. While multiple tree species in Taipei are susceptible to termite attack, recent incidents involving *A. cunninghamii* on the study campus highlighted a specific vulnerability that warranted focused investigation. Recent research has underscored the susceptibility of hoop pines to termite-induced damage, often culminating in unanticipated tree collapse (Lin et al. 2016). Such collapses can pose significant threats to human safety and property, given that termite-infested trees frequently become unstable because of damage to their trunk bases and main stems. In Taiwan, termites from the *Coptotermes* genus, notably the Formosan subterranean termite (*Coptotermes formosanus* Shiraki), are recognized as major contributors to forest and tree deterioration (Liang et al. 2020). Surveys reveal that, following tree damage caused by typhoons, these termites target the heartwood of standing tree trunks, resulting in hollowing and structural impairment within the stem (Lai 2019).

The assessment and management of tree-related risks are critical for upholding the safety and well-being of forests and individual trees. In forest resource management, early detection and appraisal of potential hazards play a key role in averting damages and ensuring the long-term viability of forests. Consequently, the realms of tree risk assessment and management have acquired considerable importance. Heightened concerns about public safety and the preservation of urban trees have accentuated the need for the development and application of rapid, precise, and cost-effective technologies to identify decay and other structural vulnerabilities within trees (Li et al. 2022; Martiansyah et al. 2022).

While visual tree assessment has long been a valuable tool involving the visual inspection of external tree defects, instrumental measurement of internal flaws, and assessment of wood strength, it often falls short in detecting termite-induced damage within tree trunks, where these insects primarily operate. In response, non-destructive testing techniques employing 2D imaging methods have been developed for the assessment and examination of wooden materials. Acoustic techniques have proven highly effective for detecting and evaluating decay and voids within various tree trunks, offering a vital means of ensuring tree safety and health (Allison et al. 2020; Goh et al. 2018; Linhares et al. 2021; Soge et al. 2021). Stress wave testing, which detects internal defects by measuring the velocity of mechanical waves propagated through the trunk, has emerged as a powerful tool for assessing the internal condition of trees. Termite-damaged areas, containing internal voids or decayed wood, typically exhibit reduced stress wave velocity compared to sound wood, allowing for their detection and mapping (Lin et al. 2016; Wei et al. 2022). The non-invasive nature of stress wave and ultrasonic assessments makes them practical and feasible for tree inspections.

Selection of *A. cunninghamii* as the subject of this research arises from the discovery of termite infestation by *C. formosanus*, commonly referred to as the Formosan subterranean termite, within this tree species on the campus of a university in Taipei. The presence of termite colonies within these trees carries long-term implications. However, quantitative *in situ* monitoring of subterranean termite feeding in urban trees remains challenging (Thant et al. 2022), meaning that for these specific trees, the rate and extent of termite feeding remain unclear. To systematically monitor and manage these trees, a detailed program of inspections and analyses is indispensable. Our principal objective is to acquire an extensive understanding of termite invasion patterns, as well as the rates and patterns of damage inflicted by termites on the internal wood of *A. cunninghamii* trees. To achieve this objective, we monitored termite activity in *A. cunninghamii* using non-destructive 2D stress wave imaging at multiple time points (six inspections at 2-month intervals) and tree heights (30–180 cm). This approach allowed us to detect and assess termite feeding behavior, shedding light on termite invasion patterns and the extent of their internal damage. The outcomes of this research endeavor will provide invaluable insights for tree risk assessment and management, while also contributing to strategies for the prevention and control of termite infestations

Materials and methods

Materials

This study was conducted within the Gongguan Campus of National Taiwan Normal University (NTNU, 25.00790°N, 121.53711°E), in Taipei, Taiwan. The background for this research stems from an incident that occurred in April 2022 when an *A. cunninghamii* tree collapsed on the campus. Subsequent examination of the internal tree trunk revealed damage caused by the Formosan subterranean termite (*C. formosanus*). To ensure the safety of all *A. cunninghamii* trees on the campus, a comprehensive survey was carried out in the immediate vicinity (within a 50-m radius) of the fallen tree to identify trees that might have been affected by termite infestation. This survey involved visual inspection for external signs of termite activity (e.g., mud tubes, damaged bark) and preliminary stress wave screening on approximately 15 *A. cunninghamii* trees in this zone. The initial goal was to establish a tree risk monitoring and management system. Selection criteria included: (1) proximity

to the original collapsed tree, (2) presence of preliminary signs of potential termite activity or internal defects suggestive of infestation based on the initial screening, and (3) accessibility for repeated measurements. The selected trees represented a range of conditions observed in the affected area. Given the presence of termite populations in the region and their potential for ongoing harm to the trees, it became necessary to conduct regular inspections of these trees to gain a deeper understanding of the invasion patterns and rates of internal termite damage.

Stress wave tomography and damage assessment

To evaluate the extent of termite feeding damage, we conducted experimental inspections on all the trees in the vicinity of the fallen tree. We selected six *A. cunninghamii* trees for long-term monitoring of termite feeding damage. Trees ranged in age from 40 to 50 years and had a breast height diameter ranging from approximately 40 to 55 cm. Considering that termite infestations primarily occur inside trees, we employed stress wave detection methods (Figure 1). Tests were conducted in June 2022, August 2022, October 2022, December 2022, February 2023, and April 2023, to examine the cross-sectional trunk areas at different height levels and assess the extent of termite damage within the trees.

We employed a FAKOPP stress wave timer (FAKOPP Enterprise, Hungary) equipped with eight probes. Measurements were taken at eight equidistant points along the circumference of the tree trunk approximately 30, 60, 90, 120, 150, and 180 cm in height from the ground along the tree trunk, targeting sections with visible or suspected signs of termite infestation (e.g., mud tubes on bark, flight holes, galleries exposed after minimal bark removal, or hollow sounds upon tapping) and areas suspected of containing decay cavities based on preliminary visual assessments or an initial campus-wide survey.

The sensors were oriented perpendicular to the longitudinal axis of the tree trunk to measure the propagation time and stress wave velocity. We conducted the strikes in sequential order at positions 1 to 8, repeating the measurements five times to obtain an average value. Throughout the testing process, we acquired a complete data matrix for the transverse stress wave detection area of each tree. Each probe act sequentially as a transmitter while the remaining seven acted as receivers. The number of unique pairwise paths for stress wave propagation was calculated as $N(N-1)/2$, where N is the number of probes. Thus, eight probes resulted in $(8\times7)/2=28$ independent propagation time measurements at each test location. The propagation path of the transverse stress wave was determined by utilizing the eight probes with both receiving and transmitting capabilities.

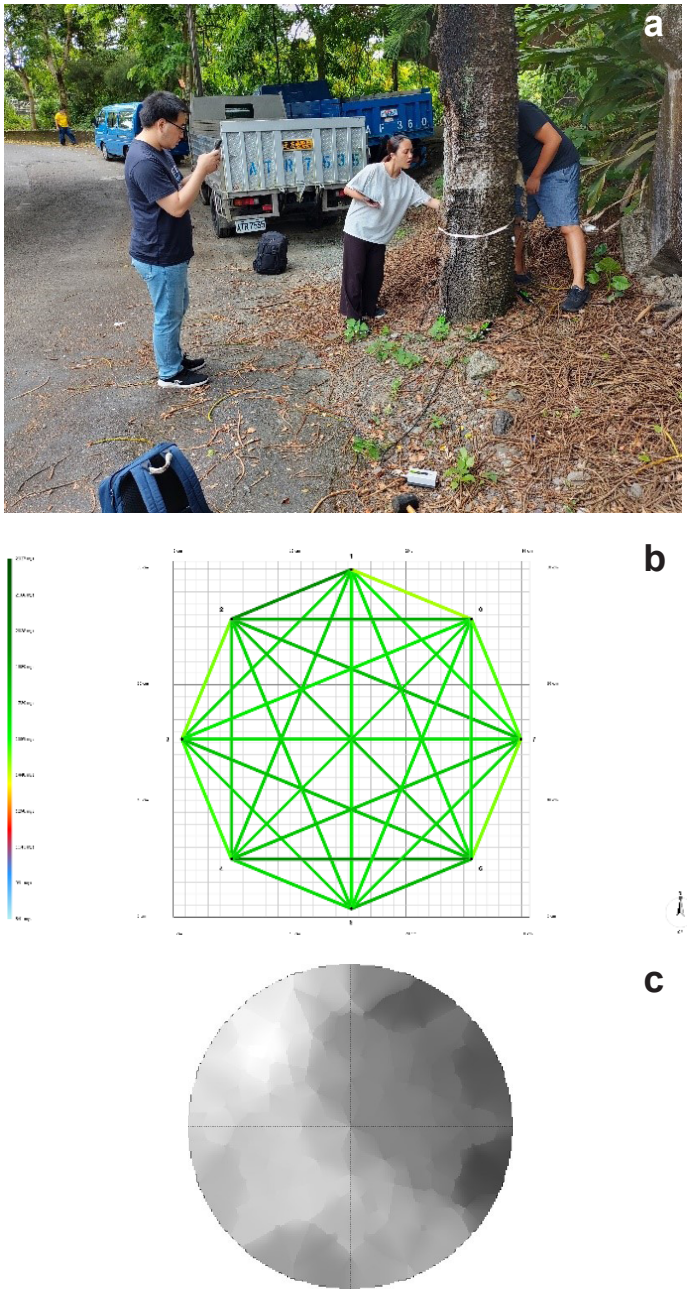

Figure 1. Acoustic tomography test on *A. cunninghamia* trees using a Fakopp stress wave tomographic tool showing (a) the sensor arrangement; (b) the paths of acoustic measurement; and (c) a grayscale image of a stress wave tomogram.

Data analyses

The cross-sections and the distances between sensors were measured with a tape measure. The software approximated the circular cross-sectional shape as the standard. All instruments were operated according to their respective operational manuals, with data computation and analysis performed using the ArborSonic software. Although raw propagation times were collected, the software internally used these times along with

precise path distances (derived from the input geometry) to generate velocity values. Concurrently, the influence of probe spacing was also handled internally by the software; thus, velocity values were inherently normalized by the software.

First, following the completion of stress wave acoustic measurements, we employed ArborSonic software to generate transverse stress wave 2D images for each cross-section. Each 2D stress wave image was accompanied by a color scale that represented the measured stress wave velocity. The scale was calibrated separately for each sample tree so that its endpoints corresponded to the maximum and minimum velocities recorded during that particular test. Secondly, we used the ArborSonic software program to generate stress wave velocity 2D images of the cross-sections, which were calculated based on the raw, unadjusted, and unnormalized propagation times obtained during the experiments.

The stress wave velocity corresponding to each pixel in the images was quantitively used to assess stress wave velocity in 2 D images. Visualization and transformation of the 2D cross-sectional images were used to generate stress wave velocity distribution maps for different positions. Each 2D stress wave image was accompanied by a color scale that represented the measured stress wave velocity. The scale was calibrated separately for each sample tree so that the endpoints corresponded to the maximum and minimum velocities recorded during that particular test. Finally, we rationalized and corrected the damage rate of termite feeding on the trunk cross-sections based on the 2D images. According to the operating manual, the damage ratio (DR, %) was operated such that when the relative velocity decrease was 0, 5, 10, 15, 20, 30, 40, 50, and >50%, the estimated decayed area was 0, 0, 0, 0–10, 10–20, 10–20, 20–40, 30–50, and >50% by ArborSonic software, respectively (FAKOPP 2020).

Gross errors or noisy signals were managed according to the operator manual guidelines, and re-measurements were performed at that sensor point. Multiple stress wave measurements were repeated at each probe to collect five data points, which were then averaged to provide a mean propagation time for each path before velocity calculation. The variability of these repeated measurements was monitored during collection to ensure signal stability.

After integrating the stress wave characteristic information and 2D images of each cross-section, we conducted sampling using an increment borer to extract 5 mm diameter increment cores from the bark to the pith of each tree trunk. The cores were assessed for wood damage and the holes were examined using an endoscope (model TON-666LNP, resolution 370,000 pixels, with built-in LED illumination, inspection depth up to 115 cm) for signs of wood decay, damage, termites, or termite mud tunnels. This inspection served as a basis for comparison and adjustment against the stress wave velocity 2D images.

Ultimately, we chose six *A. cunninghamii* trees that had experienced termite feeding damage to be monitored over the long term. Tree No. 36 was felled in September 2022, prior to the end of the test. This tree was chosen for felling because internal stress wave assessments showed that it had consistently high and widespread internal damage and was identified as a high-risk tree by campus management, necessitating its removal (Figure 2). Finally, based on the results of the aforementioned experiments, we evaluated and summarized the patterns of termite feeding damage inside the trees. Using the adjusted termite feeding damage rates on cross-sections, we provided a reference for tree inspection and risk management.

Results and discussion

Temporal patterns of termite activity

The August 2023 examinations utilizing increment borers and endoscopic tools unveiled ongoing termite activity within Trees 29 and 32, implying that termites were actively feeding on the wood within these trees. Furthermore, although termites were not observed in Trees 28, 34, and 43, traces of termite tunneling soil, such as termite galleries partially filled with soil and frass (termite tunneling soil), were detected. These findings suggested that termites had previously been active within these trees but had gradually vacated during our inspections.

Stress wave testing of Tree 29 yielded lateral stress wave 2D images, with specific findings presented in Table 1. There was a progressive manifestation of termite activity within the tree trunk from June 2022 to April 2023, primarily originating from the base of the tree below ground level and advancing upward. Damage levels within trunk cross-sections at various heights ranged from 5% to 20%, exhibiting a gradual upward trend. Particularly noteworthy was the period between February 2023 and April 2023, where damage rates surged from 13% to 20%, representing a 7% increase in 2 months. In contrast, damage rates increased at a slower pace during other periods.

Spatial dynamic of termite damage

Tree 28 exhibited an upward termite infestation pattern, likely originating from subterranean activity, with DR ranging from 3% to 17% in the lower trunk sections (Table 2). The primary increase in damage (from 11% to 17% at 30 cm) occurred between June and August 2022. Live termites were not detected by August 2023.

Figure 2. Cross-sections of *A. cunninghamia* tree (No. 36) damaged by termite infestation.

Lateral stress wave 2D images for Tree 32 showed a gradual consumption of the tree trunk by termites (Table 3), likely originating from the base of the tree within the soil below ground level and extending upwards. Consequently, the damage rate in the trunk cross-sections near the base of the tree exceeded that at higher cross-sections. Overall, damage rates within the trunk cross-sections ranged widely, from 10% to 55%. The most substantial change transpired between August 2022 and October 2022, as the damage rate more than doubled from 16% to 37%. Thereafter, damage rates stabilized, suggesting that termites primarily consume sections that had already sustained damage.

Vertical and radial patterns of termite infestation

The stress wave 2D images for tree numbers 28, 29, and 32 consistently demonstrated termite infestation commencing near the base, close to ground level, and subsequently extending upwards. This attack often commenced in the heartwood or at the heart/sap boundary before progressively infiltrating the heartwood region.

Stress wave 2D images for Tree 34 showed gradual termite infestation within the tree trunk where damage was initially observed or was more concentrated in the upper portions of the assessed trunk sections and appeared to extend downwards towards the base (Table 4). Overall, damage rates within the trunk cross-sections varied from 7% to 29%. The most notable change occurred between August and October 2022, with the damage rate escalating from 23% to 31%. Subsequently, there was a modest rise (ranging from 2% to 5%) in damage rates across various trunk cross-sections during later inspection periods.

In line with inspection results, termite infestation initially emerged 1.5 m above the ground, infiltrating the trunk cross-section from the outer side at the juncture of the sapwood and

Table 1. Transversal stress wave velocities and 2D imaging of *A. cunninghamii* (Tree No. 29) 30 cm above ground, based on six time-series sampling points collected from June 2022 to April 2023.

No	Tree height (cm)	Velocity (m/sec)	June 2022	August 2022	October 2022	December 2022	February 2023	April 2023
29	30	Max	1264	1214	1289	1312	1320	1261
		Min	967	928	986	1004	1009	964
2D			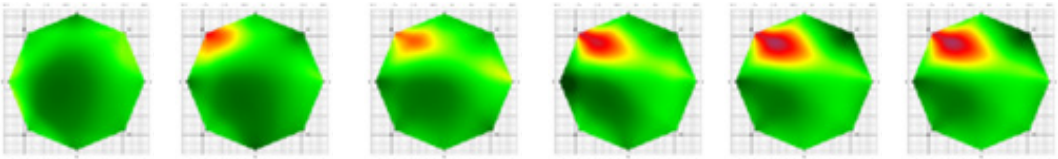					
DR (%)			0	5	6	10	13	20

DR, damage ratio (%)

Table 2. Transversal stress wave velocities and 2D imaging of *A. cunninghamii* (Tree No. 28) 30, 45 and 60 cm above the ground, based on six time-series sampling points collected from June 2022 to April 2023.

No	Tree height (cm)	Velocity (m/sec)	June 2022	August 2022	October 2022	December 2022	February 2023	April 2023
28	60	Max	1384	1337	1342	1376	1379	1342
		Min	1059	1023	1026	1052	1055	1026
2D			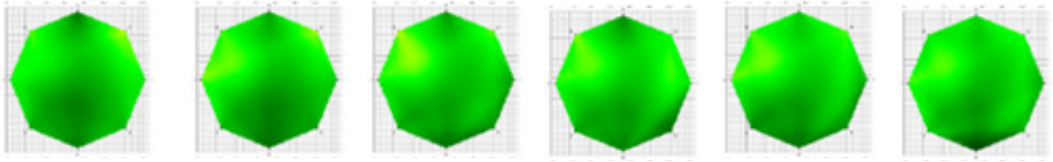					
DR (%)			0	0	0	0	0	0
28	45	Max	1331	1344	1294	1344	1314	1272
		Min	1018	1028	989	1028	1005	973
2D			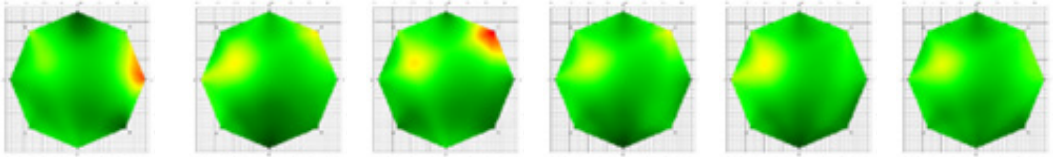					
DR (%)			3	3	4	4	4	4
28	30	Max	1195	1303	1252	1266	1308	1235
		Min	914	997	958	968	1000	945
2D			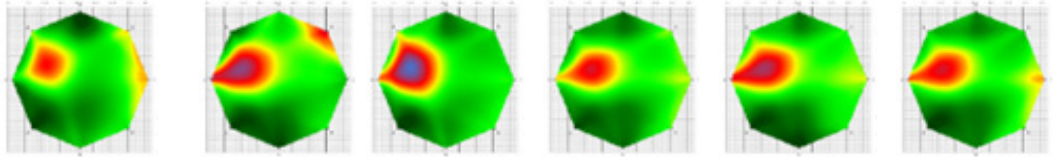					
DR(%)			11	17	17	17	17	17

DR, damage ratio (%)

heartwood, and gradually progressing towards the base and heartwood. The trunk sections 90 cm and 120 cm above the ground sustained the most substantial impact.

Stress wave 2D images for Tree 43 revealed gradual termite infestation within the tree trunk, potentially emanating from the upper sections and descending towards the base (Table 5). Overall, damage rates within the trunk cross-sections ranged from 7% to 35%. The most remarkable transition occurred between February and April 2023, with damage rates rising from 14% to 19%. Rates ranging from 2% to 4% were

Table 3. Transversal stress wave velocities and 2D imaging of *A. cunninghamii* (Tree No. 32) 30, 60, 90, 120 and 150 cm, based on six time-series sampling points collected from June 2022 to April 2023.

No	Tree height(cm)	Velocity (m/sec)	June 2022	August 2022	October 2022	December 2022	February 2023	April 2023
32	150	Max	1643	1556	1472	1571	1640	1542
		Min	1257	1190	1126	1201	1254	1180
2D			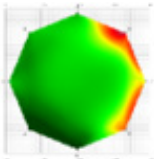	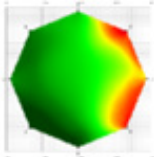	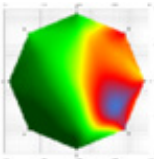	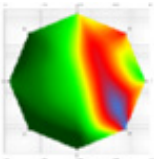	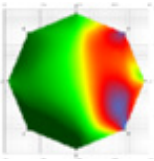	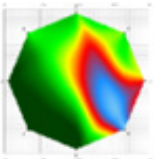
DR (%)			10	16	37	37	37	37
32	120	Max	1258	1158	1105	1157	1131	1109
		Min	962	886	845	885	865	848
2D			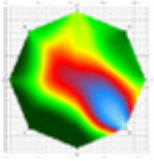	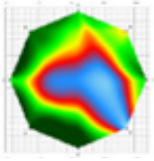	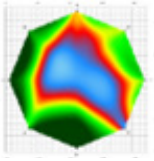	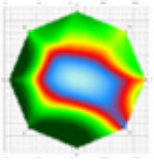	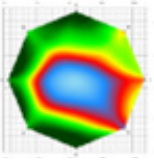	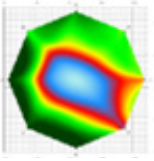
DR (%)			40	48	52	52	52	52
32	90	Max	1366	1198	1221	1236	1182	1180
		Min	1045	916	933	945	904	902
2D			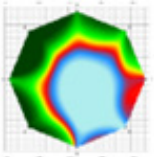	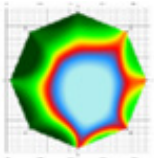	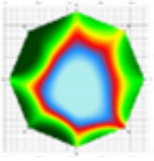	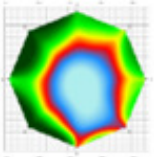	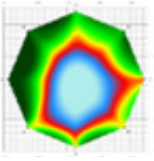	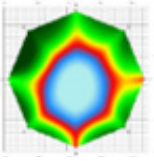
DR (%)			54	54	54	54	54	54
32	60	Max	1406	1325	1170	1276	1384	1315
		Min	1076	1013	895	976	1059	1005
2D			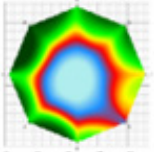	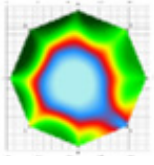	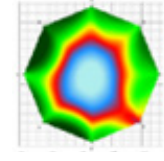	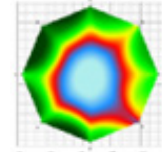	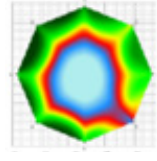	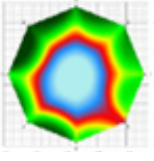
DR (%)			54	54	54	54	54	54
32	30	Max	1042	1002	1027	993	1026	996
		Min	797	766	785	760	785	762
2D			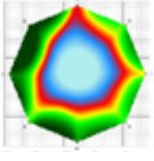	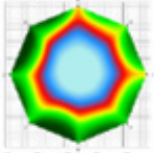	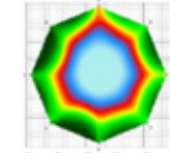	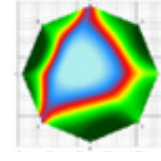	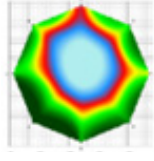	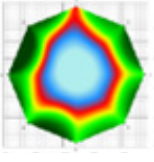
DR (%)			55	55	55	55	55	55

DR, damage ratio (%)

Table 4. Transversal stress wave velocities and 2D imaging of *A. cunninghamii* (Tree No. 34) 30, 60, 90, 120 and 150 cm, based on six time-series sampling points collected from June 2022 to April 2023.

No	Tree height (cm)	Velocity (m/sec)	June 2022	August 2022	October 2022	December 2022	February 2023	April 2023
34	150	Max	1571	1548	1519	1486	1509	1563
		Min	1202	1184	1161	1136	1154	1195
2D			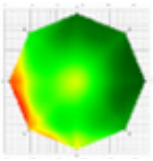	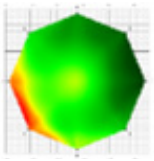	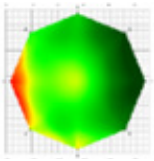	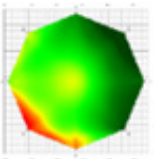	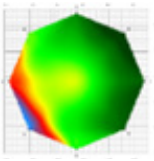	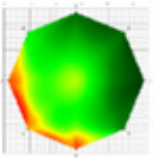
DR (%)			7	8	8	8	13	13
34	120	Max	1459	1440	1449	1387	1408	1429
		Min	1116	1101	1108	1061	1076	1093
2D			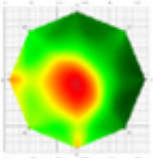	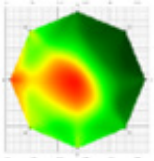	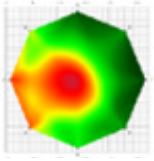	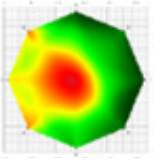	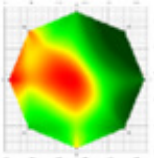	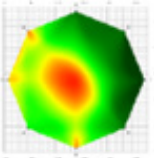
DR (%)			21	23	31	31	31	31
34	90	Max	1373	1452	1440	1438	1453	1443
		Min	1050	1110	1101	1099	1111	1104
2D			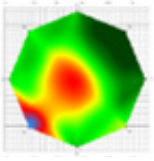	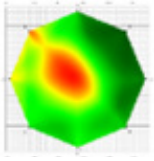	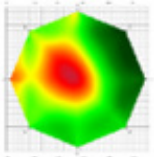	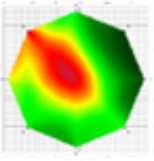	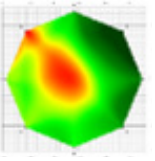	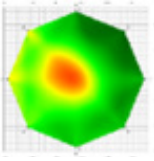
DR (%)			25	25	25	29	29	29
34	60	Max	1381	1434	1417	1416	1403	1392
		Min	1056	1097	1083	1083	1073	1064
2D			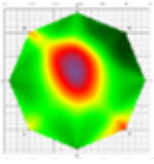	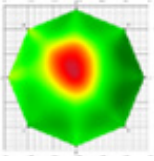	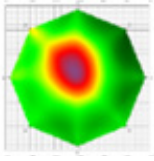	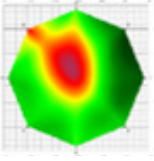	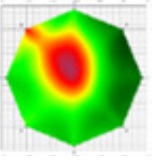	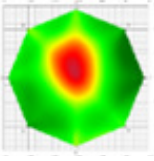
DR (%)			20	20	20	24	24	24
34	30	Max	1352	1397	1400	1362	1307	1335
		Min	1034	1068	1071	1041	999	1021
2D			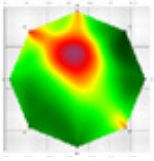	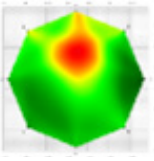	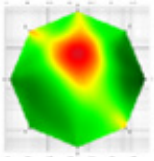	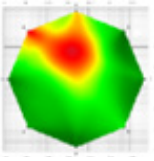	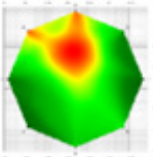	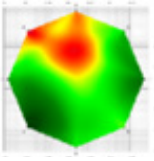
DR (%)			17	17	17	22	22	24

DR, damage ratio (%)

Table 5. Transversal stress wave velocities and 2D imaging of *A. cunninghamii* (Tree No. 43) 30, 60, 90, 120, 150 and 180 cm, based on six time-series sampling points collected from June 2022 to April 2023.

No	Tree height (cm)	Velocity (m/sec)	June 2022	August 2022	October 2022	December 2022	February 2023	April 2023
43	180	Max	1505	1513	1487	1497	1497	1475
		Min	1151	1157	1137	1144	1145	1128
2D			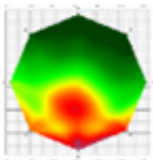	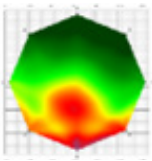	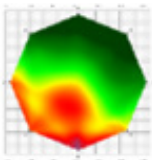	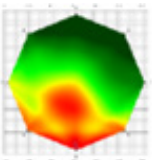	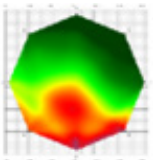	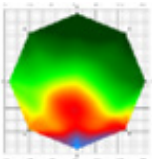
DR (%)			31	33	35	35	35	35
43	150	Max	1458	1526	1468	1537	1459	1466
		Min	1115	1167	1122	1176	1116	1121
2D			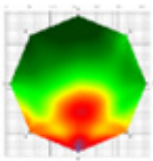	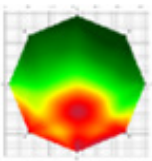	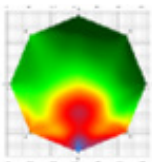	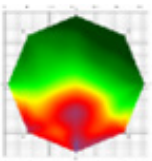	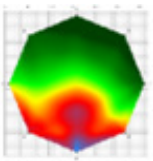	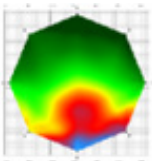
DR (%)			29	31	31	35	35	35
43	120	Max	1416	1432	1376	1428	1397	1348
		Min	1083	1095	1052	1092	1069	1031
2D			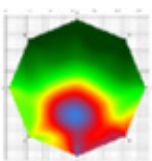	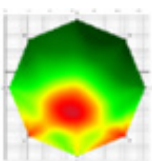	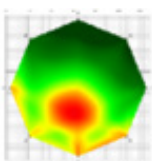	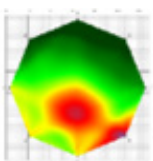	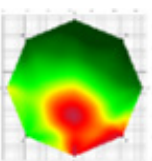	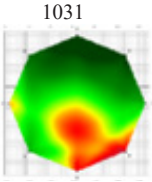
DR (%)			25	25	25	28	28	28
43	90	Max	1189	1228	1267	1373	1245	1326
		Min	909	939	969	1050	952	1014
2D			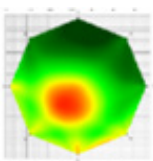	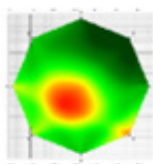	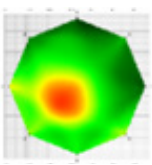	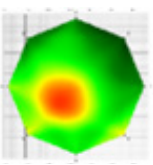	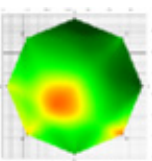	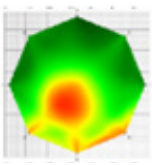
DR (%)			14	14	14	14	14	19
43	60	Max	1373	1370	1334	1384	1323	1358
		Min	1050	1048	1020	1058	1012	1038
2D			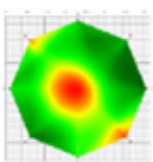	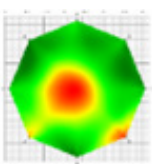	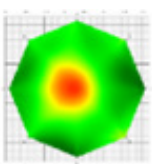	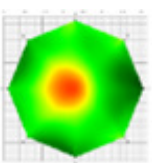	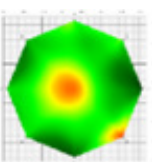	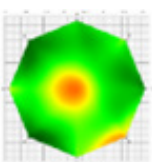
DR (%)			11	11	11	11	11	11
43	30	Max	1273	1245	1259	1302	1265	1273
		Min	974	952	963	996	968	973
2D			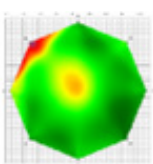	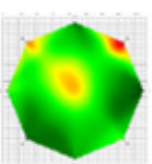	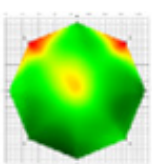	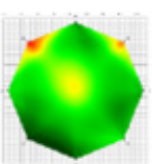	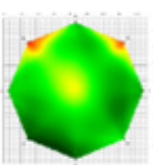	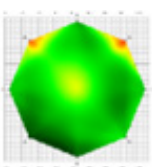
DR (%)			7	7	7	7	7	7

DR, damage ratio (%)

observed across various trunk cross-sections during different inspection periods.

Termite infestation initially occurred at 1.8 m above the ground. Trunk sections 180 cm and 150 cm above the ground experienced the most substantial impact, with higher damage rates in the upper trunk portions compared to the base.

Stress wave 2D images of Tree 36 were based on the inspections conducted in June and August 2022, before this tree was felled in September 2022 (Table 6). A visual examination was performed to assess the extent of termite damage across trunk cross-sections at varying heights (Figure 2). Visual inspection of the felled tree cross-sections allowed for detailed characterization and quantitative assessment of termite-induced damage patterns and rates (Table 6), which served to validate and calibrate the interpretation of the non-destructive stress wave data.

Visual observations indicated that termite feeding patterns involved longitudinal extension from the base upwards, followed by a tangential shift towards the earlywood, and subsequent radial movement. Termite movement patterns tended to be random, with no particular orientation. Notably, earlywood segments were the prime target of termite activity, with earlywood exhibiting more pronounced damage compared to latewood.

Termite feeding areas in Tree 36 were circular, point-like, or clustered in regions that gradually expanded and concentrated within the trunk interior. Lateral stress wave 2D images primarily detected stress wave connection signals outside the feeding areas, which served as effective evaluation indicators. Termite feeding areas were less frequent within the sapwood region and primarily manifested within the heartwood and the boundary zone between the earlywood and latewood, extending deeper into the heartwood interior. Examination of trunk cross-sections from the felled tree highlighted a noticeable water staining phenomenon in the wood surrounding the damaged areas due to termite-induced damage.

Termites in Taiwan, including species such as *Odontotermes formosanus* (Shiraki), *C. formosanus*, and *Coptotermes gestroi* (Wasmann), are recognized as significant forest pests (Lee et al. 2011) and are known to construct mud tubes on tree bark and cause feeding damage to the living tree trunk. It is important to distinguish their feeding behaviors. For instance, *O. formosanus* primarily constructs mud tubes on the surface of tree trunks and feeds on the tree bark covered by these tubes, without invading the tree interior. In contrast, species like *C. formosanus*, identified in our study, are known to cause

Table 6. Transversal stress wave velocities and 2D imaging of *A. cunninghamii* (Tree No. 36) 30, 60, 90, 120, 150 and 180 cm, based on six time-series sampling points collected from June 2022 to August 2022.

No	Tree height (cm)	Velocity (m/sec)	June 2022	August 2022
36	30	Max	1452	1434
		Min	1110	1097
2D			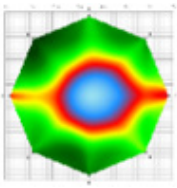	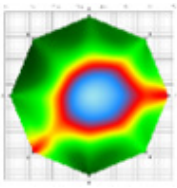
DR (%)			38	38
36	60	Max	1520	1443
		Min	1162	1104
2D			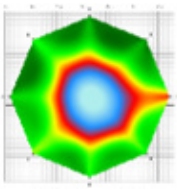	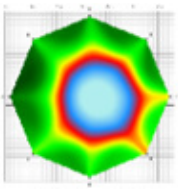
DR (%)			37	41
36	90	Max	1463	1427
		Min	1119	1091
2D			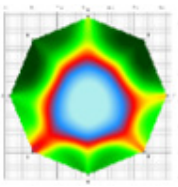	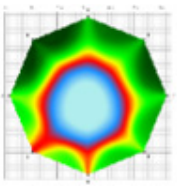
DR (%)			47	47
36	120	Max	1447	1292
		Min	1106	988
2D			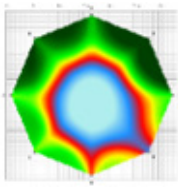	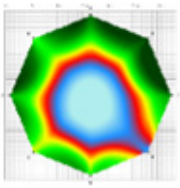
DR (%)			51	51
36	150	Max	1563	1438
		Min	1195	1100
2D			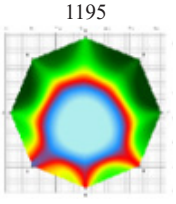	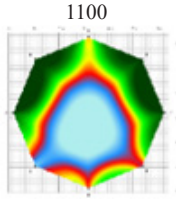
DR (%)			53	56
36	180	Max	1557	1456
		Min	1191	1114
2D			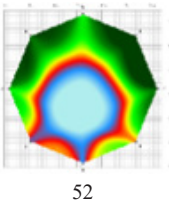	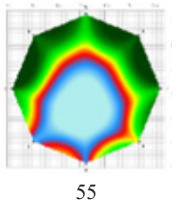
DR (%)			52	55

DR, damage ratio (%)

extensive internal damage. Chiu et al. (2020) observed that trees were primarily affected by *O. formosanus*, with varying infestation rates among different tree species associated with distinct tree characteristics. This highlights the potential for different termite species to dominate in different contexts or tree species, exhibiting varied impacts.

The aggressive feeding behavior of *Coptotermes* species significantly impacts tree health. For instance, mud tubes built by *C. gestroi* can extend as high as 6.35 m above ground on dead trunks of Luchu pine (*Pinus luchuensis* Mayr.), with 16.0% of the cross-sectional areas of the trunk being damaged by feeding. Lin et al. (2021) suggested that the feeding damage patterns of *C. gestroi* and *C. formosanus* are similar, as they tunnel into the trunk and base of trees, increasing their susceptibility to collapse. Furthermore, *C. gestroi* may tunnel into the tough bark and sapwood of trees, potentially leading to circumferential debarking and subsequent tree mortality (Chouvenc and Foley 2018). As the extent of damage caused by termite feeding varies among trees, this may have implications for the community structure within forest ecosystems (Evans et al. 2019).

This study primarily employed 2D stress wave imaging techniques to assess the extent of termite-induced damage within the trunks of six trees. While using repeated stress wave tomography on living trees differs from previous methods that mainly relied on visual inspection of tree exteriors or observations of dead trees to investigate termites, the literature indicates that variations in termite species and environmental conditions can lead to different patterns of termite feeding (Scholtz et al. 2021).

Evans et al. (2019) observed that a higher occurrence of termites and the resulting damage to trees was associated with warmer and more humid climates. Other termite species, such as *Paraneotermes simplicicornis* (Banks), *Heterotermes aureus* (Snyder), and *C. formosanus*, exhibited increased rates of wood degradation with rising temperatures (Tai 2002). Therefore, warmer climates are often associated with higher termite frequencies and increased foraging frequency, a trend consistent with the findings of Chiu et al. (2015), who noted a significant positive correlation between temperature and termite foraging activity.

Our results showed that the damage rate caused by termite infestation was highest in tree specimens No. 28, 32, and 34, and that it typically occurred between June and August, which corresponded to the hottest season of the year, when termites would be most active. Taipei City experiences the highest average temperatures between June and September, ranging from approximately 28.3°C to 30.1°C, with relative humidities ranging from 70.2% to 75.3%. This result aligns with previous research findings (Chiu et al. 2015).

However, the maximum decay cavity rate due to termite infestation in Tree 29 and 43 occurred between February and April when Taipei City experiences the highest average relative humidity, approximately 74.9% to 77.8%, and temperatures ranging from 17.2 to 22.5 °C. This corresponds to the season immediately following the end of winter when temperatures begin to rise, and relative humidity is higher, potentially stimulating termite foraging activity. Therefore, the periods of higher termite infestation rates observed in this study mainly coincided with seasons characterized by higher temperatures and relative humidity, rather than during the colder winter months.

The pathways and methods of termite infestation in residential buildings can be categorized into “trail invasion” or “swarming invasion” (Yagi 2018). In trail invasion (by subterranean termite mud tunnels), termites nest in dead trees, standing trees, or underground, extend their trails to expand their damage range and gain access to buildings in ground contact. Trail invasion is a common mode of entry, where termite trails extend vertically from the ground upward. Swarming invasion (by aerial termite swarm flight) begins with winged termites swarming in pairs. They initially select damp nesting sites and later move to locations with relatively stable humidity, temperature, and a steady food supply (King and Spink 1969). This method may involve selecting trees, especially those with decayed portions, as these areas are conducive to termite concealment.

In this study, we observed that trees damaged by termites primarily experienced internal feeding within their trunks. Based on the initial damage locations and progression patterns, we inferred these two invasion modes in our study trees. The classification of termite infestation pathways into trail invasion (subterranean) or swarm invasion (aerial) in this study was primarily inferred based on the following criteria: (1) The primary vertical location of initial and most severe damage, damage concentrated at the base of the tree (e.g., 30 cm height) and progressing upwards, was indicative of subterranean trail invasion. Conversely, damage initiated at higher points on the trunk (e.g., >1m) and progressing downwards or localized in upper sections was considered indicative of aerial swarm invasion, potentially exploiting entry points like branch wounds. (2) Presence of external signs: while not always definitive, including visible mud tubes extending from the soil up the base

of the trunk supported classification as trail invasion. Direct evidence of aerial nests was not found, so swarm invasion was largely inferred from damage patterns inconsistent with a solely subterranean origin. The feeding pattern for subterranean trail invasions typically involved vertical extension from the tree base, followed predominantly by a circular direction, and finally, a radial path. This mode of infestation was often initiated by termite trails below the soil, initially invading the base of the tree and then progressing upward, classifying it as a subterranean termite trail invasion.

Another mode of infestation occurred when termites, after swarming, initially invaded a specific height on the tree and then moved downward towards the base. This mode was associated with alates and was categorized as an above-ground termite swarm invasion pattern.

During the inspection in August 2023, it was observed that Trees 29 and 32 still exhibited live termites, while Trees 28, 34, and 43 no longer showed signs of live termites. This phenomenon of termite disappearance from Trees 28, 34, 43 by August 2023 may have been influenced by physical disturbances during the inspection activities (e.g., drilling, sensor placement) or other environmental factors, potentially causing termite populations to vacate these specific locations between inspections.

The infestation mode for Trees 34 and 43 involved a termite swarm invasion pattern, which could make them susceptible to leaving the tree due to environmental disruptions. Whether the termite populations will return to these trees for feeding in the future requires further tracking and investigation.

Laboratory consumption rates of *Reticulitermes flaviceps* Oshima and *Nasutitermes parvonasutus* Light have been investigated on four different wood species (Tai 2002). Consumption rates ranged between 2.35 and 6.38 milligrams per day. Consumption rate of wood is influenced by several factors, including tree species, wood moisture content, termite colony condition, colony size, temperature, and humidity. It is noteworthy that these two termite species exhibited higher consumption rates on less dense wood species (Tai 2002).

Morales-Ramos and Rojas (2001) reported that laboratory feeding rate of the Formosan subterranean termite (*C. formosanus*) on Parana pine (*Araucaria angustifolia*), a highly preferred wood species, was approximately 0.49 milligrams per day. This rate was much lower than the rate reported by Tai (2002). In addition, a report by Jasmi and Ahmad (2011) mentions that hoop pines (*A. cunninghamii*), which have lower wood density, were attacked by *Coptotermes curvignathus* Holmgren, resulting in a damage rate of 15.9%. This accounted for 74% of the overall termite infestation rate (Jasmi and Ahmad 2011).

Secondary metabolites produced during wood decomposition may also influence interactions between termites and the wood. Therefore, variations in wood density and the production of secondary metabolites among different tree species result in different termite species showing preferences and ease of feeding on specific types of wood (Lai 2019).

Our study focused on hoop pine, *A. cunninghamii*, which is characterized by lower density, and we found that termites preferred less dense earlywood over latewood. Termites also initially targeted the sapwood/heartwood boundary. This behavior may be influenced by the secondary metabolites produced by living sapwood in the trees. Notably, termites were observed in our study to less frequently damage the sapwood region. Sapwood typically has higher moisture content, different chemical composition (e.g., fewer extractives, more starches) and is physiologically more active compared to heartwood (Li et al. 2019). These factors, or the proximity of sapwood to the external environment, might influence termite preference. Consequently, termites primarily consumed and extended their damage from the boundary between the sapwood and heartwood or the heartwood region, gradually progressing further into the heartwood.

The concept of tree defense known as the compartmentalization of decay in trees (CODIT) model, describes a self-protective system within trees where four conceptual zones—referred to as "reaction zones"—develop inside the wood to isolate and limit the spread of decay or injury (Morris et al. 2016; Pearce and Rutherford 1981; Shigo 1984; Smith 2020). In the first stage of the defense mechanism, physiological changes occur within the wood at Zones 1 (longitudinal), 2 (radial), and 3 (tangential). The final and strongest defense mechanism is the barrier zone produced by the formation of new tissue (Dunster et al. 2013). Typically, the direction in which decay in wood is most likely to expand follows a pattern of longitudinal first, then radial, and finally tangential. Visual inspection confirmed the localized internal decay zones observed in our acoustic data

In this research case, termites initially fed longitudinally, primarily along the tangential earlywood, and finally spread radially. This difference in feeding behavior compared to typical fungal decay spread patterns described by CODIT may be attributed to distinctions between active termite excavation and fungal decay processes. However, darker wood stains were observed near the wood surface affected by termite feeding

damage in the felled Tree 36 and noted in some endoscopic views. Wounding and subsequent microbial colonization, even if initiated by termites, can trigger CODIT responses in trees (Yatsko et al. 2024). This staining could therefore potentially represent a physiological response, such as the formation of a reaction zone (Wall 3 or even Wall 4, if cambial activity is involved) to internal wood damage and associated microbial activity caused or facilitated by termite feeding. Whether this observed staining fully aligns with defined CODIT walls would require further histological and chemical investigation for confirmation. It is important to note that while termite galleries represent a direct removal of wood, any associated staining or discoloration patterns would be the tree response to wounding and invasion by opportunistic microorganisms.

The generalizability of our findings may be constrained by the relatively small sample size. Although the trees were of a similar age range (40–50 years), variations in individual tree physiology, microclimate, and precise wood moisture content (which was not measured) could have influenced stress wave velocities and termite activity. We attempted to mitigate this by focusing on relative changes within individual trees. Furthermore, stress wave imaging possesses inherent resolution limitations. Previous research (Ostrovsky et al. 2017) indicated that stress wave technology only detected defects or decay when they occupied more than 2.8%–5% of the cross-sectional area, meaning that very small, isolated cavities or incipient decay might not be detected by this method. Accuracy can also be affected if the software does not adequately account for irregular trunk geometries. Species level identification of termite species was not possible for some trees where only remnant damage was present. Finally, the classification of infestation pathways was largely inferred from damage patterns rather than direct observation of alate colonization or extensive subterranean tunneling.

Conclusions

C. formosanus infested urban *A. cunninghamii* trees through both subterranean tunneling and aerial swarm invasions. Termite feeding damage was primarily concentrated in the heartwood, progressing longitudinally before moving tangentially through the preferred earlywood and then radially. Damage rates increased most substantially during warmer, humid seasons, with observed increases as high as 21% over a 2-month period. These findings demonstrate the value of repeated non-destructive stress wave imaging for monitoring the spatiotemporal dynamics of termite infestations, which is crucial for risk assessment and management of urban trees.

Acknowledgments

We would like to express our special thanks to National Taiwan Normal University for providing the project and financial support that enabled us to conduct the investigation on campus tree safety risks. The authors also gratefully acknowledge Professor Hou-Feng Li from National Chung Hsing University for his assistance in identifying the termite samples.

References

Allison RB, Wang X, Senalik CA (2020) Methods for nondestructive testing of urban trees. Forests 11(12):1341. https://doi.org/10.3390/f11121341.

Chiu CI, Li HF, Yeh HT, Tsai MJ (2015) Termite survey of Zelkova serrata plantations in moderate and low altitude areas of Taiwan. J Experiment Forest National Taiwan University 29(2):69–77. https://doi.org/10.6542/EFNTU.2015.29(2).1.

Chiu CI, Yeh HT, Yu JC, Li HF, Tsai MJ (2020) Termite occurrence on tree trunk affected by tree species, tree size, and its crown coverage. J Experiment Forest National Taiwan University 34(1):15–24. https://doi.org/10.6542/EFNTU.202003_34(1).0002.

Chouvenc T, Foley JR (2018) *Coptotermes gestroi* (Wasmann) (Blattodea [Isoptera]: Rhinotermitidae), a threat to the Southeastern Florida urban tree canopy. Fla Entomol 101(1):79–90. https://doi.org/10.1653/024.101.0115.

Dunster JA, Smiley ET, Matheny N, Lilly S (2013) Tree risk assessment manual. International Society of Arboriculture, Champaign. 198 p.

Evans TA, Forscher BT, Trettin CC (2019) Not just urban: The Formosan subterranean termites, *Coptotermes formosanus*, is invading forests in the Southeastern USA. Biol Invasions 21:1283–1294. https://doi.org/10.1007/s10530-018-1899-5.

FAKOPP (2020) Manual for the ArborSonic 3D Acoustic tomography. User's manual v6.5. 63pp.

Goh CL, Rahim RA, Rahiman MHF, Talib MTM, Tee ZC (2018) Sensing wood decay in standing trees: A review. Sensor Actuat A-Phys 269:276–282. https://doi.org/10.1016/j.sna.2017.11.038.

Jasmi AH, Ahmad AH (2011) Termite incidence on an Araucaria plantation forest in Teluk Bahang, Penang. Insects 2(4):469–474. https://doi.org/10.3390/insects2040469.

King EG Jr, Spink WT (1969) Foraging Galleries of the Formosan Subterranean Termite, *Coptotermes formosanus*, in Louisiana. Ann Entomol Soc Am 62:536–542. https://doi.org/10.1093/AESA/62.3.536.

Lee HF, Yeh HT, Wang YN, Tsai MJ (2011) Termite diversity and damage pattern in tropical botanical garden of Taiwan. J Experiment Forest National Taiwan University 25(2):139–147. https://doi.org/10.6542/EFNTU.201106_25(2).0005.

Li Y, Deng X, Zhang Y, Huang Y, Wang C, Xiang W, Xiao F, Wei X (2019) Chemical Characteristics of Heartwood and Sapwood of Red-Heart Chinese Fir (*Cunninghamia lanceolata*). For Prod J 69(2):103–109. https://doi.org/10.13073/FPJ-D-18-00042.

Li H, Zhang X, Li Z, Wen J, Tan X (2022) A review of research on tree risk assessment methods. Forests 13(10):1556. https://doi.org/10.3390/f13101556.

Lai, YY (2019) Termite infestation survey of protected old trees and baiting Formosan subterranean termite (Blattodea: Rhinotermitidae) in mango trees. National Chung Hsing University, master's thesis. 57 p. https://nchu.primo.exlibrisgroup.com/permalink/886NCHU_INST/2sntbr/alma990071951130107976

Liang WR, Maruyama M, Kanao T, Iwata R, Li HF (2020) Discovery of termitophilous rove beetles associated with Formosan subterranean termite *Coptotermes formosanus* in Taiwan, with the first larval description for

the tribe Termitohospitini (Coleoptera: Staphylinidae). Acta Entomologica Musei Nationalis Pragae, 60:77–87. https://doi.org/10.37520/aemnp.2020.005.

Lin CJ, Huang YH, Huang GS, Wu ML, Yang TH (2016) Detection of termite damage in hoop pine (*Araucaria cunninghamii*) trees by nondestructive techniques. J Trop For Sci 28(1):79–87. https://doi.org/10.6542/EFNTU.2015.29(2).2.

Lin WJ, Chen GY, Chiu CI, Liang WR, Tsai MJ, Yeh,HT, Li HF (2021) Damage and reinvasion of Asia subterranean termite on tree: A case study of Luchu Pine in Xiaping Tropical Botanical Garden. J Experiment Forest National Taiwan University 35(1):49–60. https://doi.org/10.6542/EFNTU.202103_35(1).0005.

Linhares CSF, Goncalves R, Martins LM, Knapic S (2021) Structural stability of urban trees using visual and instrumental techniques: a review. Forests 12(12):1752. https://doi.org/10.3390/f12121752.

Martiansyah I, Zulkarnaen RN, Hariri MR, Hutabarat PWK, Wardani FF (2022) Tree health monitoring of risking trees in the hotel open space: A case study in Rancamaya, Bogor. J Sylva Lestari 10(2):180–201. https://doi.org/10.23960/jsl.v10i2.570.

Morales-Ramos JA, Rojas MG (2001) Nutritional Ecology of the Formosan Subterranean Termite (Isoptera: Rhinotermitidae): Feeding Response to Commercial Wood Species. J Econ Entomol 94(2):516–523. https://doi.org/10.1603/0022-0493-94.2.516.

Morris H, Brodersen C, Schwarze FWMR, Jansen S (2016) The Parenchyma of Secondary Xylem and Its Critical Role in Tree Defense against Fungal Decay in Relation to the CODIT Model. Front Plant Sci 7. https://doi.org/10.3389/fpls.2016.01665.

Myer A, Forschler B (2018) Evidence for the Role of Subterranean Termites (*Reticulitermes* spp.) in Temperate Forest Soil Nutrient Cycling. Ecosystems 22:602–618. https://doi.org/10.1007/s10021-018-0291-8.

Ostrovsky R, Kobza M, Gazo J (2017) Extensively damaged trees tested with acoustic tomography considering tree stability in urban greenery. Trees 31:1015–1023. https://doi.org/10.1007/s00468-017-1526-6.

Pearce R, Rutherford J (1981) A wound-associated suberized barrier to the spread of decay in the sapwood of oak (*Quercus robur* L.). Physiol Plant Pathol 19:359–369. https://doi.org/10.1016/S0048-4059(81)80069-0.

Scholtz O, Knight M, Eggleton P (2021) Spatial structure of rainforest termites: Two matched pioneering cross-continental case studies. Biotropica, 53. https://doi.org/10.1111/btp.12959.

Shigo, AL (1984) Compartmentalization: a conceptual framework for understanding how trees grow and defend themselves. Annu Rev Phytopathol 22:189–214.

Smith K (2020) Whither compartmentalization of decay in trees? A commentary on: 'Using the CODIT model to explain secondary metabolites of xylem in defence systems of temperate trees against decay fungi'. Ann Bot 125(5):iv–vi. https://doi.org/10.1093/aob/mcaa035.

Soge AO, Popoola OI, Adetoyinbo AA (2021) Detection of wood decay and cavities in living trees: a review. Can J Forest Res 51(7):937–947. https://doi.org/10.1139/cjfr-2020-0340.

Tai WY (2002) Wood decomposition rates and caloric content changes of *Reticulitermes flaviceps* (Oshima) and *Nasutitermes parvonasutus* (Shiraki). National Taiwan University, master's thesis. 42 p. https://ntu.primo.exlibrisgroup.com/permalink/886NTU_INST/14poklj/alma991020160699704786

Thant, M., Lin, X., Atapattu, A., Cao, M., Xia, S., Liu, S, Yang X (2022) Activity-density and spatial distribution of termites on a fine-scale in a tropical rainforest in Xishuangbanna, southwest China. Soil Ecol Lett 5:169–180. https://doi.org/10.1007/s42832-022-0141-7.

Wei X, Du C, Xu S, Tian C, Yang X, Hu L, Pang P (2022) Research on stress wave wood nondestructive testing technology. J Phys Conf Ser 2366(1):012035. https://doi.org/10.1088/1742-6596/2366/1/012035.

Yagi H (2018) Study on the assessment of structural termite deterioration in building. National Taipei University of Technology, master's thesis. 147 p. https://hdl.handle.net/11296/ce8put

Yatsko AR, Wijas B, Calvert J, Cheesman AW, Cook K, Eggleton P, Gambold I, Jones C, Russell-Smith P, Zanne AE (2024) Why are trees hollow? Termites, microbes and tree internal stem damage in a tropical savanna. Funct Ecol 39:770–782. https://doi.org/10.1111/1365-2435.14727.

A comparison of woods for acoustic guitar soundboards

*Devon Pessler**
Assistant Professor (visiting)
School of Engineering Technology, Purdue University, West Lafayette, IN, USA

Eva Haviarova
Professor of Wood Products
Department of Forestry and Natural Resources, Purdue University, West Lafayette, IN, USA

Mark French
Professor of Engineering Technology
School of Engineering Technology, Purdue University, West Lafayette, IN, USA

(Received 6 March 2025)

Abstract. The soundboards of guitars have been crafted from wood since the beginning of string instruments. Based on industry-specific criteria, soundboards have traditionally been made from spruce and a few selected tropical wood species. This paper aims to find potential U.S. hardwoods that can serve as viable options to supplement the current manufacturing needs of the guitar industry. This paper also identifies the properties within the industry-specific criteria and determines how each property contributed to the market success of the soundboard woods used in production. The woods were separated into spruces, other woods in production, and U.S. hardwoods. A decision matrix determined which U.S. hardwoods would make viable options for production-grade soundboards. Basswood has the most promise of being a supplemental option.

Keywords: Tonewoods; Acoustic guitar; Engineering materials; Soundboards

Introduction

Wood has been used for the bodies of stringed instruments since the earliest times. As stringed instruments evolved, a common form emerged: a hollow body with a flat top or soundboard and a long neck. While decorative elements varied, the structures were almost always made of wood. The acoustic guitar emerged from Europe and the United States in roughly its modern form by the middle of the 19th century (Turnbull 1974).

Soundboards, or tops, are predominantly made from a few species of conifers, mainly spruce (genus *Picea*). However, a small number of steel-string guitars use tropical woods. Most acoustic guitars have a top with an "hourglass" shape, with the lower part, or lower bout, being longer and broader than the upper part or upper bout. The soundboard's waist separates the upper and lower bouts. Figure 1 displays a basic diagram of an acoustic guitar.

Soundboards are made from quarter-sawn wood to obtain the wood with the most dimensionally stable properties. Soundboards are usually made by book-matching, "a process in which a plank is split and opened up in the same manner as opening a book" (French 2012, 138). The two boards are then joined together at a seam along the grain to make a soundboard. Book matching two boards requires large diameter logs, which can only be obtained from harvesting old-growth trees.

Traditionally, old-growth spruce trees are used to make soundboards for acoustic guitars. However, the old-growth spruce the guitar industry uses is quickly diminishing due to the expected quality of wood. The quality of wood used for guitar tops is exceptionally high; some even consider it rare (Gibson and Warren 2021). Guitar builders prefer tops with "straight, even grain with closely spaced growth rings, which is relatively stiff when flexed by hand across the grain, and rings well when held lightly and tapped with a fingertip" (French 2022, 61). The industry may need to look to other woods to keep up with its manufacturing needs. This paper aims to determine if U.S. hardwoods are a viable option for supplementing the production of acoustic guitar soundboards.

*Corresponding author. Email: dpessler@purdue.edu;
address: Knoy Hall of Technology, 401 Grant St, West Lafayette, IN 47907

Wood and Fiber Science, 57(3), 2025, pp. 136–146
https://doi.org/10.22382/wfs-2025-12

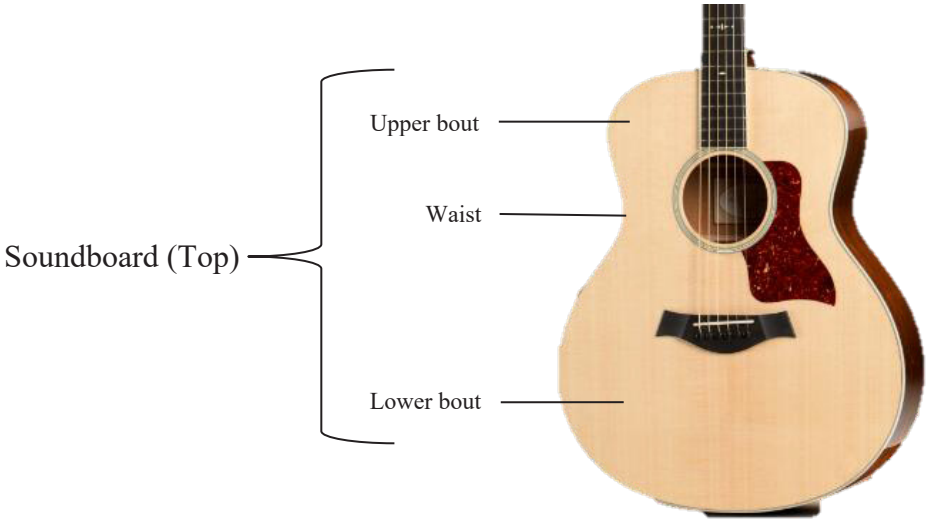

Figure 1. Basic diagram of an acoustic guitar's soundboard (Taylor Guitars 2024).

Materials and methods

Woods

Spruce is the most common material used for guitar tops. Sitka spruce (*Picea sitchensis*) is the most commonly used spruce for guitar tops, making up approximately 80 percent of all guitars in production worldwide (CMUSE 2022). Taylor Guitars, a major American guitar manufacturer, makes 85%–90% of their guitars with Sitka spruce tops (Taylor Guitars 2024). Other spruces used in acoustic guitar soundboards are Engelmann (*Picea engelmannii*), red (*Picea rubens*), white (*Picea glauca*), European (*Picea abies*), and Lutz (*Picea* x lutzii).

Due to the limited supply of the quality spruce wood necessary for acoustic guitar soundboards, the market currently offers alternatives to spruce-top guitars. Most of the major American guitar companies, including Fender, Taylor, and Martin, offer tops that are not of spruce. Fender uses hardwoods such as mahogany (*Swietenia macrophylla*), sapele (*Entandrophragma cylindricum*), and agathis (*Agathis australis*). Taylor uses hardwoods such as mahogany, koa (*Acacia koa*), walnut (*Juglans nigra*), big leaf maple (*Acer macrophyllum*), and softwoods like western red cedar (*Thuja plicata*) and sinker redwood (*Sequoia sempervirens*). Martin uses sinker redwood.

One untapped resource that has the potential to be wood for acoustic guitar soundboards is domestic U.S. hardwoods. A few domestic hardwoods, like walnut, are rarely used for soundboards but are commonly used for other guitar parts. This paper considers basswood (*Tilia americana*), swamp ash (*Fraxinus genus*), yellow poplar (*Liriodendron tulipifera*), black cherry (*Prunus serotina*), birch (*Betula alleghaniensis*), and red alder (*Alnus rubra*) as possible soundboard options. These woods were chosen because they are either used in the production of other stringed instruments or other parts within the acoustic guitar body.

Given this selection of woods for guitar-making, this paper looks to prove if domestic U.S. hardwoods can supplement the existing materials based on their structural, acoustic, and aesthetic characteristics. Based on the number of hardwoods in industry standard guitars, domestic U.S. hardwoods should be a viable supplemental option.

Method

Choosing the right wood for an acoustic guitar soundboard is vital to the instrument as the soundboard is responsible for its tonal quality (Pessler 2024). This study selected three types of wood: spruces used in acoustic guitar production, non-spruce wood used in guitar production, and U.S. domestic hardwoods known to be associated with guitar soundboards. Using the selection criteria commonly used among luthiers, the acoustic, structural, and aesthetic properties of spruce and non-spruce wood used in acoustic guitar production were ranked based on a decision matrix.

After the values were recorded and ranked, the study applied the same method to the selected U.S. domestic hardwoods. The hardwood properties were then compared to that of the properties of the spruce and non-spruce wood used in acoustic guitar production.

Selection criteria

Pedgley et al. (2009) state that "regardless of material, all acoustic guitar soundboards must satisfy three basic design criteria: structural, acoustic, and aesthetic" (p. 160). Their paper elaborates on these criteria by explaining that

> "the designer's task is to devise a soundboard with freedom to move (to satisfy acoustic criteria), whilst at the same time resisting twisting, bowing and other displacements that can arise from string tension (to satisfy structural criteria); and assuming the structural and acoustic criteria are met, the final requirement is for the soundboard to possess attractive sensorial properties (to satisfy aesthetic criteria)" (p. 160).

Structural criteria

The material properties are a crucial factor in selecting wood for tops. The four significant material properties are density, stiffness, hardness, and strength. Guitar builders use low-density wood, as it makes the guitar lightweight and has more tonal complexity (C.F. Martin & Co., Inc. 2025a). Merchel et al. (2019) furthered this idea by concluding that low density and low Young's modulus of the soundboard positively impact the guitar's sound quality. The relationship between Young's modulus and density is used to determine a widely referenced metric for selecting tops: specific stiffness. Specific stiffness, or stiffness-to-weight ratio, is Young's modulus in the longitudinal direction, E_L, divided by the density, ρ, of the material and is denoted as (Gore and Gilet 2011). Young's modulus is known as the modulus of elasticity (MOE).

Guitars are designed to have the lowest damping possible. Wood's hardness is related to its internal damping, as harder woods have low damping and accentuate higher frequencies (Acoustic Guitarist 2025). The Janka hardness scale measures wood hardness. Woods with higher Janka hardness values have less internal damping. Damping is also an acoustic property and can be found via modal testing.

Wood strength is a secondary material property, as stiffness is proportional to compression strength parallel to the grain. When strength is increased, so is stiffness. A stiff soundboard is also a strong soundboard, so wood with higher strength would better resist the tension of the strings across the guitar's bridge.

Acoustic criteria

Soundboard materials are characterized by four acoustic properties: material speed of sound, sound radiation coefficient, characteristic impedance, and damping. Ideally, acoustic guitar soundboard woods have a high speed of sound, high sound radiation coefficient, low characteristic impedance, and low damping.

The speed of sound through an orthotropic material, like wood, varies depending on the direction of the grain in relation to the measurement. This occurs because a material's speed of sound is dependent on material properties. The material's speed of sound, c, equation is

$$c = \sqrt{\frac{E_L}{\rho}} \tag{1}$$

"Light wood with high stiffness along the grain has a higher speed of sound" (French 2022, 248). The speed of sound through a material is directly proportional to the material's sound radiation coefficient and characteristic impedance. A material's sound radiation coefficient, R, relates to how quickly sound can radiate from the material. A high sound radiation coefficient means a louder sound. The sound radiation coefficient (SRC) equation is

$$R = \frac{c}{\rho} = \sqrt{\frac{E_L}{\rho^3}} \tag{2}$$

Bucur (2006) stated that high-quality resonance wood should have the highest sound radiation coefficient and the lowest acoustic impedance. The material's acoustic impedance of acoustic guitar soundboards is the mechanical input impedance. This term is purely resistive and real (Rossing and Fletcher 2004). Mechanical input impedance, Z_0, is expressed by its equation,

$$Z_0 = c\rho = \sqrt{E_L \rho} \tag{3}$$

The soundboard's ability to efficiently radiate sound is fundamental to the guitar's overall tonal characteristics and projection. The ideal soundboard would ring like a bell, meaning the higher resonance frequencies of the soundboard ring for a more extended period. Every resonance frequency rings in the same number of cycles. The bell-like sound radiates more cycles, thus reaching higher frequencies. Higher frequencies can be heard when there is low damping.

Damping refers to absorbing or dissipating vibrational energy in the context of an acoustic guitar soundboard. Damping can be calculated via the half-power bandwidth method. According to ASTM (2017), the half-power bandwidth, also known as the 3dB method, works by

> "using the response curve from each mode, measure the resonant frequency and the frequencies above and below the resonant frequency where the value of the response curve is 3 dB less (the 3 dB down points)

than the value at resonance. The frequency difference between the upper 3 dB down point and the lower 3 dB down point is the half-power bandwidth of the mode. The modal loss factor (η) is the ratio of the half-power bandwidth to the resonant frequency" (p. 6).

This method is predicated on the following equation:

$$\eta = 2\zeta = \frac{1}{Q} = \frac{\Delta f_{3dB}}{f_n} \quad (4)$$

Where ζ is the damping ratio, Q is the quality factor, Δf_{3dB} is the difference between the left and right frequencies (in Hz) when moving 3dB down the FRF, and f_n is the frequency (in Hz) of the n^{th} mode. The quality factor is inversely related to damping. So, to achieve the desired low damping, Q needs to be an enormous value (French 2022). This variable is unitless. This method is depicted in Figure 2.

Aesthetic criteria

The end user (guitar player) visually values the aesthetics of guitars. Usually, the player must be attracted to how the guitar looks so that they will consider playing the instrument. On one end of the spectrum, some players will only consider an instrument they think is attractive. It does not matter how good it sounds in those cases – the player will never know. On the other end of the spectrum, other players may give the unattractive guitar a chance if they know who made the guitar and what materials went into making it. Pedgley et al. (2009) surmise that "wood is a material rich in visual, tactile, and olfactory properties and is regarded as a memento of the power, beauty, and lifecycle of nature" (p. 162).

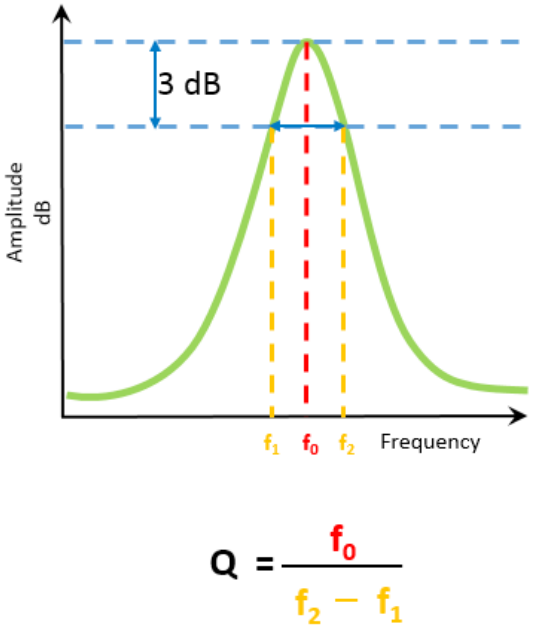

Figure 2. Depiction of the half-power bandwidth method (Siemens 2020).

Decision matrix

A decision matrix was used to compare the wood's material properties within each group. To summarize the tables in the Results section, let us look at the guitar industry's benchmark material, Sitka spruce. Using Table 1, Sitka spruce has a density of 425 kg/m^3, MOE of 11.03 GPa, specific stiffness of 27.5 x 10^6 m^2/s^2, Janka hardness of 2270 N, and compression strength parallel to the grain of 38.2 MPa. Based on the score ranges in Table 4, Sitka spruce has a density that falls within the score of "1", MOE score of "0", specific stiffness score of "5", Janka hardness score of "5", and strength score of "5". Using the weight multipliers in Table 2, the weighted score of Sitka spruce's density is "1" multiplied by four, which equals "4". Its weighted score for MOE is "0" multiplied by three, which equals "0". The weighted score of specific stiffness for Sitka spruce is "5" multiplied by five, which equals "25". Sitka spruce's Janka hardness weighted score is "5" multiplied by one, which equals "5". Finally, the weighted score for compression strength parallel to the grain is "5" multiplied by two, which equals "10". These weighted values are presented in Table 6, as well as the total scores that were used to create Figure 3. This method was used for the non-spruce wood soundboards in production material property rankings. The decision matrices were used to establish which material properties the guitar industry favors so that the U.S. hardwoods selected in this paper could be compared to what was already in production.

Results

Spruces as soundboards

Through the decades, guitar builders have found that old-growth spruce woods fit the criteria best. Old-growth woods are used for their size, as well as their stable and predictable properties. Table 1 shows the material properties and aesthetics of commonly used spruce woods for acoustic guitar soundboards, sourced from Eric Meier's book, *Wood! Identifying and using Hundreds of Woods Worldwide* (2015) and Lisa Black's thesis, *Tonewood: An Environmental Perspective* (2013).

The spruces can be ranked based on the material properties of density, modulus of elasticity (MOE), specific stiffness, hardness, and compression strength parallel to the grain. Using a decision matrix, the species can be objectively ranked on a scale from zero to five. Tables 2–5 show the breakdown of the decision matrix.

Table 1. Mechanical property values and grain pattern descriptions for spruces used as guitar soundboards.

Woods	Scientific name	Density, ρ (kg/m^3)	MOE, E_L (GPa)	Specific stiffness, (10^6 m^2/s^2)	Janka hardness, J (N)	Strength, σ (MPa)	Grain pattern
Sitka	*Picea sitchensis*	425	11.03	27.5	2270	38.2	Fine, even texture; consistently straight (Meier 2015, 184)
Engelmann	*Picea engelmannii*	385	9.44	24.5	1740	31.5	Fine, even texture; consistently straight; small knots are common (Meier 2015, 183)
White	*Picea glauca*	425	9.07	21.3	2140	32.6	Fine, even texture; consistently straight (Meier 2015, 183)
Red	*Picea rubens*	435	10.76	24.7	2180	33.6	Fine, even texture; consistently straight (Meier 2015, 183)
European	*Picea abies*	405	9.70	24.0	1680	35.5	Fine, even texture; consistently straight (Meier 2015, 183)
Lutz	*Picea* x lutzii	425	10.05	24.4	2205	35.4	Texture and luster of white spruce (Black, 2013)

Table 2. Weights of material properties.

	Low	High	Weights
Density, ρ	5	0	4
MOE, E_L	5	0	3
Specific stiffness,	0	5	5
Janka hardness, J	0	5	1
Strength, σ	0	5	2

Table 3. Ranking assignments for each mechanical property.

	Density ρ	MOE E_L	Specific stiffness	Janka hardness J	Strength σ
5	0–394	0–9.25	26.5 +	2170 +	38 +
4	395–404	9.26–9.65	26.4–25.5	2169–2070	37.9–36.5
3	405–414	9.66–10.05	25.4–24.5	2069–1970	36.4–35
2	415–424	10.06–10.45	24.4–23.5	1969–1870	34.9–33.5
1	425–434	10.46–10.85	23.4–22.5	1869–1770	33.4–32
0	435 +	10.86 +	22.4–0	1769–0	31.9–0

Table 4. Unweighted rankings of spruces.

	Sitka	White	Engelmann	Red	European	Lutz
Density	1	1	5	0	3	1
MOE	0	5	4	1	3	3
Specific stiffness	5	0	3	3	2	3
Janka hardness	5	4	0	5	0	4
Strength	5	1	0	2	3	3
Totals	16	11	12	11	11	14

Table 5. Weighted rankings of spruces.

	Sitka	White	Engelmann	Red	European	Lutz
Density	4	4	20	0	12	4
MOE	0	15	12	3	9	9
Specific stiffness	25	0	15	15	10	15
Janka hardness	5	4	0	5	0	4
Strength	10	2	0	4	6	6
Totals	44	25	47	27	37	38

Table 6. Acoustic properties of spruces.

	Density, ρ (kg/m^3)	MOE, E_L (GPa)	Speed of sound, c (m/s)	SRC, R (m^4/(kg-s))	Mechanical impedance, z (kg/(m^{2}s))
Red	435	10.76	4,973.5	11.43	2,163,469
Engelmann	385	9.44	4,951.7	12.86	1,906,410
European	405	9.70	4,893.9	12.08	1,982,044
Lutz	425	10.05	4,862.8	11.44	2,066,700
Sitka	425	11.03	5,094.4	11.99	2,165,121
White	425	9.07	4,619.7	10.87	1,963,352

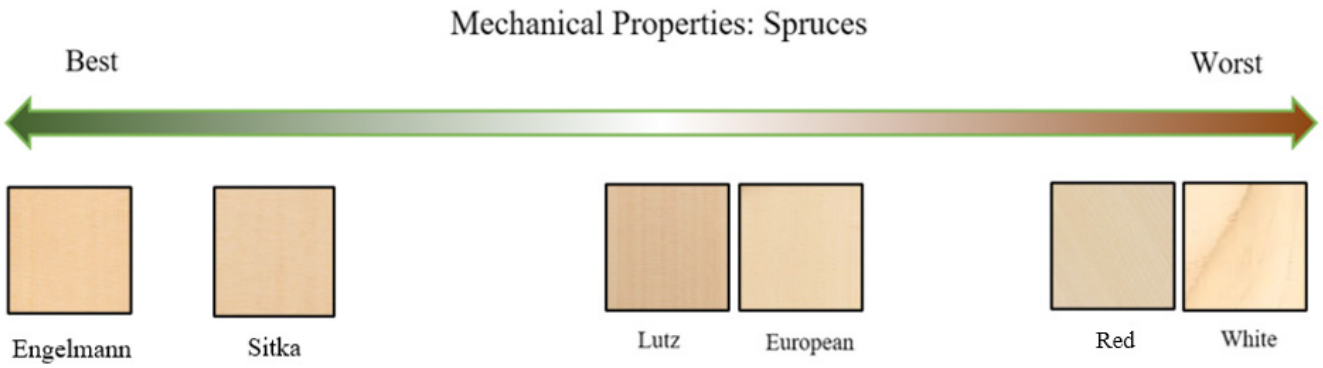

Figure 3. Ranking spruces by material properties (Taylor Guitars 2024b, 2024c, 2024d; Forestry 2023).

Table 2 shows how the material properties are scored. Lower values are desired for density and MOE, so a score of "5" is given. A score of "0" is given to a spruce with high density. For specific stiffness, hardness, and strength, the opposite is true. Higher values are desired, so a score of "5" is given to the wood with the highest values. Table 2 also shows the weighted importance of each material property. The material properties are numbered from most significant to least, with a score of "5" being most significant and a score of "1" for least significant. The weighted score values were assigned to each material property based on the industry's majority consensus.

Table 3 applies a value range to each number ranking for each material property. For example, let's take the material property of density. The highest value of 435 was placed in the "0" category because a high-density value is not desirable. The lowest value of 385 needed to be in the "5" category so that the full range of scores was used. The best way to incrementally distribute the density values among the scores was to group them in counts of ten. The rest of the density scores were determined by looking at Table 1 and seeing where they fell on the chart.

Table 4 shows the scores of each material property based on the value ranges in Table 3. The scores were totaled without weighted values. This table shows the total scores of the material properties for each spruce as if they were equally considered. Table 4 shows that Sitka spruce is the best wood for acoustic guitar soundboards.

Table 5 shows the final weighted decision matrix, and Figure 3 depicts the results of Table 5. The weighted scores were found by adding the values in Table 4 with the weights in Table 2, Table 5, and Figure 3 show that if only material properties were considered when selecting materials for a soundboard, then Engelmann spruce would be the desired wood.

The material properties and aesthetics of tonewoods are only two influences on selecting a top for an acoustic guitar. The third is the material's acoustic properties. Table 6 shows the calculated speed of sound, sound radiation coefficient, and mechanical impedance of each spruce based on the equations in the previous section (Wegst 2006).

The data in Table 6 show that Sitka spruce has the highest speed of sound, and Engelmann spruce has the lowest mechanical impedance and highest sound radiation coefficient, attributed to its low density. Figure 4 shows the order in which the spruces are used in industry, from most common to rarely used.

Non-Spruce Soundboards in Production

Gore (2011) states that western red cedar and redwood show attributes of good woods for an acoustic guitar top. These woods' material properties and grain pattern affect their status as an acceptable replacement for spruce tops. Table 7 shows the material properties and grain pattern of the listed alternative wood for a guitar soundboard, sourced from Meier (2015). The woods listed below are both hardwoods and softwoods.

With Sitka spruce as a benchmark, Agathis is the only species with relatively close specific stiffnesses. The following two closest woods are western red cedar and sinker redwood. Western red cedar and sinker redwood are attractive alternatives due to their low densities. Sapele and Hawaiian Koa are the strongest materials in this selected group.

Based on the material properties, the current alternative tonewoods were ranked using the decision matrix method as the spruce woods. Tables 8–10 show the breakdown of the decision matrix, and Figure 5 shows the species ranked from best to worst mechanical properties.

The grain pattern is the next deciding factor. Of the selected tonewoods, Agathis comes closest to being the best alterna-

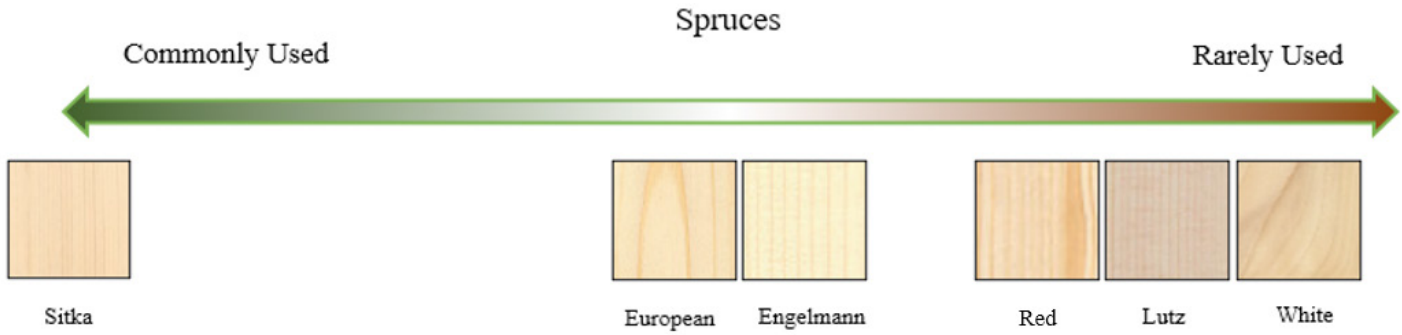

Figure 4. Order of use in industry for spruces (Taylor Guitars 2024b, 2024c, 2024d; Forestry 2023).

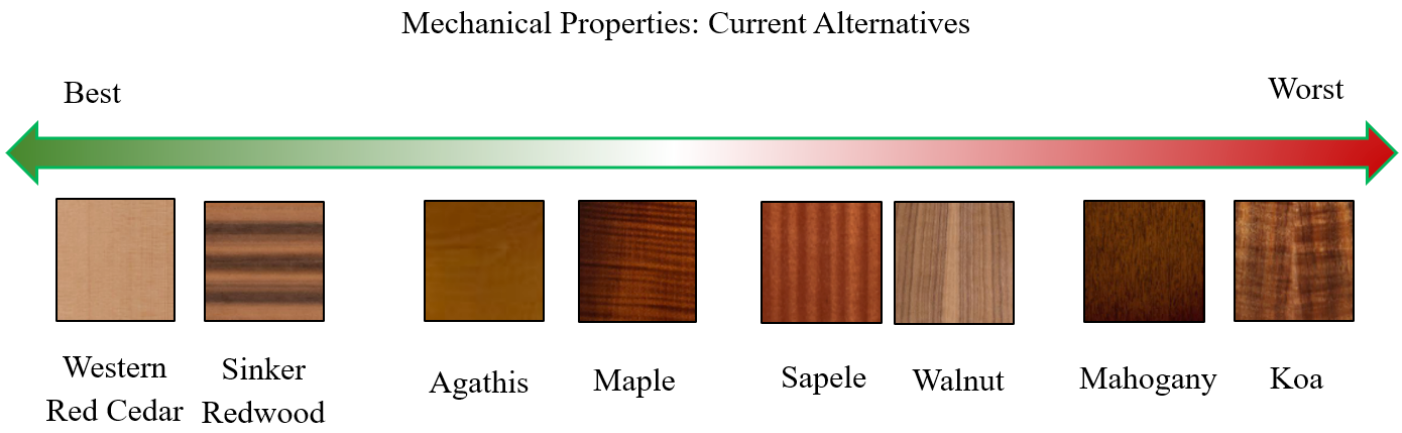

Figure 5. Ranking current alternatives by material properties (C.F. Martin & Co., Inc. 2025a; Taylor Guitars 2024a, 2024d; Andy king50 (2011))

Table 7. Mechanical property values and grain pattern descriptions for alternative tonewoods.

	Woods	Wood type	Scientific name	Density ρ (kg/m^3)	MOE E_L (GPa)	Specific stiffness (10^6 m^2/s^2)	Janka Hardness J (N)	Strength Σ (MPa)	Grain pattern
Often used	Western red cedar	Softwood	*Thuja plicata*	370	7.66	20.7	1560	31.4	Straight grain with coarse texture (Meier 2015, 240)
	Mahogany	Hardwood	*Swietenia macrophylla*	590	10.06	17.1	4020	46.6	Medium and uniform texture; grain can be straight, interlocked, irregular or wavy (Meier 2015, 230)
Less used	Koa	Hardwood	*Acacia koa*	610	10.37	17.0	5180	48.7	Uniform medium to coarse texture; usually slightly interlocked and sometimes wavy (Meier 2015, 50)
	Agathis	Hardwood	*Agathis australis*	540	11.87	22.0	3230	42.3	Usually straight, with a fine, even texture (Meier 2015, 58)
	Sinker redwood	Softwood	*Sequoia sempervirens*	415	8.41	20.3	2000	39.2	Straight, coarse texture (Meier 2015, 224)
Rarely used	Walnut	Hardwood	*Juglans nigra*	610	11.59	19.0	4490	52.3	Usually straight, but can be irregular; medium texture (Meier 2015, 146)
	Sapele	Hardwood	*Entandrophragma cylindricum*	670	12.04	18.0	6280	60.4	Interlocked; fine uniform texture (Meier 2015, 122)
	Maple	Hardwood	*Acer macrophyllum*	545	10.00	18.3	3780	41.0	Straight, fine, even texture (Meier 2015, 54)

Table 8. Ranking assignments for each mechanical property.

	Density ρ	MOE E_L	Specific stiffness	Janka hardness J	Strength σ
5	0–445	0–8.04	21.5 +	5650 +	59 +
4	446–520	8.05–9.04	21.4–20.5	5649–5000	58.9–54
3	521–595	9.05–10.04	20.4–19.5	4999–4350	53.9–49
2	596–670	10.05–11.04	19.4–18.5	4249–3700	48.9–44
1	671–745	11.05–12.04	18.4–17.5	3699–3050	43.9–39
0	746 +	12.05 +	17.4–0	3049–0	38.9–0

Table 9. Unweighted rankings of current alternative tonewoods.

	Western red cedar	Mahogany	Koa	Agathis	Walnut	Sinker redwood	Sapele	Maple
Density	5	3	2	3	2	5	2	3
MOE	5	2	2	1	1	4	1	3
Specific stiffness	4	0	0	5	2	3	1	1
Janka hardness	0	2	4	1	3	0	5	2
Strength	0	2	2	1	3	3	5	5
Totals	14	9	10	11	11	15	14	14

Table 10. Weighted rankings of current alternative tonewoods.

	Western red cedar	Mahogany	Koa	Agathis	Walnut	Sinker redwood	Sapele	Maple
Density	20	12	8	12	8	20	8	12
MOE	15	6	6	3	3	12	3	9
Specific stiffness	20	0	0	25	10	15	5	5
Janka hardness	0	2	4	1	3	0	5	2
Strength	0	4	4	2	6	6	10	10
Totals	55	24	22	43	30	53	31	38

tive when favoring grain patterns. Maple is another species that has a desired grain pattern. The final criterion is based on the wood's acoustic properties. Table 11 shows the calculated speed of sound, mechanical impedance, and sound radiation coefficient of each current alternative tonewood.

Agathis has the desired high speed of sound, and western red cedar has the preferred lowest mechanical impedance and the most significant sound radiation coefficient. Figure 6 shows the order of the current alternatives, from most common to rarely used.

Domestic hardwoods as possible woods for soundboards

Some domestic species are used in production for solid body electric guitars, like red alder, basswood, ash, and yellow poplar (Ahvenainen 2019). Table 12 shows several selected domestic species with material properties and aesthetics that compare to the woods already in soundboard production, sourced from Meier (2015).

Basswood has the closest specific stiffness to spruce and has the ideal grain pattern for building an acoustic guitar top. Yellow poplar is another species with a higher specific stiffness, but the surface texture can be coarse, requiring filling before finishing. Birch has many sought-after qualities; however, it has a very high density, which leads to low specific stiffness. Basswood, black cherry, and red alder have grain patterns ideal for guitar tops.

Table 11. Acoustic properties of current alternative tonewoods.

	Density, ρ (kg/m^3)	MOE, E_L (GPa)	Speed of sound, c (m/s)	Mechanical impedance, z (kg/(m^{2}s))	SRC, R (m^4/(kg-s))
Western red cedar	370	7.66	4,550.0	1,683,508	12.3
Mahogany	590	10.06	4,129.3	2,436,268	7.0
Koa	610	10.37	4,123.1	2,515,094	6.8
Agathis	540	11.87	4,688.4	2,531,758	8.7
Walnut	610	11.59	4,358.9	2,658,928	7.1
Sinker redwood	415	8.41	4,501.7	1,868,194	10.8
Sapele	670	12.04	4,239.1	2,840,211	6.3
Maple	545	10.00	4,283.5	2,334,524	7.9

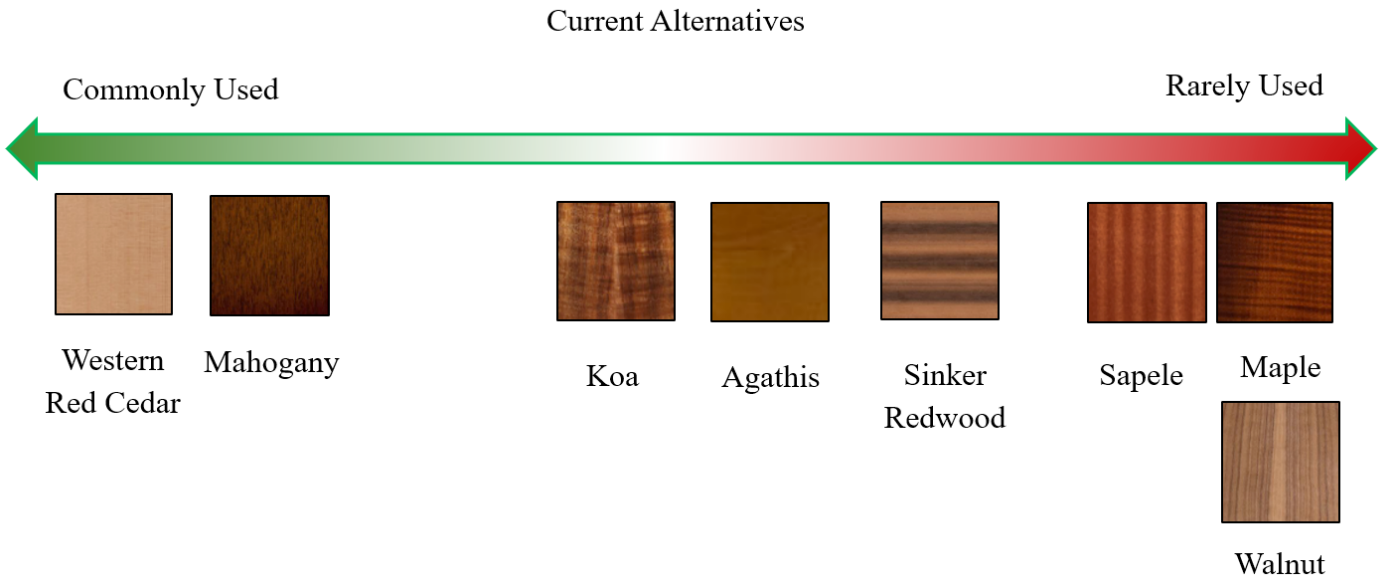

Figure 6. Order of use in industry for current alternatives (C.F. Martin & Co., Inc. 2025a; Taylor Guitars 2024a, 2024d; Andy king50 2011)

Table 12. Material properties and grain pattern descriptions for possible alternative U.S. hardwood tonewoods.

Woods	Scientific name	Density ρ (kg/m^3)	MOE E_L (GPa)	Specific Stiffness (10^6 m^2/s^2)	Janka hardness J (N)	Strength Σ (MPa)	Grain pattern
Basswood	*Tilia americana*	415	10.07	24.3	1820	32.6	Straight, with a fine, even texture (Meier 2015, 242)
Swamp ash*	*Fraxinus genus*	510	11.00	21.6	3780	41.2	Typically straight and regular; medium to coarse texture (Meier 2015, 131-132)
Yellow poplar	*Liriodendron tulipifera*	455	10.90	24.0	2400	38.2	straight, uniform grain, with a medium texture (Meier 2015, 156)
Black cherry	*Prunus serotina*	560	10.30	18.4	4230	49.0	Usually straight; fine, even texture (Meier 2015, 202)
Birch	*Betula alleghaniensis*	690	13.86	20.1	5610	56.3	straight or slightly wavy, with a fine, even texture (Meier 2015, 69)
Red alder	*Alnus rubra*	450	9.52	21.2	2620	40.1	Generally straight; moderately fine, uniform texture (Meier 2015, 60)

"Swamp Ash" has mechanical property values and grain pattern descriptions like black ash, except for the density. According to the Wood Database (Meier 2025), the listed density is the average density of swamp ash.

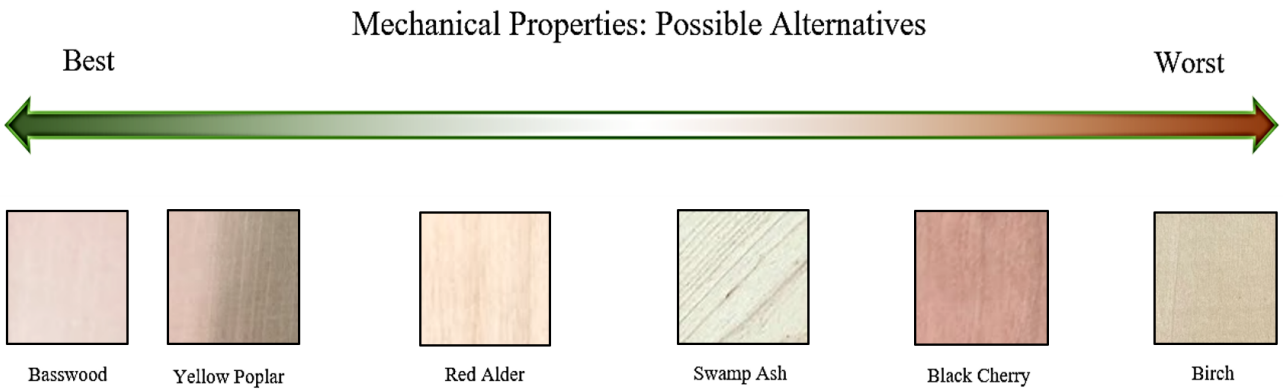

Figure 7. Ranking possible alternative U.S. hardwood tonewoods by material properties (Stephen Ondich 2020)

Table 13. Ranking assignments for each mechanical property.

	Density ρ	MOE E_L	Specific stiffness	Janka hardness J	Strength σ
5	0–450	0–9.75	24 +	4950 +	52.5 +
4	451–500	9.76–10.75	23.9–23	4949–4300	52.4–48.5
3	501–550	10.76–11.75	22.9–22	4299–3650	48.4–44.5
2	551–600	11.76–12.75	21.9–21	3649–3000	44.4–40.5
1	601–650	12.76–13.75	20.9–20	2999–2350	40.4–36.5
0	651 +	13.76 +	19.9–0	2349–0	36.4–0

A decision matrix was used to rank the wood species based on their material properties with the same methods as the other two wood groups. Tables 13–15 show the breakdown of the decision matrix, and Figure 7 shows the order of the woods from the best to the worst mechanical properties.

Material properties and aesthetics are essential for selecting tops; however, they are not the only factors to consider. Acoustic properties are just as important. Table 16 shows the calculated speed of sound, mechanical impedance, and sound radiation coefficient of each possible alternative tonewood.

Table 14. Unweighted rankings of possible U.S. hardwood tonewoods.

	Basswood	Swamp ash	Yellow poplar	Black cherry	Birch	Red alder
Density	5	3	4	2	0	5
MOE	4	3	3	4	0	5
Specific stiffness	5	2	5	0	1	2
Janka hardness	0	3	1	3	5	1
Strength	0	2	1	4	5	1
Totals	14	14	14	13	11	14

Table 15. Weighted rankings of possible U.S. hardwood tonewoods.

	Basswood	Swamp ash	Yellow poplar	Black cherry	Birch	Red alder
Density	20	12	16	8	0	20
MOE	12	9	9	12	0	15
Specific stiffness	25	10	25	0	5	10
Janka hardness	0	3	1	3	5	1
Strength	0	6	2	8	10	2
Totals	57	40	53	31	20	48

Table 16. Acoustic properties of possible U.S. hardwood tonewoods.

	Density, ρ (kg/m³)	MOE, E_L (GPa)	Speed of sound, c (m/s)	Mechanical impedance, z (kg/(m²s))	SRC, R (m⁴/(kg-s))
Basswood	415	10.07	4,926.0	2,044,272	11.9
Swamp ash*	510	11	4,644.2	2,368,544	9.1
Yellow poplar	455	10.9	4,894.5	2,226,993	10.8
Black cherry	560	10.3	4,288.7	2,401,666	7.7
Birch	690	13.86	4,481.8	3,092,475	6.5
Red alder	450	9.52	4,599.5	2,069,783	10.2

With mechanical, visual, and acoustic properties similar to those of the commonly used top woods, basswood is the clear choice as a possible hardwood alternative for guitar tops.

Discussion

Old-growth spruce tops are not a sustainable resource for the guitar industry. Major guitar manufacturers have started to move towards sustainable tonewoods, but they still use spruce for most of their acoustic guitar production. This paper demonstrates that alternative tonewoods are suitable substitutes for spruce when using mechanical, acoustic, and aesthetic characteristics. The domestic U.S. hardwoods that were most suitable were basswood and yellow poplar. With options to supplement spruce for acoustic guitar soundboards, the next step is to build guitars with tops made from basswood and yellow poplar and test them to prove whether they are practical candidates.

References

Acoustic Guitarist, The (2025) A Guide to Acoustic Guitar Tonewoods. 24 March 2025. https://theacousticguitarist.com/acoustic-guitar-tonewoods/.

Ahvenainen P (2019) Anatomy and mechanical properties of woods used in electric guitars. IAWA 40(1):106-S6. DOI:10.1163/22941932-40190218

Andy king50 (2011) Kauri museum kauri wood. Andy king50, CC BY-SA 3.0 <https://creativecommons.org/licenses/by-sa/3.0>, via Wikimedia Commons, https://commons.wikimedia.org/wiki/File:Kauri_museum_kauri_wood.JPG.

ASTM-American Society for Testing and Materials (2017) Standard Test Method for Measuring Vibration-Damping Properties of Materials. ASTM International. https://compass.astm.org/.

Black LR (2013). Tonewood: An Environmental Perspective." Master's thesis, California State University, Northridge, May. 88-89. https://scholarworks.calstate.edu/concern/theses/5t34sn93k

Breedlove Guitar Company (2021). Sustainability: Organic Collection. Accessed September 2, 2022. https://breedlovemusic.com/instruments/acoustic-guitars/sustainability .

Bucur V (2006) Acoustics of Wood (2nd edition). J Acoust Soc Amer 119 (6). doi:10.1121/1.2197787.

C.F. Martin & Co., Inc. (2025a) Acoustic Guitar Wood Types: A Guide. https://www.martinguitar.com/learn-wood-materials.html.

C.F. Martin & Co., Inc. (2025b) Custom K-1 Major Kealakai. https://www.martinguitar.com/guitars/Custom-Major-Kealakai.html.

CMUSE (2022) *Lutz Spruce vs Sitka Spruce - Which Tonewood Is Better?* 22 June. Accessed August 1, 2022. https://www.cmuse.org/lutz-spruce-vs-sitka-spruce/.

Ellis A, Saufley C, Gerken T (2008) The Future of Tonewood. February: 80–86. https://www.proquest.com/magazines/future-tonewood/docview/198687385/se-2.

Forestry (2023) *White Spruce Lumber.* 27 June. Accessed November 9, 2023. https://forestry.com/lumber/white-spruce-lumber/.

French RM (2022) Acoustic Guitar Design. Switzerland: Springer.

French RM (2012) Structure of the Guitar. In *Technology of the Guitar*, 138. New York: Springer.

Gibson C, Warren A (2021). "The guitar industry's hidden environmental problem." 28 May 2021. Accessed May 26, 2023. https://phys.org/news/2021-05-guitar-industry-hidden-environmental-problem.html.

Gore T (2011) Wood for Guitars. J Acoust Soc Am 12 (1).

Gore T, Gilet G (2011) The sound radiation coefficient. In Gore and Gilet, Contemporary Acoustic Guitar Design and Build, Australia: Trevor Gore, pp. 4-19–4-20.

Herrod, C. 2018. *Wood Scarcity.* Luthiers Mercantile International, Inc., 10 November. Accessed August 3, 2022. https://www.lmii.com/blog/2017/10/07/wood-scarcity/.

Meier, E. (2025) The Wood Database. https://www.wood-database.com/

Meier E (2015) WOOD! Identifying and Using Hundreds of Woods Worldwide. Whitethorn, CA: The Wood Database.

Merchel S, Altinsoy ME, Olson D (2019). Perceptual evaluation of bracewood and soundboard wood variations on the preference of a steel-string acoustic guitar. J Acoust Soc Am 146 (4):2608–2618. doi:10.1121/1.5129395.

Music Trades Magazine (2020). How to secure sustainable wood for the guitar industry. Music Trades Magazine 168(2):60. https://www.musictrades.com/

Pedgley O, Norman E, Armstrong R (2009). Materials-inspired innovation for acoustic guitar design. Mimarlık Fakültesi Dergisi 26 (1):157–175.

Pessler D (2024). An Objective Material Selection Metric for Acoustic Guitar Soundboards. Doctoral dissertation, Purdue University Graduate School. https://doi.org/10.25394/PGS.25582773.v1.

Rossing TD, Fletcher NH (2004) Continuous Systems in One Dimension: Strings and Bars. In Rossing and Fletcher, Principles of Vibration and Sound, New York: Springer-Verlag, pp. 33–64.

Siemens. (2020). How to calculate damping from a FRF? Accessed November 15, 2023. https://community.sw.siemens.com/s/article/how-to-calculate-damping-from-a-frf.

Stephen Ondich (2020) Swamp ash lumber. Stephen Ondich, CC BY-SA 4.0 <https://creativecommons.org/licenses/by-sa/4.0>, via Wikimedia Commons, https://commons.wikimedia.org/wiki/File:84_Southern_White_Ash-1.jpg.

Taylor Guitars (2024a) Body woods. Accessed October 23, 2023. https://www.taylorguitars.com/guitars/acoustic/features/woods/body-woods.

Taylor Guitars (2024b) Engelmann Spruce. Accessed August 3, 2022. https://www.taylorguitars.com/guitars/acoustic/features/woods/top-woods/european-spruce.

Taylor Guitars (2024c) Sitka Spruce. Accessed August 3, 2022. https://www.taylorguitars.com/guitars/acoustic/features/woods/top-woods/sitka-spruce.

Taylor Guitars (2024d) Top Woods. Accessed October 23, 2023. https://www.taylorguitars.com/guitars/acoustic/features/woods/top-woods.

Turnbull H (1974) The Guitar, from the Renaissance to the Present Day. New York, Charles Scribner's Sons.Wegst, UGK (2006) Wood for sound. Am J Bot 93 (10):1369–1565.

Near-infrared spectral signatures differentiate blue stain and brown rot fungi in conifer and broadleaf trees

*Emmanuel A. Boakye**
Natural Resources Canada
Canadian Forest Service, Edmonton, AB T6H-3S5, Canada
emmanuel.boakye@nrcan-rncan.gc.ca / eaaboakye@yahoo.com

*Jennifer Klutsch**
Natural Resources Canada
Canadian Forest Service, Edmonton, AB T6H-3S5, Canada
jennifer.klutsch@nrcan-rncan.gc.ca

Cyriac S. Mvolo
Natural Resources Canada
Canadian Forest Service, Edmonton, AB T6H-3S5, Canada
cyriac.mvolo@nrcan-rncan.gc.ca

Andre G. Duarte
Natural Resources Canada
Canadian Forest Service, Edmonton, AB T6H-3S5, Canada
andregalvd@gmail.com

(Received 30 May 2025)

Abstract. Colonization by blue stain and brown rot fungi affects timber quality in distinct ways. Blue stain fungi cause discoloration without reducing wood properties, while brown rot fungi degrade wood tissues, resulting in brittleness and brown coloration. Given these chemical differences, we investigated whether near-infrared spectroscopy (NIRS) could distinguish between these fungal types. We hypothesized that early fungal attack would produce unique spectral signatures, allowing for rapid identification. Wood disc samples were collected from white spruce, lodgepole pine, and trembling aspen in Fox Creek, northwest Alberta, Canada, ca. 4 months after a wildfire. The trees were colonized by fungi associated with blue and brown sapwood discoloration and analyzed using NIRS. In white spruce, we found consistent and significant absorbance differences between blue- and brown-discolored sapwood across each 100 nm segment. In lodgepole pine, the most distinct differences occurred in the 1650–1750 nm, 2050–2150 nm, and 2350–2450 nm ranges. For trembling aspen, differences were evident across most 100 nm intervals, except 2150–2250 nm. Permutational multivariate analysis of variance (PERMANOVA) indicated greater spectral dissimilarity between fungal types in white spruce and trembling aspen, with less pronounced differences in lodgepole pine. Our findings suggest that NIRS can effectively classify fungal-discolored wood in white spruce and trembling aspen within the first year following wildfire. However, its application to lodgepole pine in the same timeframe may be less reliable.

Keywords: Fungal colonization; Blue stain fungi; Brown rot fungi; Wood discoloration; Near-infrared spectroscopy (NIRS); Spectral signatures

Introduction

Canada's boreal forest plays a vital role in domestic and international wood markets, contributing 1.2% to the national GDP in 2022 and accounting for 12% of global wood supply (Natural Resources Canada 2022, 2023). However, threats like fires, pests, and diseases threaten the forest health and wood quality (Gauthier et al. 2015). From 1984 to 2016, wildfires and insect outbreaks caused 53.7% of forest biomass loss, surpassing the 43.8% from industry harvesting (Wulder et al. 2020). In 2023, wildfires burned over twice the previous record area of 6.7 million hectares set in 1989 (Jain et al. 2024). Between 1998 and 2009, insects like the mountain pine beetle killed an estimated 675 million m³ of pine in Western Canada (Natural Resources Canada 2020). With temperatures projected to rise between 2°C and 6°C by the end of the century, increasing fire and pest activity could threaten the forests' economic viability (Natural Resources Canada 2019).

Wildfires significantly impact timber value, as burned trees may become unsuitable for commercial use, and salvaged

* Corresponding author

wood often has lower product value (Watson and Potter 2004; Bousfield et al. 2023). The heat from wildfires triggers pyrolysis, a chemical decomposition that alters the wood's structure and composition, reducing moisture content, darkening coloration, decreasing mechanical strength, and increasing brittleness (Mensah et al. 2023). These changes make the wood prone to cracking and degrade key mechanical properties, such as tensile strength and bending strength, rendering it unsuitable for structural applications (González-Peña et al. 2009; Piernik et al. 2022). Additionally, fire-damaged trees can become vulnerable to fungal, bacterial, and insect attack, which accelerates decay and further reduces the wood's commercial value.

Fungal growth in burnt wood is favored by conditions such as mild temperatures, moderate to low moisture levels, and increased aeration as the wood dries (Schmidt 2006; McCarthy et al. 2012). The fungal colonization in sapwood is distinguished by patterns like blue and brown discoloration. Blue stain fungi, generally from the class Ascomycota, do not degrade lignin or cellulose (McCarthy et al. 2012; Lundell et al. 2014). Instead, they invade living wood and produce melanin to protect themselves from environmental stressors, breaking down non-structural components like triglycerides and oleic acid. This activity results in discoloration appearing as shades of blue but causes minimal structural damage (Lundell et al. 2014). In contrast, fungi that cause brown rot are typically associated with the class Basidiomycota and often cause severe damage that degrades cellulose (McCarthy et al. 2012; Lundell et al. 2014). This leaves behind a brown rot characterized by brittle, cracked residues composed mainly of lignin that significantly compromises the wood's structural integrity (McCarthy et al. 2012; Lundell et al. 2014). Both blue stain and brown rot fungi reduce the cosmetic quality of timber, but brown rot fungi also render it unsuitable for structural use (McCarthy et al. 2012).

Given the potential for widespread fungal damage in burnt wood, tools that quickly and accurately assess wood properties and the presence of fungal-caused discolouration are essential for early intervention to minimize damage (Pohleven et al. 2002; Guillén and Machuca 2008). In this regard, near-infrared spectroscopy (NIRS) can be an efficient tool for analyzing these characteristics. By utilizing the near-infrared (NIR) region of the electromagnetic spectrum (700 to 2500 nm), NIRS measures how electromagnetic energy is scattered or absorbed by wood tissues, providing understanding into their composition and quality (Tsuchikawa and Kobori 2015). The light interacts with the overtone and combination vibrations of chemical bonds (e.g., C-H, O-H, N-H) within organic compounds, producing NIRS spectra that can be analyzed to obtain information about the chemical properties of organic materials (Chen et al. 2015; Tsuchikawa and Kobori 2015). This technique is valuable for forest management because it offers rapid data acquisition, high accuracy, and requires minimal sample preparation, making it ideal for large-scale studies (Tsuchikawa 2007; Tsuchikawa and Kobori 2015; Hein et al. 2017).

NIRS is particularly useful for analyzing wood composition and assessing quality changes due to fungal damage. Previous studies demonstrated that NIRS can capture molecular-level alterations in wood coloration from fungal activity. Via et al. (2007) observed distinct absorbance shifts due to blue stain in longleaf pine; Kelley et al. (2002) and Barton et al. (1995) detected lignin and carbohydrate degradation from white and brown rot fungi; and Fackler et al. (2007) and Fackler and Schwanninger (2012) monitored decay progression and mass loss. Building on this, Burud et al. (2014) used hyperspectral NIRS imaging to quantify blue stain in Norway spruce. Unlike visual inspection, which detects only advanced discoloration, NIRS provides an accurate alternative, identifying early-stage and subsurface decay in wood that may not be identified by visual methods. By detecting chemical changes such as lignin or cellulose degradation, NIRS enables fungal damage detection before visible signs emerge, thus representing a more refined and precise method in wood quality assessment (Pohleven et al. 2002; Guillén and Machuca 2008).

This study builds on previous research by using NIR spectroscopy to assess the effects of blue stain and brown rot fungi on NIR absorbance in two coniferous and a deciduous tree species, focusing on white spruce (*Picea glauca* (Moench) Voss), lodgepole pine (*Pinus contorta* Douglas ex Loudon), and trembling aspen (*Populus tremuloides* Michx.). Since fungal infestations alter organic chemical bonds in wood, we aimed to determine whether colonization influenced NIR absorbance in species-specific ways, as NIR is sensitive to molecular vibrations of organic compounds (Tsuchikawa and Kobori 2015; Deepa et al. 2024). We expected that differences in how blue stain and brown rot fungi interact with sapwood would allow for the differentiation of their spectral characteristics. To this end, we hypothesized that the unique chemical and physical alterations caused by each fungal type would manifest in distinct spectral patterns, enabling reliable wood quality assessment. This is the first step in evaluating the potential of NIR as a tool for understanding the role of fungi in wood degradation in fire-killed trees. Based on these results, future work will aim to identify fungi species associated with these stains and further clarify their contribution to wood decay.

Materials and methods

Wood samples

In 2023, a forest inventory was conducted in the native forests near Fox Creek, Alberta (54.476°N, 116.783°W), to assess the impact of fire on wood quality. This area has a history of periodic disturbances, primarily wildfire, that shape the composition and structure of its boreal forests. During the inventory, some harvested trees were found to be infested with fungi. The sampled tree species included white spruce (average age based on ring counts = 88 years), lodgepole pine (average age = 77 years), and trembling aspen (average age = 73 years), all of which are common in Alberta's boreal forests. Discs from the infested trees were collected at a height of 2 m from the base to ensure consistency in wood properties. The wood exhibited minimum degradation but advanced discoloration (Figure 1). The presence of fungi associated with blue stain and brown rot (Table 1) was confirmed by the Mycology Research Laboratory of the Canadian Forest Service in Edmonton, Canada.

Acquisition of spectra in the NIR region

Spectral readings were collected from the flat transverse surface of the wood sample discs. For each disc, five scan locations were selected per observed type (e.g., blue stain or brown rot) to capture variation across the visibly stained regions (Table 1), along with five additional scans from clear areas confirmed as unstained by visual inspection. In cases where multiple stain types were present on a single disc, five scans were taken for each type. Control discs taken from trees with no visible staining were scanned at five locations across the clear surface.

Clear scans from visibly unstained areas on stained discs enabled direct comparisons of near-infrared spectral characteristics within a consistent tree-specific context. Control scans from entirely unstained discs of the same species served as a baseline reference free of fungal influence.

To ensure uniform surface conditions, the samples were lightly pre-sanded to remove chainsaw marks that could interfere with spectral readings. Sanding was applied consistently across each sample. Measurements were conducted at room temperature (approximately 22°C) to control for environmental effects on the readings and were performed using a single NeoSpectra-Scanner (Si-Ware Systems Inc., USA). The device features a 10-mm collection window, and its software reports spectra from 1350 to 2550 nm at a step of 2.5 nm, with a wavelength resolution of 16 nm. The scanner lens was positioned on the dried wood surface and held steady during each scan to minimize interference from ambient light. At each measurement location, three spectra were collected and averaged to reduce noise.

Table 1. Summary of data samples showing the number of trees and total scans per species under four wood conditions. Total scans refer to the number of measurements taken on wood discs from each species under each condition. Control refers to scans from completely unstained discs collected from healthy trees of the same species. Clear refers to scans from visibly unstained areas on otherwise stained discs.

Wood condition	Species	Number of trees	Total scans
Blue stain fungi	Lodgepole pine	5	25
	Trembling aspen	3	15
	White spruce	6	30
Brown rot fungi	Lodgepole pine	3	15
	Trembling aspen	5	27
	White spruce	3	15
Clear	Lodgepole pine	6	30
	Trembling aspen	6	30
	White spruce	7	35
Control	Lodgepole pine	5	25
	Trembling aspen	5	25
	White spruce	5	25

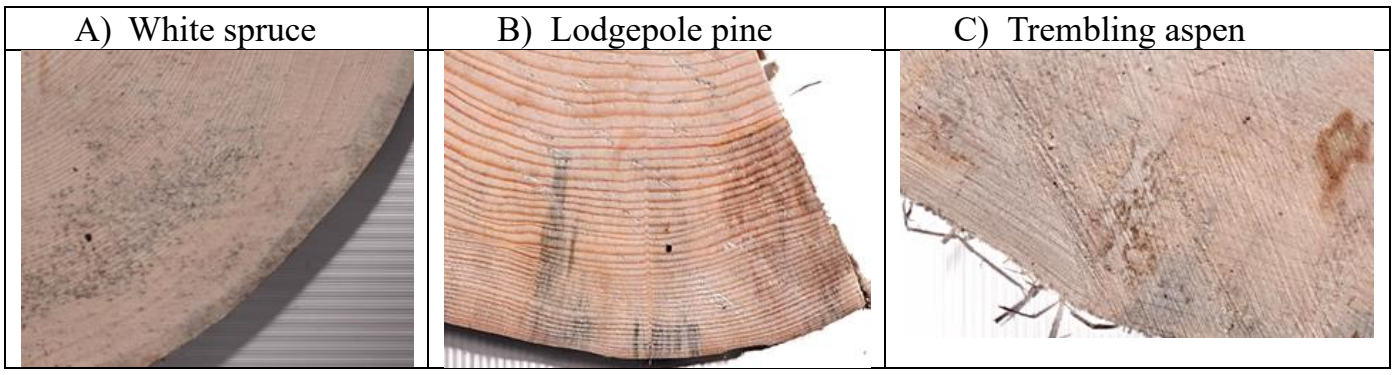

Figure 1. Cross-section segments of white spruce, lodgepole pine, and trembling aspen showing brownish and bluish stains on the wood surface.

Spectral pre-processing

Near-infrared spectroscopy data pose challenges due to broad, overlapping absorption bands that can shift depending on physical, chemical, and structural factors. These shifts and overlaps can obscure the resolution of spectral features and make direct interpretation difficult. To address these issues, derivatives are commonly used for baseline correction in spectroscopy (Savitzky and Golay 1964). The first derivative removes additive shifts, while the second eliminates linear increases and sharpens peaks. The application of these derivatives also enhances resolution, resolves overlapping peaks, and highlights spectral details.

With these considerations, two pre-processing techniques were applied to enhance spectral features and reduce noise:

1. No pre-treatment: Using raw or original absorbance values.
2. Savitzky-Golay smoothing with first- and second-order derivatives: This method, proposed by Savitzky and Golay (1964), was implemented with a window size of 13 data points and a polynomial order of 2. These parameters were selected based on exploratory analysis and their effectiveness in resolving overlapping peaks and correcting baselines, as demonstrated in previous studies (e.g., Via et al. 2007).

The signal package (signal developers, 2023) in R software (R Core Team 2024) was used for the Savitzky-Golay filtering of the spectral data.

Data Analysis

Spectral data were analyzed to identify regions with absorbance peaks and assess differences in mean absorbance across four wood conditions: clear wood, blue-stained wood, brown rot wood, and control samples. The spectral range was divided into 100-nm segments to capture localized variations in absorbance, and the average absorbance within each segment was compared across the wood conditions. A Kruskal-Wallis test was applied to each segment, followed by Dunn's post-hoc test to determine specific differences between the wood conditions. A permutational multivariate analysis of variance (PERMANOVA) was conducted on similarity matrices based on Euclidean distances using the *vegan* package in R (Oksanen et al. 2024). PERMANOVA was chosen because it evaluates for differences among groups in multivariate space without assuming normality. This analysis assessed whether the centroids representing each wood condition were significantly different, indicating variation in spectral patterns across treatments. To mitigate the risk of too few unique permutations, the Monte Carlo method was used to obtain reliable p-value estimates. If PERMANOVA indicated significant differences among the wood conditions, pairwise comparisons were performed to assess the statistical significance of the Euclidean distances between the wood condition centroids.

Results and discussion

Spectral properties of stained and unstained wood across species

We observed variations in the spectral properties (Figure 2) of white spruce, lodgepole pine, and trembling aspen across four conditions: blue stain fungi, brown rot fungi, clear wood, and control wood. In white spruce (Figure 2A), brown rot fungi exhibited the highest absorbance across most wavelengths, especially around 1450 nm, 1900 nm, and 2350 nm. Blue stain fungi followed closely with slightly lower absorbance, while the control and clear wood conditions showed lower values, with clear wood consistently having the lowest absorbance overall. Additionally, significant differences in mean absorbance between the blue stain and brown rot fungi were consistently observed at 100-nm intervals along the spectral curve.

In the 1st derivative plot of white spruce (Figure 2A), the spectral curves across conditions were generally similar, though some differences appeared around 1550 nm and 2150 nm, where the brown rot showed slightly higher peaks. The control, brown rot, and blue stain fungi curves overlapped closely, while the clear condition displayed a slightly different pattern, particularly around 1750 nm and 2350 nm. In the 2nd derivative plot, minor variations emerged between the conditions. The blue stain, brown rot, and control conditions deviated more visibly from the clear wood, especially between 1750 nm and 1950 nm, and at 2350 nm, where their patterns were distinct. Additionally, no significant differences in mean absorbance were detected between the blue and brown rot fungi for both the first and second derivatives at 100-nm intervals along the spectral curve.

For lodgepole pine (Figure 2B), the patterns were similar, with blue stain fungi showing the highest overall absorbance, particularly between 1900 and 2350 nm. Brown rot fungi and clear wood exhibited moderate absorbance, with brown rot fungi slightly higher than clear wood across most wavelengths, while the control had the lowest absorbance. The peak around 1900 nm was especially pronounced in the blue stain fungi sample. Additionally, significant differences in mean absorbance between blue and brown rot fungi were consistently observed at 100-nm intervals along the spectral curve.

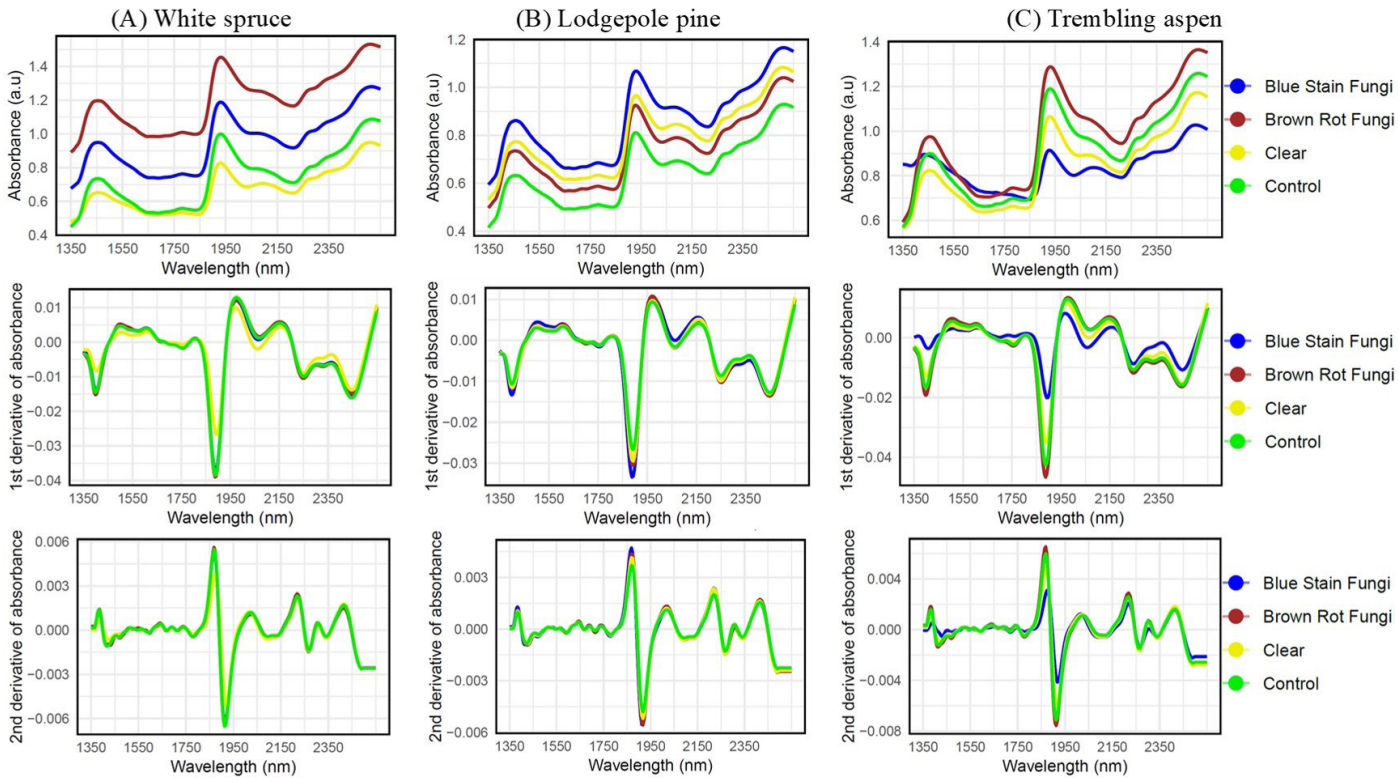

Figure 2. Average absorbance (top row), first derivative ($dA \cdot dw^{-1}$, middle row), and second derivative ($d^2A \cdot dw^{-2}$, bottom row) spectra as functions of wavelength (1350–2450 nm) for each species. The four wood conditions are color-coded: blue stain fungi (blue), brown rot fungi (brown), clear wood (yellow), and control (green). Each curve represents the mean spectrum for its respective condition.

In the first derivative curves of lodgepole pine (Figure 2B), there was a clearer distinction between blue stain fungi and brown rot fungi, especially around 1950 nm. Clear wood and the control overlapped significantly across most regions, with minimal variation between them, particularly in the 1550–1950 nm range. Significant differences in mean absorbance between the blue and brown rot fungi were observed in the wavelength intervals of 1650–1750 nm, 2050–2150 nm, and 2350–2450 nm.

The second derivative curves (Figure 2B) showed similar trends. The blue and brown rot fungi samples displayed distinct patterns around 1950 nm, while clear wood and the control remained closely aligned throughout the spectrum, with minor variation between them. Significant differences in mean absorbance between the blue and brown rot fungi were evident in the intervals of 1650–1750 nm, 1950–2050 nm, and 2050–2150 nm.

For trembling aspen (Figure 2C), the brown rot fungi showed the highest absorbance, particularly between 1750 and 2350 nm, with distinct peaks around 1900 nm and 2350 nm. Control and clear wood followed similar patterns but exhibited lower absorbance compared to the brown rot fungi. In contrast, the blue stain fungi consistently displayed the lowest absorbance across the wavelength range. At 100-nm intervals along the spectral curve, significant differences in mean absorbance were observed between the blue and brown rot fungi at most wavelengths, except for the intervals 1450–1550, 1550–1650, 1650–1750, and 1750–1850.

In the first derivative of trembling aspen (Figure 2C), differences were more pronounced around 1950 nm, where the brown rot fungi separated more clearly from the other spectra. The curves for clear wood and control samples largely overlapped across most regions, while the blue stain fungi showed some separation around 1850 nm. Additionally, at 100-nm intervals, significant differences in mean absorbance were consistently detected between the blue and brown rot fungi, except in the 2150–2250 nm range.

In the second derivative (Figure 2C), the brown and blue stain fungi exhibited sharper peaks around 1850 nm and 1950 nm, whereas the clear wood and control curves remained closely aligned, showing minimal variation in these regions. Again, significant differences in mean absorbance were observed at 100-nm intervals between the blue and brown rot fungi,

except for the intervals 1350–1450, 1750–1850, 1950–2050, 2250–2350, and 2350–2450 nm.

Our results demonstrate that NIRS can distinguish between brown rot and blue stain fungi in white spruce, lodgepole pine, and trembling aspen, based on distinct spectral signatures (Figure 2, Table 2) that reflect underlying chemical and physical changes. The variations in absorbance with wavelength, particularly at 1900 nm, 1950 nm, and 2350 nm, emerged as consistent markers for distinguishing blue stain and brown rot fungi across all three species (Figure 2). These wavelengths were reliable indicators due to their consistent presence in multiple spectral analyses (raw, 1st derivative, and 2nd derivative) across species. Specifically, the 1900 nm and 1950 nm regions are sensitive to water and hydroxyl (-OH) groups associated with cellulose and water molecules (Via et al. 2008;

Table 2. PERMANOVA and pairwise comparisons of wood stained/rot or unstained by fungi. F represents the F-statistic, and p represents the p-value from PERMANOVA. Significant at p value less than 0.05. A dash indicates that the overall PERMANOVA was not significant enough to warrant pairwise comparisons.

A. White spruce						
Source/Comparison	F	p	F	p	F	p
	Raw Absorbance		1st Derivative		2nd Derivative	
Overall PERMANOVA	31.647	0.001	9.589	0.001	9.396	0.001
Pairwise comparison						
Control vs. brown rot fungi	52.408	0.001	0.19	0.711	0.203	0.757
Control vs. clear	4.342	0.032	26.817	0.001	25.43	0.001
Control vs. blue stain fungi	18.003	0.002	0.293	0.562	0.239	0.692
Brown rot fungi vs. clear	77.166	0.001	22.452	0.001	20.633	0.001
Brown rot fungi vs. blue stain fungi	10.442	0.006	0.224	0.664	0.204	0.78
Clear vs. blue stain fungi	40.142	0.001	20.64	0.001	21.756	0.001
B. Lodgepole pine						
Source/Comparison	F	p	F	p	F	p
	Raw Absorbance		1st Derivative		2nd Derivative	
Overall PERMANOVA	4.763	0.006	1.341	0.256	1.469	0.214
Pairwise comparison						
Control vs. blue stain fungi	14.676	0.001	-	-	-	-
Control vs. brown rot fungi	5.57	0.019	-	-	-	-
Control vs. clear	6.508	0.011	-	-	-	-
Blue stain fungi vs. brown rot fungi	2.842	0.097	-	-	-	-
Blue stain fungi vs. clear	1.251	0.277	-	-	-	-
Brown rot fungi vs. clear	0.447	0.503	-	-	-	-
C. Trembling aspen						
Source/Comparison	F	p	F	p	F	p
	Raw Absorbance		1st Derivative		2nd Derivative	
Overall PERMANOVA	2.0674	0.102	14.056	0.001	11.269	0.001
Pairwise comparison						
Control vs. brown rot fungi	-	-	1.693	0.161	1.505	0.205
Control vs. clear	-	-	4.265	0.038	4.304	0.034
Control vs. blue stain fungi	-	-	29.252	0.001	23.936	0.001
Brown rot fungi vs. clear	-	-	11.724	0.001	10.121	0.004
Brown rot fungi vs. blue stain fungi	-	-	50.507	0.001	34.153	0.001
Clear vs. blue stain fungi	-	-	12.119	0.002	8.729	0.002

Sundaram et al. 2015). Blue stain fungi alter water distribution and cellulose structure, leading to significant absorption differences at these wavelengths. Similarly, the 2350 nm region is linked to lignin, which contains aromatic structures and fewer hydroxyl groups (Belt et al. 2022; Fackler and Schwanninger 2012). Unlike lignin-degrading fungi, brown rot fungi do not significantly alter lignin, and the resulting spectral consistency at this wavelength emphasizes the importance of their minimal impact on this component, aiding in their differentiation.

Our findings also highlight tree species-specific differences in the wavelengths that distinguish blue stain and brown rot fungi (Figure 2). For white spruce, subtle but visible distinctions appeared in the raw spectral curve around 1450 nm, 1900 nm, and 2350 nm, where brown rot fungi exhibited higher absorbance, likely due to chemical changes caused by fungal activity. Additional observations in the derivative plots, such as around 1550 nm and 2150 nm, provided further insights into spectral patterns. In lodgepole pine, blue stain fungi exhibited the highest absorbance in the raw curve between 1900–2350 nm, peaking around 1900 nm, suggesting links to fungal metabolite concentrations. Derivative plots further differentiated key intervals, including 1650–1750 nm, 1950–2150 nm, and 2350–2450 nm, emphasizing the utility of derivative analyses (Schwanninger et al. 2011). For trembling aspen, brown rot fungi showed dominant absorbance from 1750–2350 nm, particularly at 1900 nm and 2350 nm, while derivative plots revealed variability around 1850 nm and 1950 nm. These results demonstrate the potential of these wavelengths as reliable markers for species identification and wood quality assessment, aligning with findings from previous studies (Ramirez et al. 2015; Lang et al. 2017).

Multivariate analysis of NIR spectral differences among wood conditions and species

PERMANOVA and follow-up pairwise comparisons were used to assess the NIR spectral similarity among the different wood conditions: blue stain, brown rot, clear, and control for the species white spruce, lodgepole pine, and trembling aspen. Despite some overlap in the multivariate ordination plots, significant differences were detected among the four wood conditions based on the original (raw) absorbance values, as well as the first and second derivatives.

For white spruce, a significant difference was observed between the blue stain and brown rot fungi for the raw absorbance, whereas the first and second derivatives showed no significant difference between the two fungal groups (Table 2A, Figure 3A). Various degrees of significance were also noted between the clear/control and both the blue stain and brown rot conditions (Table 2A).

For lodgepole pine (Table 2B, Figure 3B), the raw absorbance values showed no significant difference between the blue stain and brown rot conditions. Unlike clear wood, there was a significant difference in absorbance values between the control and both the brown rot and blue stain fungi. For the first and second derivatives, the overall PERMANOVA was not significant, so no pairwise comparisons were conducted between the different wood conditions (Table 2B).

In the case of trembling aspen (Table 2C, Figure 3C), PERMANOVA showed no significant differences in absorbance values between the blue stain, brown rot fungi, and their clear and control wood counterparts. However, PERMANOVA for the first and second derivatives revealed significant differences between the brown rot and blue stain fungi conditions. Significant differences were predominantly recorded between the control and clear wood, each compared separately to the brown rot and blue stain conditions.

Our results revealed species-specific differences in the spectral properties and the relative utility of raw absorbance versus derivative data for differentiating fungal stains (Figure 3, Table 2). In white spruce, significant differences between blue stain and brown rot fungi were observed in the raw absorbance spectra, particularly when compared to the clear and control wood conditions. However, the first and second derivatives did not reveal significant differences between the two fungal discoloration types. This suggests that the spectral changes induced by blue stain and brown rot fungi in white spruce are more detectable in the raw spectra. The lack of differentiation in the derivative plots may be due to the tendency of derivative processing to emphasize subtle spectral features while reducing broader signals, which could obscure meaningful changes if the fungal-induced variations are not sharply defined. Additionally, the spectral sampling interval of the instrument and the use of 100-mm spatial increments may have contributed to signal averaging, further limiting the detection of localized fungal effects. Nevertheless, pronounced differences were observed between stained and unstained wood (both clear and control conditions), confirming that NIR spectroscopy was effective in detecting fungal degradation relative to unaffected wood (Via et al. 2008).

These species-specific differences in PERMANOVA outcomes likely reflected underlying biological and chemical processes. In white spruce, the consistent and pronounced spectral shifts across brown rot, blue stain, and unstained (clear and control)

wood suggest that fungal colonization leads to substantial and predictable chemical changes, which are readily captured by raw spectra. In contrast, lodgepole pine exhibited more subtle and overlapping spectral responses, indicating that fungal impact may be less chemically pronounced or more spatially variable, making detection less reliable. For trembling aspen, the blue stain spectrum appeared atypical compared to all other spectra, potentially due to pigment accumulation, unique host-fungus interactions, or sampling variation. This irregularity likely contributed to the lack of significant group separation in the raw data. However, applying derivative transformations helped reveal meaningful contrasts in aspen by removing baseline noise and highlighting finer spectral details. These findings emphasize that both species-specific wood chemistry and spectral preprocessing approaches influence the detectability of fungal degradation in NIR spectra.

The ability to detect spectral changes caused by blue stain and brown rot fungi depends on whether raw or derivative spectra are used (Figures 2 and 3, Table 2). Derivative transformations, like first or second derivatives, are often applied to spectroscopic data to enhance spectral features and elimi-

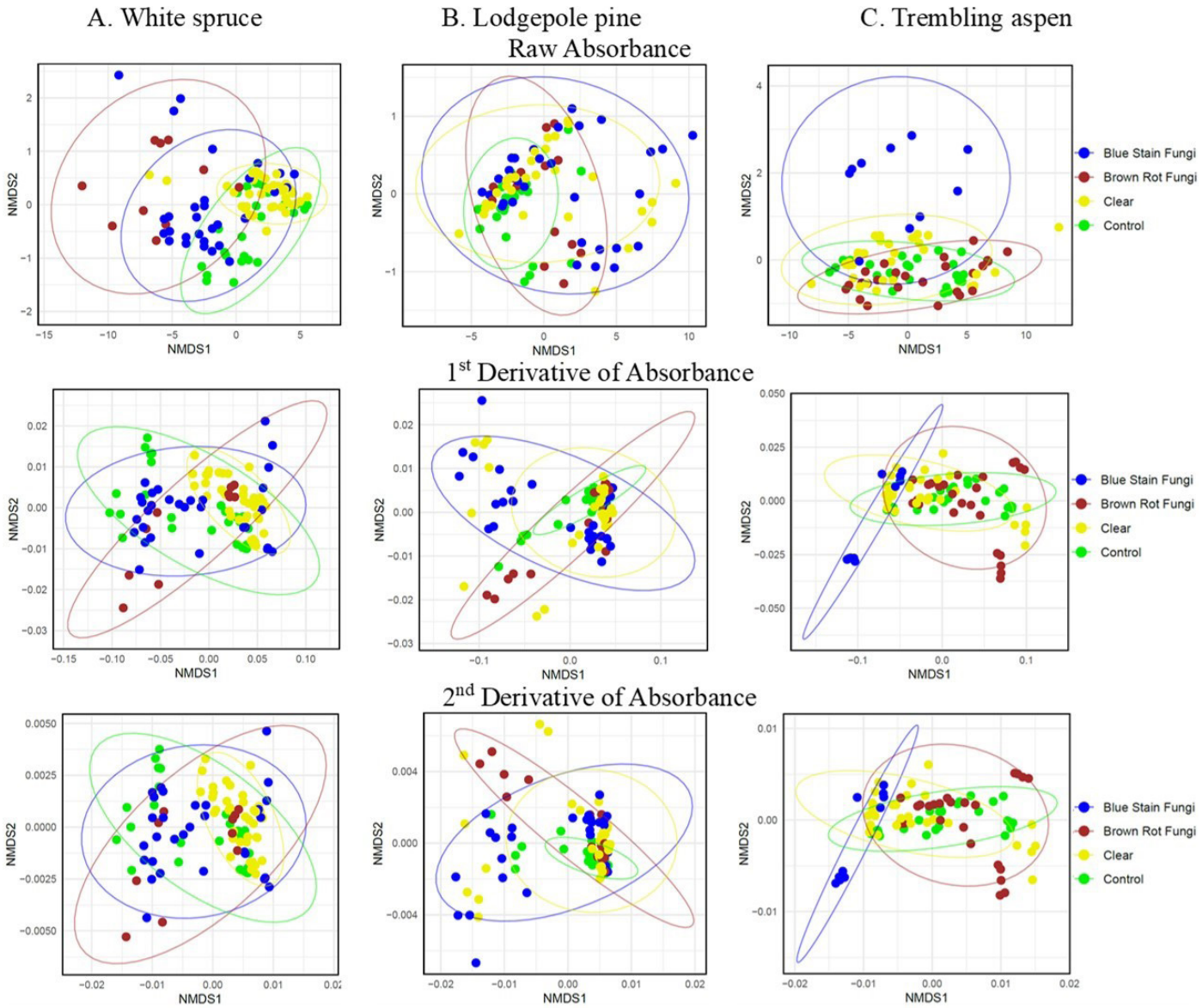

Figure 3. NMDS ordination from PERMANOVA showing spectral variability across four wood stain conditions in different tree species. Each column represents a species, and rows display raw absorbance (top), first derivative (middle), and second derivative (bottom). The four wood conditions: blue stain fungi (blue), brown rot fungi (brown), clear wood (yellow), and control (green) are represented using non-metric multidimensional scaling (NMDS) plots. Ellipses indicate the dispersion and overlap within each wood stain condition.

nate baseline variations. However, these transformations can sometimes reduce the ability to detect fungal-induced spectral changes due to increased noise. For example, Via et al. (2007 and 2008) identified significant differences in the raw spectra of longleaf pine affected by blue stain at specific wavelengths (e.g., 354–364 nm, 424–1104 nm, and 1114–1354 nm). These differences became less detectable after applying derivative transformations, highlighting that raw spectra alone can effectively identify fungal stains without requiring additional processing.

Regarding the observed significant differences between control and clear wood, although both were visually unstained, subtle chemical differences may exist due to residual microbial activity that could have influenced the clear samples prior to NIR measurement, making them spectrally distinct from the control set. This suggests that unstained regions on stained discs (clear wood) may not be chemically equivalent to wood from entirely non-colonized unstained trees (control), potentially reflecting early or localized biochemical alterations.

Conclusions

This study highlighted the potential of NIR spectroscopy to detect and differentiate fungal stains and rots in wood, with performance varying across tree species. In white spruce, raw absorbance spectra effectively distinguished stain from rot fungi. In trembling aspen, derivative analysis enhanced sensitivity to subtle spectral differences. However, in lodgepole pine, spectral overlap limited differentiation, suggesting a need for further exploration of the biochemical similarities among fungal types and the resulting wood degradation. These findings emphasize the importance of developing rapid, reliable methods for fungal identification, especially as climate-driven disturbances such as wildfires could alter the prevalence of fungal impacts on salvaged logs. Accurate detection can support informed forest management, efficient processing, and improved timber valuation.

Nonetheless, several factors limited the interpretation and generalizability of our results. Species-specific traits of trees such as age, size, site conditions, growth history, natural wood color, and durability, as well as sampling location, can influence spectral patterns. Moreover, because the samples were naturally stained in the field, we had no experimental control over fungal colonization or wood condition. While this enhanced ecological relevance, it necessitated caution in interpreting the results. These limitations were not directly evaluated in this study but should be systematically addressed in future research to strengthen model robustness and applicability. Moving forward, we plan to integrate genetic analyses to identify fungal species, explore the causes of staining, and clarify fungal functional roles. Combining NIR spectroscopy with complementary techniques will improve fungal discrimination and deepen understanding of the underlying spectral mechanisms.

Acknowledgment

The authors express their gratitude to the Canadian Wood Fibre Centre within Natural Resources Canada for providing financial support. We also extend our appreciation to the students who assisted with field data collection and sample processing for measurements. Additionally, we acknowledge the valuable comments provided by colleagues at the Canadian Wood Fibre Centre on the submitted manuscript.

References

Barton FE, Himmelsbach DS, Akin DE, Sethuraman A, Eriksson KE (1995) Two-dimensional vibrational spectroscopy III: interpretation of the degradation of plant cell walls by white rot fungi. J. Near Infrared Spectrosc, 3(1), 25-34.

Belt T, Awais M, Mäkelä M (2022) Chemical characterization and visualization of progressive brown rot decay of wood by near infrared imaging and multivariate analysis. Front Plant Sci 13:940745. https://doi.org/10.3389/fpls.2022.940745

Bousfield CG, Lindenmayer DB, Edwards DP (2023) Substantial and increasing global losses of timber-producing forest due to wildfires. Nat Geosci 16(12):1145-1150.

Burud I, Gobakken LR, Flø A, Kvaal K, Thiis TK (2014) Hyperspectral imaging of blue stain fungi on coated and uncoated wooden surfaces. Int Biodeterior Biodegrad 88, 37-43. https://doi.org/10.1016/j.ibiod.2013.12.002

Chen Q, Zhang D, Pan W, Ouyang Q, Li H, Urmila K, Zhao J (2015) Recent developments of green analytical techniques in analysis of tea's quality and nutrition. Trends Food Sci Technol 43(1):63-82. https://doi.org/10.1016/j.tifs.2015.01.009

Deepa MS, Shukla SR, Kelkar BU (2024) Overview of applications of near infrared (NIR) spectroscopy in wood science: recent advances and future prospects. J Indian Acad Wood Sci 1-24.

Fackler K, Schwanninger M (2012) How spectroscopy and microspectroscopy of degraded wood contribute to understand fungal wood decay. Appl Microbiol Biotechnol 96:587-599. https://doi.org/10.1007/s00253-012-4369-5

Fackler K, Schwanninger M, Gradinger C, Srebotnik E, Hinterstoisser B, Messner K (2007) Fungal decay of spruce and beech wood assessed by near-infrared spectroscopy in combination with uni-and multivariate data analysis.

Gauthier S, Bernier P, Kuuluvainen T, Shvidenko AZ, Schepaschenko DG (2015) Boreal forest health and global change. Science 349(6250):819-822. http://www.jstor.org/stable/24749186

González-Peña MM, Curling SF, Hale MD (2009) On the effect of heat on the chemical composition and dimensions of thermally-modified wood. Polym Degrad Stab 94(12):2184-2193.

Guillén Y, Machuca Á (2008) The effect of copper on the growth of wood-rotting fungi and a blue-stain fungus. World J Microbiol Biotechnol 24:31-37. https://doi.org/10.1007/s11274-007-9434-3

Hein PRG, Pakkanen HK, Dos Santos AA (2017) Challenges in the use of Near Infrared Spectroscopy for improving wood quality: A review. Forest

Syst 26(3):eR03. https://doi.org/10.5424/fs/2017263-11892

Jain P, Barber QE, Taylor SW, Whitman E, Castellanos Acuna D, Boulanger Y, Chavardès RD, Chen J, Englefield P, Flannigan M, Girardin MP, Hanes CC, Little J, Morrison K, Skakun RS, Thompson DK, Wang X, Parisien M-A (2024) Drivers and impacts of the record-breaking 2023 wildfire season in Canada. Nat Commun 15:Article 6764. https://doi.org/10.1038/s41467-024-51154-7

Kelley SS, Jellison J, Goodell B (2002) Use of NIR and pyrolysis-MBMS coupled with multivariate analysis for detecting the chemical changes associated with brown-rot biodegradation of spruce wood. FEMS Microbiology Letters, 209(1), 107-111. https://doi.org/10.1111/j.1574-6968.2002.tb11117.x

Lang C, Almeida DR, Costa FR (2017) Discrimination of taxonomic identity at species, genus and family levels using Fourier Transformed Near-Infrared Spectroscopy (FT-NIR). For Ecol Manage 406:219-227.

Lundell TK, Mäkelä MR, de Vries RP, Hildén KS (2014) Genomics, lifestyles and future prospects of wood-decay and litter-decomposing basidiomycota. Adv Bot Res 70:329-370.

Mensah RA, Jiang L, Renner JS, Xu Q (2023) Characterisation of the fire behaviour of wood: From pyrolysis to fire retardant mechanisms. J Therm Anal Calorim 148(4):1407-1422. https://doi.org/10.1007/s10973-022-11442-0

McCarthy JK, Hood IA, Kimberley MO, Didham RK, Bakys R, Fleet KR, Brownlie RK, Flint HJ, Brockerhoff EG (2012) Effects of season and region on sapstain and wood degrade following simulated storm damage in Pinus radiata plantations. For Ecol Manage 277:81–89. https://doi.org/10.1016/j.foreco.2012.04.018

Natural Resources Canada (2023). The State of Canada's Forests: Annual Report 2023. Retrieved from https://natural-resources.canada.ca/sites/nrcan/files/forest/sof2023/NRCAN_SofForest_Annual_2023_EN_accessible-vf.pdf

Natural Resources Canada (2022). Canada's softwood lumber industry. Retrieved from https://natural-resources.canada.ca/our-natural-resources/forests/industry-and-trade/canadas-softwood-lumber-industry/19601

Natural Resources Canada (2020). Economic impacts. Retrieved from https://natural-resources.canada.ca/our-natural-resources/forests/insects-disturbances/forest-pest-management/economic-impacts/13387

Natural Resources Canada (2019). Changes in temperature. Retrieved from https://www.canada.ca/en/environment-climate-change/services/climate-change/canadian-centre-climate-services/basics/trends-projections/changes-temperature.html

Oksanen J, Simpson GL, Blanchet FG, Kindt R, Legendre P, Minchin PR, O'Hara RB, Solymos P, Stevens MHH, Szoecs E, Wagner H, Barbour M, Bedward M, Bolker B, Borcard D, Carvalho G, Chirico M, De Caceres M, Durand S, Evangelista HBA, FitzJohn R, Friendly M, Furneaux B, Hannigan G, Hill MO, Lahti L, McGlinn D, Ouellette M-H, Ribeiro Cunha E, Smith T, Stier A, Ter Braak CJF, Weedon J (2024) vegan: Community ecology package (Version 2.6-6.1) [R package]. CRAN. https://CRAN.R-project.org/package=vegan

Piernik M, Woźniak M, Pinkowski G, Szentner K, Ratajczak I, Krauss A (2022) Impact of the heat treatment duration on color and selected mechanical and chemical properties of scots pine wood. Materials 15(15):5425.

Pohleven F, Humar M, Amartey S, Benedik J (2002) Tolerance of wood decay fungi to commercial copper-based wood preservatives. IRG/WP 02-30291.

Ramirez JA, Posada JM, Handa IT, Hoch G, Vohland M, Messier C, Reu B (2015) Near-infrared spectroscopy (NIRS) predicts non-structural carbohydrate concentrations in different tissue types of a broad range of tree species. Methods Ecol Evol 6(9):1018–1025.

R Core Team (2024) R: A language and environment for statistical computing. R Foundation for Statistical Computing, Vienna, Austria. https://www.R-project.org/.

Savitzky A, Golay MJ (1964) Smoothing and differentiation of data by simplified least squares procedures. Anal Chem 36(8):1627–1639.

Schmidt O (2006) Wood and tree fungi. Springer-Verlag Berlin Heidelberg.

signal developers (2023) signal: Signal processing. Retrieved from https://r-forge.r-project.org/projects/signal/

Si-Ware Systems. (2023). NeoSpectra Scanner. Retrieved April 8, 2025, from https://www.si-ware.com/neospectra-product-pages/scanner

Sundaram J, Mani S, Kandala CV, Holser RA (2015) Application of NIR reflectance spectroscopy on rapid determination of moisture content of wood pellets. Am J Anal Chem 6(12):923–932.

Schwanninger M, Rodrigues JC, Fackler K (2011) A review of band assignments in near infrared spectra of wood and wood components. J Near Infrared Spectrosc 19(5):287–308.

Tsuchikawa S, Inagaki T, Ma T (2023) Application of near-infrared spectroscopy to forest and wood products. Curr For Rep 9:401–412. https://doi.org/10.1007/s40725-023-00203-3

Tsuchikawa S, Kobori H (2015) A review of recent application of near-infrared spectroscopy to wood science and technology. J Wood Sci 61:213–220. https://doi.org/10.1007/s10086-015-1467-x

Tsuchikawa S (2007) A review of recent near-infrared research for wood and paper. Appl Spectrosc Rev 42(1):43–71.

Via BK, So CL, Eckhardt LG, Shupe TF, Groom LH, Stine M (2008) Response of near-infrared diffuse reflectance spectra to blue stain and wood age. J Near Infrared Spectrosc 16(1):71–74.

Via B, Eckhardt L, So C, Shupe T, Groom L, Stine M (2007) The response of visible/near-infrared absorbance to wood-staining fungi. Wood Fiber Sci 38(4):717–726.

Watson P, Potter S (2004) Burned wood in the pulp and paper industry: a literature review. For Chron 80(4):473–477.

Wulder MA, Hermosilla T, White JC, Coops NC (2020) Biomass status and dynamics over Canada's forests: Disentangling disturbed area from associated aboveground biomass consequences. Environ Res Lett 15.